



THE HONG KONG
POLYTECHNIC UNIVERSITY

香港理工大學

Pao Yue-kong Library

包玉剛圖書館

Copyright Undertaking

This thesis is protected by copyright, with all rights reserved.

By reading and using the thesis, the reader understands and agrees to the following terms:

1. The reader will abide by the rules and legal ordinances governing copyright regarding the use of the thesis.
2. The reader will use the thesis for the purpose of research or private study only and not for distribution or further reproduction or any other purpose.
3. The reader agrees to indemnify and hold the University harmless from and against any loss, damage, cost, liability or expenses arising from copyright infringement or unauthorized usage.

IMPORTANT

If you have reasons to believe that any materials in this thesis are deemed not suitable to be distributed in this form, or a copyright owner having difficulty with the material being included in our database, please contact lbsys@polyu.edu.hk providing details. The Library will look into your claim and consider taking remedial action upon receipt of the written requests.

**MODELING EXPLICIT TROPOSPHERIC
OXIDATION THROUGH IDENTIFYING
VOLATILE ORGANIC COMPOUND (VOC)
SOURCES, THEIR IMPACT ON AIR QUALITY
AND THEIR SIGNATURE IN SOUTH CHINA**

HAIRONG CHENG

Ph.D

The Hong Kong Polytechnic University

2010

The Hong Kong Polytechnic University
Department of Civil and Structural Engineering

**Modeling explicit tropospheric oxidation through
identifying volatile organic compound (VOC) sources,
their impact on air quality and their signatures in
South China**

By
Hairong CHENG

**A thesis submitted in partial fulfillment of the
requirements for the Degree of Doctor of Philosophy**

May 2010

CERTIFICATE OF ORIGINALITY

I hereby declare that this thesis entitled “Modeling explicit tropospheric oxidation through identifying volatile organic compound (VOC) sources, their impact on air quality and their signatures in South China” is my own work and that, to the best of my knowledge and belief, it reproduces no material previously published or written nor material which has been accepted for award of any other degree or diploma, except where due acknowledgment has been made in text.

Signed:

Name:

Abstract

Photochemical smog, characterized by high concentrations of ozone (O_3) and fine particles, is of great concern in the urban areas, in particular megacities and city clusters like the Pearl River Delta (PRD). Ambient O_3 and its precursors were simultaneously measured for the first time at a site within the inland PRD region (WQS) and a site in Hong Kong (TC) from 22 October to 01 December 2007, in order to improve our understanding of the interplay of O_3 pollution between Hong Kong and the inland PRD region, to explore the relationships between O_3 and its precursors, and to identify the key volatile organic compound (VOC) species and emission source categories contributing to the O_3 formation. Ratio analyses for trace gases and VOCs and back trajectory calculation revealed that the air masses arriving at WQS were more aged due to regional influence, whereas the air masses at TC were mainly affected by local emissions and/or regional transport.

An observation-Based Model (OBM) was employed to determine the O_3 -precursor relationship. At both sites, O_3 production was found to be VOC-limited. Anthropogenic hydrocarbons played a key role in O_3 production, while reducing NO emissions aided the build up of O_3 concentrations. The contribution of carbonyls to O_3 formation was firstly input in the OBM by using measured data, the results showed that the net O_3 production derived from the OBM agreed better with the observed O_3 increment after hourly carbonyl concentrations were included. When adding carbonyls to the OBM, the derived

P_{O_3-NO} peak increased by 64% and 47%, and the HO_2 peak increased by 43% and 39%, at WQS and TC, respectively. These results highlight the importance of carbonyls in the photochemistry in this region.

To further identify which VOC species and emission source categories were likely to contribute most to regional O_3 formation in the PRD region, a photochemical trajectory model, was developed and used for the first time to simulate the formation of photochemical pollutants at WQS, Guangzhou during photochemical pollution episodes between 12 and 17 November, 2007. The simulated diurnal variations and mixing ratios of O_3 were in good agreement with observed data, indicating that the photochemical trajectory model provides a reasonable description of O_3 formation in the PRD region. Calculated photochemical ozone creation potential (POCP) indices for the region indicated that alkanes and oxygenated organic compounds had relatively low reactivity, while alkenes and aromatics presented high reactivity. Analysis of the emission inventory found that the sum of 60 of the 139 VOC species accounted for 91% of the total POCP-weighted emission. A further investigation of the relative contribution of the main emission source categories to O_3 formation suggested that mobile source was the largest contributor to regional O_3 formation (40%), followed by biogenic sources (29%), VOC products-related (23%), industry (6%), biomass burning (1%), and power plants (1%). The findings obtained in this study would advance our knowledge of air quality in the PRD region, and provide useful information to local government on effective control of

photochemical smog in the region.

PUBLICATIONS

1. **Cheng H R**, Guo H*, Wang X M, Saunders S M, Lam S H M, Jiang F, Wang T J, Ding A J, Lee S C, Ho K F. On the relationship between ozone and its precursors in the Pearl River Delta: Application of an Observation-Based Model (OBM). *Environmental Science and Pollution Research* 17, 547-560, 2010.
2. **Cheng H R**, Guo H*, Saunders S M, Lam S H M, Wang X M, Jiang F, and Wang T J, 2010. Assessing photochemical ozone formation in the Pearl River Delta with a photochemical trajectory model, *Atmospheric Environment*, [doi:10.1016/j.atmosenv.2010.07.019](https://doi.org/10.1016/j.atmosenv.2010.07.019).
3. **Cheng H R**, Guo H*, Saunders S M, Wang X M, 2010. Roles of volatile organic compounds in photochemical ozone formation in the atmosphere of the Pearl River Delta, southern China. *Clean Air and Climate Change*, invited paper. In press.
4. Guo H, Jiang F, **Cheng H R**, Simpson I J, Wang X M, Ding A J, Wang T J, Saunders S M, Wang T, Lam S H M, Blake D R, Zhang Y L, Xie M. Concurrent observations of air pollutants at two sites in the Pearl River Delta and the implication of regional transport. *Atmospheric Chemistry and Physics* 9, 7343-7360, 2009.
5. Jiang F, Guo H*, Wang T J, **Cheng H R**, Wang X M, Simpson I J, Ding A J, Saunders S M, Lam S H M, Blake D R, 2010. A photochemical smog episode in the Pearl River Delta: Field observation and model simulation, *Journal of Geophysical Research*, In press.
6. Guo H*, Kwok N H, **Cheng H R**, Lee SC, Li Y S, Hung W T, 2009. Formaldehyd and volatile organic compounds in Hong Kong homes:

Concentrations and impact factors. *Indoor Air* 19, 206-217.

7. Zhang Y L, Guo H*, Wang X M, Simpson I J, Barletta B, Blake D R,

Meinardi S, Rowland F S, **Cheng H R**, Saunders S M, Lam S H M, 2010.

Emission patterns and spatiotemporal variations of halocarbons in the Pearl River

Delta region, southern China. *Journal of Geophysical Research* 115, D15309,

[doi:10.1029/2009JD013726](https://doi.org/10.1029/2009JD013726).

8. Guo H*, Simpson I J, Ding A J, Wang T, Saunders S M, Wang T J, **Cheng H**

R, Barletta. B, Meinardi S, Blake D R, Rowland F S, 2010. Carbonyl sulfide,

dimethyl sulfide and carbon disulfide in the Pearl River Delta of southern China:

Impact of anthropogenic and biogenic sources. *Atmospheric Environment* 44,

3805-3813

CONFERENCE PRESENTATIONS

1. **Cheng HR**, Guo H, Jiang F, Wang TJ, Saunders SM, Wang XM (2009). (Oral Presentation) Photochemical formation in Pearl River Delta (PRD) assessed by photochemical trajectory model. The 16th Chinese Conference on Atmospheric Science and Technology, 21-24 October, 2009, Nanjing, China.
2. Lam SHM, **Cheng HR**, Guo H, Saunders SM, Wang XM, Simpson IJ, Ding AJ, Wang T, Blake DR (2009). (Oral Presentation) Ozone and its precursors in the PRD, China : An MCM Modelling approach. The 2nd International Workshop on Regional Air Quality Management in Rapidly Developing Economic Regions, 9-10 November, 2009, Guangzhou, China.
3. Jiang F, Guo H, Wang TJ, **Cheng HR**, Ding AJ (2009). (Oral Presentation) A photochemical smog episode in the Pearl River Delta: Field observation and model simulation. The 16th Chinese Conference on Atmospheric Science and Technology, 21-24 October, 2009, Nanjing, China.
4. Guo H, Wang XM, Zhang YL, Jiang F, Wang TJ, **Cheng HR**, Blake DR, Simpson IJ, Saunders Sam (2009). (Oral Presentation) An ozone episode event observed in PRD region and its implication to cross-boundary transport. The 2nd International Workshop on Regional Air Quality Management in Rapidly Developing Economic Regions, 9-10 November, 2009, Guangzhou, China.

ACKNOWLEDGMENTS

I would like to express my sincere gratitude to Dr GUO Hai, my chief supervisor, for his invaluable guidance and support. Without his understanding, encouragement, and continuous support, this project would not have been completed. I also thank him for providing me a very good opportunity to take a short-term visiting to the University of Western Australia. But most of all, I thank him for kindly offering me opportunities to explore my own interests. His scientific knowledge and insight proved to be invaluable to my work.

I also appreciated the friendship, help, and encouragement from my friends, Luo Chunlin, Jiang fei, Lin Zhenghao, Liu Qian, Yang Jing, Wang Dawei et al.

Finally, I would like to thank my family for their constant support, understanding, and patience through my PhD study.

CONTENTS

CERTIFICATE OF ORIGINALITY	I
ABSTRACT	II
PUBLICATIONS	V
CONFERENCE PRESENTATIONS	VII
ACKNOWLEDGMENTS	IX
CONTENTS	X
LIST OF TABLES	XV
LIST OF FIGURES	XVI

Chapter 1 Overview

1.1 Introduction	1
1.2 Aims and objectives	8
1.3 Structure of the thesis	8

Chapter 2 Literature review

2.1 Ozone (O ₃) in the atmosphere.....	10
2.2 Ozone studies around the world.....	12
2.2.1 Historic trends in ozone concentrations.....	13
2.2.2 Seasonal variations of ozone concentrations.....	15
2.3 Ozone studies in Hong Kong, the inland PRD and other regions of China.....	17
2.3.1 Temporal trends in ozone concentrations in the PRD	

region.....	17
2.3.2 Occurrence of elevated ground-level ozone mixing ratios and ozone pollution episodes in Hong Kong.....	18
2.3.4 Ozone studies in the inland PRD.....	21
2.3.5 Meteorological conditions favouring ozone pollution in the PRD region.....	22
2.3.6 Ozone studies in the other regions in China.....	23
2.4 NO _x in the PRD region.....	25
2.5 Volatile organic compound (VOCs) in Hong Kong and the inland PRD region.....	28
2.5.1 Ambient VOC level in the PRD region.....	28
2.5.2 Temporal variations of VOCs in the PRD region.....	33
2.5.3 Source apportionment of VOCs in the PRD region.....	34
2.6 Contributions of VOCs to ozone formation.....	36
2.6.1 Methodology development in assessing VOC contribution to ozone formation.....	37
2.6.2 VOC contribution to ozone formation in the PRD region....	39
2.7 Model simulation of ozone formation in the atmosphere.....	41
2.7.1 Model simulation on the relationship between O ₃ and its precursors.....	43
2.7.2 Studies undertaken using the observation-based model.....	46
2.7.3 Studies undertaken using the photochemical trajectory	

model.....	48
------------	----

Chapter 3 Methodology

3.1 Sampling sites.....	51
3.2 Meteorological condition.....	52
3.3 Measurement techniques.....	53
3.3.1 Continuous measurements of O ₃ , CO, SO ₂ and NO _x	53
3.3.2 Sampling and analysis of carbonyls.....	56
3.3.3 Sampling and analysis of NMHCs.....	57
3.3.4 Quality control and quality assurance for VOC and carbonyl analyses.....	58
3.4 Backward air mass trajectories.....	59
3.5 Observation-based model (OBM).....	60
3.5.1 Model description.....	60
3.5.2 The chemical mechanism (Carbon-Bond IV mechanism)...	63
3.6 The photochemical trajectory model.....	64
3.6.1 Model description.....	64
3.6.2 Master chemical mechanism.....	65
3.6.3 Photochemical ozone creation potential.....	68

Chapter 4 Concurrent observation of air pollutants at two sites in the Pearl

River Delta

4.1 Introduction.....	70
4.2 General climate condition.....	73

4.3 Temporal variations of trace gases at WQS and TC.....	75
4.3.1 Day-to-day variations.....	75
4.3.2 Diurnal variations.....	78
4.4 Characteristics of air masses in inland PRD and Hong Kong...	81
4.5 Air mass classification with trajectories.....	85
4.6 Summary.....	92

Chapter 5 Observation based model (OBM) evaluation on the relationship between ozone and its precursors

5.1 Introduction.....	93
5.2 Diurnal variations of O ₃ and its precursors.....	97
5.3 Observation-based model (OBM).....	101
5.3.1 Hourly primary production of carbonyls.....	102
5.3.2 OBM-calculated net O ₃ production with and without carbonyls.....	105
5.3.3 Impact of carbonyls on HO ₂ and P _{O₃-NO}	111
5.4 Ozone–precursor relationships.....	113
5.5 The relative effects of VOC species on O ₃ formation.....	116
5.6 Summary.....	122

Chapter 6 Photochemical trajectory modeling of ozone (O₃) formation in the PRD region

6.1 Introduction.....	125
6.2 Photochemical trajectory model (PTM).....	130

6.2.1 Model description.....	130
6.2.2 Master chemical mechanism.....	130
6.2.3 Emission inventories.....	132
6.2.4 Meteorological and air quality data.....	135
6.3 Comparison of simulated and observed data.....	136
6.4 Contribution of individual VOCs to O ₃ formation.....	140
6.4.1 The base case model experiment to calculate the POCP values.....	140
6.4.2 Ccomparison of POCPs with previous studies.....	145
6.4.3 The Contribution of VOC species to O ₃ formation.....	150
6.5 The contributions of VOC emission sources to O ₃ formation....	155
6.6 Summary.....	156
Chapter 7 Conclusions.....	159
Reference	163

LIST OF TABLES

- Table 2.1 Mixing ratios of selected hydrocarbons in the PRD region
- Table 3.1 Gradient separation of C₁ – C₉ aldehyde and ketone derivatives
- Table 4.1 Statistics of meteorological parameters at the TC and WQS sites
- Table 4.2 Daily maximum 1-h O₃ (ppbv) on eight O₃ episode days at WQS, and an O₃ episode day and a-near O₃ episode day at TC during VOCs sampling days.
- Table 4.3 Mean concentrations of trace gases at daytime and nighttime and the diurnal difference
- Table 4.4 Proportion of air masses associated with each track and the corresponding concentrations of trace gases.
- Table 4.5 Proportion of each air mass associated with each track and the corresponding concentrations of NMHCs during the VOC sampling period
- Table 5.1 Daily maximum 1-h O₃ (ppbv) on eight O₃ episode days at WQS, and an O₃ episode day and a-near O₃ episode day at TC during VOCs sampling days
- Table 5.2 PCA results for selected NMHCs and CO at WQS
- Table 5.3 PCA results for selected NMHCs and CO at TC
- Table 6.1 POCP values for 139 volatile organic compounds relative to ethene
- Table 6.2 60 key volatile organic compounds included in the photochemical trajectory model together with their mass emission rates, POCPs and POCP-weighted emissions
- Table 6.3 The top 15 VOCs with the highest reactivities (POCPs), and emission rates in the PRD region.

LIST OF FIGURES

- Fig.3.2. Flow chart indicating the major reactions, intermediate classes and product classes considered in the MCM protocol
- Fig.4.1. Mean sea level pressure and wind field on 1000 hPa between 22 October and 1 December 2007
- Fig.4.2. Time series of O₃, CO, NO, SO₂, temperature, wind speed and direction and solar radiation measured at WQS from 23 October to 01 December, 2007
- Fig.4.3. Time series of O₃, CO, NO, SO₂, temperature, wind speed and direction, and solar radiation measured at TC from 23 October to 01 December, 2007.
- Fig.4.4. Mean diurnal variations of trace gases and total NMHCs, other trace gases and wind fields between 23 October to 1 December (total NMHCs were averaged using all VOC samples from 8 sampling days)
- Fig.4.5. A scatter plot of CO measured at TC vs. WQS
- Fig.4.6. Scatter plots of (a) *m,p*-xylene to ethylbenzene (b) *i*-butane to propane at TC and WQS during the VOC sampling period.
- Fig.4.7. Three typical back trajectories for each site at the 200 m height level.
- Fig.4.8. Four typical back trajectories for each site at the 50 m height level during the VOC sampling period.
- Fig.5.1. Diurnal variations of O₃, NO, CO, and TVOC on O₃ episode days at WQS and TC
- Fig.5.2. Comparison of net photochemical O₃ production calculated by the OBM with the observed O₃ increments at WQS (top) and TC (bottom).

Fig.5.3. Back trajectories of air masses with 3 hours interval arrived at WQS (27 Oct and 13 Nov) and TC (26 Oct and 23 Nov)

Fig.5.4. Model simulated HO₂ and P_{O₃-NO} with and without carbonyl input on 26 October at WQS (left) and TC (right)

Fig.5.5. RIRs for O₃ precursors at WQS and TC

Fig.5.6. Average RIR values for individual VOC species at WQS and TC

Fig.6.1. Location of sampling site in Guangzhou, China (WQS)

Fig.6.2. Comparison of simulated (red dots) and observed (blue lines) O₃ and NO_x concentrations at WQS, TC, and C/W from November 12-17, 2007.

Fig.6.3. Backward trajectories of air parcels whose arrival time at WQS was 3 p.m. from 12-17 November, 2007.

Fig.6.4. Temporal variations of meteorological parameters at WQS between 12 November and 17 November, 2007

Fig.6.5. climatological chart of wind field and surface pressure at 15:00 on 13 November, 2007

Fig.6.6. Comparison of POCP values of target VOCs in the PRD region (using MCM v3.1) with those reported in Europe (using MCM v3).

Fig.6.7. Comparison of POCP and MIR values for 56 volatile organic compounds, which are available in both MCM (this study) and MIR (Carter, 1994)

Fig.6.8. Source contributions to anthropogenic VOC emissions (A) and source contributions to regional ozone formation (B)

Chapter 1

Overview

1.1 Introduction

Photochemical smog, characterized by high concentrations of O₃ and fine particles, is of great concern in the urban areas, in particular megacities and city clusters like the Pearl River Delta (PRD) (Chameides et al., 1992; Wang et al., 1998; Zhang, 1998a; Wang and Kwok, 2003). O₃ is not directly emitted into the atmosphere but is a photochemical product via a series of complex chemical reactions among volatile organic compounds (VOCs) and nitrogen oxides (NO_x) in the presence of sunlight. Although VOCs and NO_x have been confirmed as the key precursors of O₃, the development of an effective strategy for reducing O₃ pollution in megacities is still problematic due to the nonlinear dependency of O₃ formation on NO_x and VOCs (Cardelino and Chameides, 1995; Sillman, 1999). A number of VOC groups, including alkenes, aromatics, and carbonyls, participate in the photochemical formation of O₃. However, different VOC species react at different rates and with different reaction mechanisms. For example, the initial reaction rates of VOCs with the OH radical vary by factors of 10,000, and their different molecular structures mean that they possess intrinsically different potentials for photochemical O₃ formation. Furthermore, they are also emitted into the atmosphere at different mass emission rates, depending on the local and

regional industries, land-use and biogenic sources. Hence, the relative contribution of VOCs to the photochemical O₃ formation varies from one compound to another (Atkinson, 1990; Carter, 1994) and from region to region (Derwent et al., 1996; Chang et al., 2005; Cheng et al., 2009).

The PRD region on the coast of South China is situated at 21°17'-23°56'N and 111°59'-115°25'E, and covers 4.17×10⁴ km². This region is one of the most populated city clusters in China, where major cities include Hong Kong, Shenzhen, Guangzhou, Dongguan, and Huizhou. With the astonishing economic growth, rapid industrialization and urbanization, the PRD region is facing more and more serious O₃ pollution, gaining much attention due to the important role in atmospheric chemistry, climate change, and air quality (NRC, 1991; Wang and Kwok, 2003; Guo et al., 2009). High concentrations of O₃ at ground level can cause adverse effects on human health, visibility and global climate change (NRC, 1991; Godish, 2004). O₃ pollution has been studied and elevated ground-level O₃ concentrations have been reported in the PRD region in recent decades (Wang and Kwok, 2003; Wang et al., 2003; Guo et al., 2009; Shao et al., 2009; Zheng et al., 2010). Ambient O₃ levels have been monitored in Hong Kong since the early 1980s by the Environmental Protection Department (EPD) of Hong Kong through a network of ambient air-quality monitoring stations. Wang et al. (2009) reported the first continuous record of surface O₃ in Hok Tsui, Hong Kong from 1994 to 2007, a background air monitoring station of South China. A linear fit to the

14-year record shows that the O₃ concentration increased by 0.58 ppbv/yr. Recently, Zheng et al. (2010) demonstrated that there were 3~5 ppbv increases in 1 h-average O₃ and 8~11 ppbv increases in 1 h-max O₃ in 2007 compared to the values in 2006 across the PRD region.

The local versus regional contributions to O₃ episodes in the PRD region have been intensively discussed in recent years (Lee et al., 2002; So and Wang, 2003; Ding et al., 2004; Huang et al., 2005; Lam et al., 2005; Zhang et al., 2007). Most of these studies showed the high elevated O₃ concentrations in Hong Kong were influenced by regional transport from the inland PRD region, or a combination of the local and regional transport. For example, Ding et al. (2004) reported that the high concentrations of O₃ observed at the coastal sites in Hong Kong in September, 2001 were mainly due to the transport of pollution from inland areas of the PRD. Lam et al. (2005) found that regional transport contributed 60–90% of the O₃ level observed in urban and rural areas of Hong Kong during 18-22 August, 1999. Zhang et al. (2008) reported that between 50–100% of the O₃ increase observed in Hong Kong during the O₃ episodes in 2002 can be explained by photochemical generation within the Hong Kong area by using an observation-based model. Lee et al. (2002) reported that the emissions from power plants in Hong Kong were mainly responsible for the O₃ episodes in Hong Kong during 1994–1999, and at the same time the emissions from upwind sources in mainland China also have contributed to these O₃ episodes. However, all of these studies were conducted in

Hong Kong. The relative contributions of local photochemical formation versus regional transport to O₃ episodes are not fully understood. Furthermore, there are only limited studies on O₃ pollution carried out in the inland PRD region (Zhang et al., 2008; Shao et al., 2009; Zheng et al., 2010). The cause of O₃ episodes in the inland PRD, considered as a major cause for O₃ episodes in Hong Kong, are still unclear.

Moreover, the relationships between O₃ and its precursors have been studied in the PRD region. Most previous studies have shown that O₃ production was VOC-limited in the PRD region (So and Wang, 2004; Huang et al., 2005; Zhang et al., 2007; Zhang et al., 2008). So and Wang et al. (2004) reported that the ratios of total non-methane hydrocarbons (NMHCs) to nitrogen oxides were found to be 2 to 10 (ppbC/ppbv) indicating that the formation of photochemical O₃ in Hong Kong was controlled by the levels of NMHCs. By analyzing some high O₃ episode cases, Zhang et al. (2007) found that the formation of O₃ throughout Hong Kong was limited by VOCs, especially reactive aromatics, and high NO concentrations suppressed O₃ production. Recently, it was reported that photochemical production of O₃ was sensitive to VOCs at an urban site in Guangzhou and a rural site, Xinken, downwind of Guangzhou (Zhang et al., 2008). Although the latter two studies provide a view of O₃-precursor relationships by using an observation-based model (OBM) in Hong Kong and the inland PRD region, respectively, some limitations still remain. For example, it is well known that

some carbonyl species, including formaldehyde, are abundant in the atmosphere due to various sources. These carbonyls usually have relatively high photochemical reactivities (Atkinson 1990, 2000; Carter 1994). However, in the previous OBM studies, the contribution of carbonyls to O₃ formation was either not considered or, if considered, it was only discussed using approximate simulated carbonyl concentrations, principally due to the lack of field measurement data of carbonyls (Cardelino and Chameides, 2000; Zhang et al., 2007; Zhang et al., 2008). Moreover, previous modeling simulations were mainly based on limited daily VOC samples (five to six samples per day), although during the O₃ episode events, the concentrations of O₃ precursors, i.e., VOCs and NO_x, varied significantly with time. Hence, inadequate VOC samples collected daily for model simulation input could significantly affect the model output (Zhang et al., 2007). Given that source emissions and source profiles of O₃ precursors in the inland PRD and Hong Kong have changed significantly due to rapid urbanization and industrialization in mainland China and implementation of control measures in Hong Kong in more recent years (Streets et al., 2006), the contributions of VOCs and NO_x to the formation of O₃ in this region could vary significantly.

As such, simultaneous measurement data of O₃ and its precursors (i.e., VOCs and NO_x) in the inland PRD and Hong Kong are urgently needed in order to improve our understanding of the interaction between O₃ pollution in Hong Kong and the inland PRD region, identify the O₃-precursor relationships, and determine

which VOC species and emission source categories were likely to contribute most to regional scale O₃ formation in the PRD region. An intensive field measurement study was conducted concurrently at a site within the inland Pearl River Delta (PRD) and a site in Hong Kong (TC) from 22 October to 1 December, 2007.

Though the measurements are limited for one particular month, leaving an incomplete picture of ongoing photochemistry throughout the year, this study period represents a significant season when the prevailing autumn/winter monsoons bring polluted continental air masses to the downwind sampling sites. The sunny and dry weather, coupled with the subsidence of air in most of the time during this season, provides conditions favorable for photochemical formation of ozone (Lam et al., 2001, 2005; Wang et al., 1998, 2003; Lam et al., 2001, 2005).

Two models, an observation-based model (OBM) and a photochemical trajectory model (PTM), are used to determine the O₃-precursor relationships and identify which VOC species and emission source categories, are likely to contribute most to regional scale O₃ formation in the PRD region. The OBM, which uses measurements of ambient concentrations of O₃ and its precursors as input, is a useful tool to simulate O₃ photochemical production and destruction and to explore the O₃-precursor relationships. In the OBM, observed concentrations rather than emission inventories are used to drive the photochemical simulations and thereby ensure that the calculations are carried out for the measured mix of NO_x and VOCs. Because the OBM is relatively easy and inexpensive to operate

and makes use of data that are increasingly available, it can be used to analyze a wide range of O₃ episodes, and thus, could prove to be a relatively cost-effective tool for the analysis of the O₃–precursor relationships (Cardelino and Chameides, 1995). On the other hand, since the OBM uses observed concentrations to model the O₃ formation, it can not be used in a predictive mode to estimate exactly how much emission reduction is needed to reduce O₃ concentrations. For this reason, OBM is a supplement to, rather than substitute for more sophisticated emission based models. The second model is a photochemical trajectory model, employing the most up-to date version of a near-explicit photochemical mechanism (MCM v3.1) describing the oxidation of 139 non-methane VOC. As the MCM is a near-explicit chemical mechanism describing the detailed degradation of a large number of emitted organic compounds and the resulting generation of O₃ and other secondary pollutants under conditions appropriate to the atmospheric boundary layer, it describes the complex chemistry of VOCs as explicitly as realistically possible, leading to the inclusion of a vast number of chemicals and reactions. In this study, a PTM was developed to simulate the formation of photochemical pollutants observed at WQS, Guangzhou during a photochemical pollution episode between 12 and 17 November, 2007. The PTM is applied under a near-real situation in south-east China under anticyclone conditions to identify which VOC species and emission source categories, are likely to contribute most to regional scale O₃ formation in the PRD region.

1.2 Aims and objectives

An intensive field measurement study was carried out simultaneously in the inland PRD region and Hong Kong. The high quality measurement data enables a set of scientific analyses on the relationships between O₃ and its precursors, and on the identification of key VOC species and emission source categories contributing to O₃ formation. Besides their scientific values, the results will also help the local governments in developing effective O₃ control strategies.

The major objectives of this study are as follows:

- Characterize the spatio-temporal distributions and abundance of trace gases, VOCs, and carbonyls in Hong Kong and the inland PRD region;
- Modify an observation-based model to assess the relationship between ground-level O₃ and its precursors (*i. e.* VOCs and NO_x) in the PRD region;
- Modify a photochemical trajectory model (PTM) to simulate the formation of photochemical pollutants and identify key VOC species and emission source categories that contribute most to the regional scale O₃ formation in the PRD;
- Compare and validate the results as obtained by the PTM model and the OBM model.

1.3 Structure of the thesis

The thesis is composed of seven chapters. Chapter 1 provides the background of this study. Chapter 2 presents a brief literature review on the general

characteristics of O₃ and its precursors, and the relationship between them. Chapter 3 describes methodology including sampling sites, measurement techniques, data analysis, quality control and quality assurance (QA/QC), and model description. Chapter 4 gives an overview of the chemical and physical characteristics of regional air pollution in the study region. Chapter 5 illustrates the relationship between O₃ and its precursors in the PRD by using an observation-based model. Chapter 6 discusses the photochemical O₃ formation in the PRD region using a photochemical trajectory model (PTM). Chapter 7 highlights the major findings, the significant contributions and the implications of the study.

Chapter 2

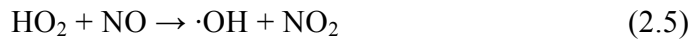
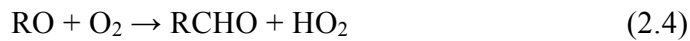
Literature review

2.1 Ozone (O₃) in the atmosphere

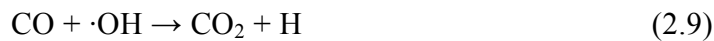
O₃ is a key trace gas in the atmosphere. It is both beneficial and harmful depending on its location and concentration. In the stratosphere (10-50 km altitude), O₃ is beneficial to the environment because it provides a very efficient shield that blocks harmful solar ultraviolet (UV) radiation from reaching the ground and thus helps to protect living organisms at the Earth's surface (Manahan, 2001; Godish, 2003). In the troposphere (0 -10 km in altitude), O₃ plays an important role in atmospheric chemistry, climate change, and air quality (NRC, 1991; Godish, 2004). It determines the oxidizing capacity of the atmosphere through generation of the principal oxidizing agent, the hydroxyl radical (\bullet OH). It is also an infrared absorber (i.e. a greenhouse gas) (Lelieveld and Dentener, 2000; Staehelin et al., 2001) in the atmosphere. However, high concentrations of O₃ (e. g. > 100 ppb) at ground-level can cause adverse effects on human health, agricultural crops, and forests (NRC, 1991).

There are two sources of tropospheric O₃. One is the injection from the stratosphere, and the other is from photochemical production involving in a series of complex chemical reactions among volatile organic compounds (VOCs) and nitrogen oxides (NO_x) in the presence of sunlight (Sillman, 1999) . The simplified

general reactions leading to O₃ formation are summarized as follows:



where an initial reaction between RH and an $\cdot\text{OH}$ radical results in the production of two O₃ molecules and an aldehyde (RCHO). Additional O₃ molecules can then be produced from the degradation of RCHO. In addition, O₃ can be generated from CO oxidation *via*



followed by reactions (2.5), (2.6) and (2.7).

Despite the fact that VOCs and NO_x have been identified as the two key precursors to photochemical O₃ formation, it is difficult to determine whether O₃ production in an urban area is NO_x-limited or VOC-limited. Much of the difficulty in controlling O₃ concentration can be traced to its complex chemistry. The rate of O₃ production is a nonlinear function of the mixture of VOCs and NO_x in the

atmosphere. The relationships among O₃ and its precursors are often site specific, therefore, a effective O₃ mitigation strategy requires an in-depth understanding of the sources, patterns, and formation of photochemical O₃ and its precursors, as well as their relationships in the specific region (Cardelino and Chameides, 1995; Sillman, 1999).

2.2 Ozone studies around the world

Extensive O₃ studies have been conducted to characterize tropospheric O₃ in different places in the world (Jacob et al., 1999; Hidy, 2000; Kleinman, 2000; Jaffe et al., 2003; Vingarzan and Taylor, 2003; Chou et al., 2006; Oltmans et al., 2006; Derwent et al., 2007b; Jaffe and Ray, 2007; Krzyscin et al., 2007; Jenkin, 2008; Kurokawa et al., 2009; Tanimoto, 2009; Wang et al., 2009).

Due to the complex interactions of chemical and meteorological factors, the trends of ground-level O₃ concentration varied in terms of both sign and magnitude. Ground-level O₃ concentrations in urban and rural areas of industrialized regions are strongly linked to the changes in anthropogenic emissions of O₃ precursors. While in remote areas, O₃ precursor emissions from distant source regions, biomass burning, and atmospheric circulation all play important roles in the O₃ concentrations (Jaffe et al., 2003; Parrish et al., 2004; Jaffe and Ray, 2007; Oltmans et al., 2008).

2.2.1 Historic trends in ozone concentrations

The long-term trends of ground-level O₃ concentrations have been reported in many regions around the world including those in Europe, North America, and Asia (Lin et al., 2000; Vingarzan and Taylor, 2003; Vingarzan, 2004; Oltmans et al., 2006; Jenkin, 2008; Tanimoto, 2009).

A review by Vingarzan (2004) showed that the surface O₃ background trend was very inconsistent among monitoring stations. Across the world an increasing O₃ trend for 22 background stations, while a declining trend for 8 background stations, has been reported.

In Europe, Jenkin (2008) investigated the average trends of O₃ concentrations at 13 rural sites from 1990-2006 and at 5 urban sites from 1993-2006 in the UK. The study found a gradual increase in the north-hemispheric baseline O₃ concentration, resulting from global scale effects and thereby influencing the baseline levels of O₃ brought into the UK from the Atlantic Ocean. Oltmans et al. (2006) also reported a significant increase in O₃ concentration with an overall increase of 12.6 (±0.8) % /decade from 1978 to 2004 at Zugspitze, Germany.

In the U.S., Lin et al. (2000) examined the O₃ trends using the database generated from observations at the EPA monitoring sites in the US. They found that the distribution of O₃ had shifted over time, with the highest percentile concentrations showing a decrease and the lowest percentile showing an increase. They hold the opinion that the increase was due to an increase in background O₃,

largely due to increasing emissions from Asia. At Lassen National Park in Northern California, a 15-year record of surface O₃ was evaluated using back trajectories (Jaffe et al., 2003). A positive trend in O₃ concentrations was found in both the Pacific-marine and continental air masses. However, analysis by Oltmans et al. (2006) found no trend at a coastal California site or several National Parks in the western United States.

In Canada, Vingarzan and Taylor (2003) reported that decreasing trends were found for annual O₃ for stations in the eastern portion of southern British Columbia between 1985 and 2000. These trends were consistent with local decline in O₃ precursors. In contrast, increasing trends were found for annual O₃ in the western portion of southern British Columbia, where the geographical locations are less affected by locally produced O₃.

In Asia, an evaluation of observation data at Okinawa, Japan from 1989 to 1997 reported an O₃ increase of 2.5% year⁻¹ in Asian continental air during the winter–spring period (Lee et al., 1998). Tanimoto et al. (2009) reported that O₃ concentrations were increased in Japan during springtime at a remote mountainous site between 1998 and 2006. The springtime background levels have increased at the rate of 0.6 ppbv yr⁻¹. The number of high-O₃ days doubled during 2003-2006 compared to 1999-2002, likely due to rapid increase in anthropogenic emissions from East Asia (Tanimoto, 2009). Chou et al. (2006) reported the trends in the annual averages of O₃ and O₃-max (daily maximum 1 h O₃), increased by 58% and

26%, respectively, in Taipei, China for the period 1994-2003. As the emissions of O₃ precursors, NO_x and VOCs decreased significantly in the same period. Chou et al. explained that the increasing trend of O₃ in Taipei was due to the reduced titration by NO.

2.2.2 Seasonal variations of O₃ concentrations

O₃ concentrations throughout the troposphere showed clear seasonal variations at different locations. The seasonal cycle of O₃ in the troposphere is controlled by a number of processes, such as proximity to large source areas of O₃ precursors, geographical location and meteorological factors (Vingarzan and Taylor, 2003).

Previous studies showed that the annual cycle of O₃ over mid-latitudes exhibits two principal modes of seasonal behaviour, a broad summer maximum typical of populated and industrialized areas and a spring maximum typical of remote regions and associated with background conditions (Vukovich et al., 1985; Ancellet and Beekmann, 1997; Monks, 2000; Tanimoto et al., 2002; Carnero et al., 2010). For example, Tanimoto et al. (2002) reported that seasonal variations of O₃ showed a spring maximum and a summer minimum in Japan, which are consistent with previous field observations made in Europe and North America. O₃ concentrations also showed a clear spring maximum characteristic of the seasonal O₃ cycles in very clean and remote atmospheres in the northern hemisphere based

on the measurement from 1876-1886 at the Montsouris (near Paris, France) (Volz and Kley, 1988).

In contrast to the above sites, there are many studies at surface sites reported a broad summer maximum of O₃ concentration (Tiwari et al., 2008; Carnero et al., 2010). For example, Tiwari et al. (2008) stated that daytime 12-hourly mean O₃ concentrations varied from 45.18 to 62.35 ppbv during summer, and from 28.55 to 44.25 ppbv during winter in Varanasi, India during 2002-2006. Elevated O₃ levels during the summer months can be attributed to high temperature, which favours photochemical production of O₃. Relatively low levels of O₃ during the winter might be due to greater atmospheric stability and an increased incidence of nocturnal inversions, which might enhance the chemical scavenging of O₃ and dry deposition. Carnero et al. (2010) also reported that O₃ concentrations in Spain present a seasonal variability with higher values in summer months, while in wintertime, lower values are recorded. The high levels in summer could be due to the photochemical production *in situ* and also to horizontal or vertical O₃ transport.

While the existence of a broad summer maximum is often associated with the photochemical production of O₃, which is formed by reactions involving VOCs and NO_x in the presence of strong solar radiation, the origin of the spring maximum remains under continued debate. One of the ideas linking the spring maximum is the photochemical activity, which results from increased solar

radiation acting upon a pool of accumulated NO_x and hydrocarbons built up during the winter period (Penkett and Brice, 1986; Simpson, 1995).

2.3 Ozone studies in Hong Kong, the inland PRD and other regions of China

With the astonishing economic growth, rapid industrialization and urbanization, China is facing more and more serious O₃ pollution problems, gaining much attention due to its important role in atmospheric chemistry, climate change, and air quality.

Most of the studies related to O₃ pollution have been reported in the three major city clusters of China (i.e., Beijing-Tianjing, PRD and Yangze River Delta) while O₃ pollution in other regions of China are much less reported (Wang et al., 1998, 2001a, 2001b, 2003; Ding et al., 2004,2008; Huang et al., 2005; Tie et al., 2006; Zhang et al., 2007; Xu et al., 2008; Zhang et al., 2008; Zheng et al., 2010).

Ambient O₃ levels have been monitored in Hong Kong since the early 1980s, by the Environmental Protection Department (EPD) of Hong Kong through a network of ambient air-quality monitoring stations (http://www.epd.gov.hk/epd/english/environmentinhk/air/data/air_data.html).

2.3.1 Temporal trends in ozone concentrations in the PRD region

Wang et al. (2009) recently reported a continuous record of surface O₃ in a background air monitoring station at Hok Tsui, Hong Kong from 1994 to 2007. A

linear fit to the 14-year record showed that the O₃ mixing ratio increased by 0.58 ppbv yr⁻¹. The authors pointed out that the increasing background O₃ in the South China coastal region is associated with the increasing NO₂ column concentration in upwind Eastern China, indicating that the pronounced increase in NO_x (and possibly VOCs as well) emissions in Eastern China is likely the main cause of the increasing O₃ levels at Hok Tsui.

2.3.2 Occurrence of elevated ground-level ozone mixing ratios and ozone pollution episodes in Hong Kong

Elevated ground-level O₃ mixing ratios and O₃ pollution episodes have often been reported in the PRD region in the past decades (Wang et al., 1998, 2001a, 2001b, 2002a, 2003; Lam et al., 2001; So and Wang, 2003; Wang and Kwok, 2003; Huang et al., 2005; Lam et al., 2005; Guo et al., 2009; Zheng et al., 2010). To date, the highest mixing ratio of O₃ recorded to date was 203 ppbv measured in a suburb of Hong Kong (Tai O) in autumn, 2004 (Zhang et al., 2007).

Wang et al. (1998) firstly reported that four O₃ pollution episodes were observed at a non-urban coastal location in Hong Kong in 1994, and the hourly average O₃ mixing ratios exceeded 100 ppbv and in one case reached as high as 162 ppbv. They found that recirculation of urban air caused by the reversal of surface winds was an important mechanism of transporting the “aged” urban plumes to the monitoring site. Huang et al. (2005) reported that the number of O₃

episode days was 7 in 1999 and 2000, 13 in 2001, and 18 in 2002 and 2003 in Hong Kong. The synoptic patterns associated with tropical cyclones originating in the North Pacific Ocean and the South China Sea were found to be the most optimal weather conditions for the occurrence of O₃ episodes in Hong Kong.

In Hong Kong, high O₃ concentrations usually occur in autumn and reach the year-round low in summer, exhibiting strong seasonal variations (Wang et al., 1998, 2001b; Lam et al., 2001). For example, Wang et al. (1998) reported that O₃ mixing ratios reached the typical value of about 20 ppbv during 1994-95 at Cape D'Aguilar (Hok Tsui) of Hong Kong, while O₃ mixing ratios tended to be the highest in autumn with typical values of 50-60 ppbv. This unique seasonal cycle, different from those observed in North America and Europe, where a spring or spring-summer maxima is widely observed, may be attributed to the Asia monsoon circulation.

In summer, winds are generally from the south, southeast, or southwest, bringing in clean marine air to Hong Kong. Furthermore, the summer monsoon introduces unstable conditions, with clouds, boundary layer venting and heavy rainfall. These conditions are not conducive to photochemical production of O₃ and accumulation of air pollutants. However, in autumn, the northeastern monsoon can carry precursors-laden air from the Asian continent to Hong Kong. The sunny and dry weather, coupled with the subsidence of air, provides conditions favorable for photochemical O₃ formation (Chan et al., 1998b; Lam et al., 2001; Wang et al.,

2001b, 2003).

Diurnal O₃ variations can provide valuable information on the interplay of emissions, chemical and physical processes on a daily cycle (Wang et al., 2001a). The O₃ mixing ratio typically reaches a maximum value in the afternoon due to active in-situ photochemical production, and shows its minimum level at night through surface deposition and nighttime reaction with primary pollutants (Wang et al., 2001a; Cheng et al., 2009).

Despite a similar diurnal trend of O₃ mixing ratios, there are different characteristics in different locations such as rural, urban or suburban site. For example, Wang et al. (2001a) observed a broad daytime O₃ peak at a relatively remote coastal site (Cape D'Aguiar, i.e. Hok Tsui), compared to a narrower but more elevated one at the downwind suburban site (Sha Lo Wan) in Hong Kong. Furthermore, the nighttime O₃ values in Hong Kong are generally higher than those observed in the inland PRD region, which may be attributed to the constant transport of O₃ by a strong wind at night and reducing deposition of O₃ over water.

The local versus regional contributions to O₃ episodes in Hong Kong of the PRD region have been widely discussed in recent years (So and Wang, 2003; Ding et al., 2004; Huang et al., 2005; Lam et al., 2005; Zhang et al., 2007). By using the chemical species ratios such as SO₂/NO_x and CO/NO_x, So and Wang (2003) pointed out that a rural site in Hong Kong was impacted by the regional air masses from the inland PRD region, whereas an urban site was predominantly affected by

local emissions (containing higher levels of NO_x) and a suburban site was influenced by both local and regional pollution. Ding et al. (2004) reported that the high O_3 mixing ratios observed at coastal sites in Hong Kong in September 2001 were mainly due to the transport of pollution from inland PRD. Lam et al. (2005) calculated the regional transport contribution to be 60–90% of the O_3 level at urban and rural areas of Hong Kong during 18-22 August, 1999. Zhang et al. (2008) reported that 50–100% of the O_3 increase observed in Hong Kong during the O_3 episodes in 2002 can be explained by photochemical generation within the Hong Kong area based on the modeling results of an observation-based model.

2.3.4 Ozone studies in the inland PRD

Relatively few studies on ground-level O_3 pollution have been conducted in the inland PRD, compared to Hong Kong. Zhang et al. (1999) revealed that severe episodes of O_3 pollution with mixing ratios as high as 150 ppbv were observed at a rural site in Guangzhou in 1998. Since then, increasingly more measurements aimed at O_3 and its precursors have been carried out to study the characteristics of the O_3 pollution in inland PRD (Zhang et al., 1999, 2008; Shao et al., 2009; Zheng et al., 2010). Results confirmed that the inland PRD in general suffers from serious O_3 pollution, particularly in the autumn season when northerly winds and clear sky conditions prevail. For example, Zhang et al. (2008) observed the O_3 mixing ratios at an urban and a rural site (Xinken) of Guangzhou in October 2004 during the PRIDE-PRD2004 campaign. They found persistently high mixing ratios of O_3

(over 100 ppbv) in most sampling days at Xinken with the maximum hourly mean mixing ratios of O₃ up to 160 ppbv. The hourly average O₃ concentrations exceeded 200µg/m³ (i.e. China's Grade III Standard) on 76% of the sampling days. Zheng et al. (2010) demonstrated that there were 3~5 ppbv increases in 1-h average O₃ mixing ratio and 8~11 ppbv increases in 1-h maximum O₃ mixing ratio in 2007, compared to the values in 2006 in the PRD region.

2.3.5 Meteorological conditions favouring ozone pollution in the PRD region

Studies have shown that meteorological factors, such as vertical mixing, temperature, solar radiation, wind speed, wind direction and cloud cover can strongly influence the formation of O₃ and its precursors (Sillman S., 2003). It is known that a well-defined boundary layer, subsidence inversion, light winds, high temperatures and high solar radiation are favorable for the formation and accumulation of high O₃ concentrations (Colbeck and Mackenzie, 1994).

In the PRD region, the meteorological characteristics of O₃ pollution have been extensively studied (Liu and Chan, 2002; Wang and Kwok, 2003; Lam et al., 2005; Wang et al., 2005; Jiang et al., 2008; Wang et al., 2009). For example, Liu et al. (2002) found that the calm winds, delicate interaction between the synoptic forcings and the local circulations and between the different sea-breeze circulations are the dominant factors responsible for the severe O₃ episode in Hong Kong on 29 and 30 December 1999. Wang et al. (2003) observed high O₃ mixing

ratios (>120 ppbv) at a rural coastal site in western Hong Kong for six consecutive days in September of 2001, and suggested that the unusually severe and prolonged pollution episode in Hong Kong was induced by a quasi-stationary tropical cyclone in the East China Sea that caused air subsidence and stagnation over the PRD. Ding et al. (2004) simulated the continuous pollution episode using MM5 modeling in Hong Kong in September 2001 and showed that the sea–land breeze has an important impact on the transport of pollutants from urban areas on the coast. Wang et al. (2005) reported that cross-border transport did play a critical role in air-quality deterioration in the PRD region. Lam et al. (2005) revealed that the cloudless sky with high temperatures and weak wind was responsible for the formation of O_3 , which was trapped by sea-breeze circulations developed under stable atmospheric conditions by investigating an O_3 episode that occurred in Hong Kong during 18–22 August 1999. By using the regional air quality model (WRF–chem), Jiang et al. (2008) simulated that high temperature, lower relative humidity, strong solar radiation, a northerly airstream, and stable boundary layer structure were conducive to formation and maintenance of photochemical pollution during September 14–19, 2001 in Hong Kong.

2.3.6 Ozone studies in other regions in China

In addition to the studies in the PRD, O_3 pollution in other regions of China including Beijing and the Yangze River Delta has also been reported (Xu et al., 1999; Shao et al., 2006; Tie et al., 2006; Xu et al., 2006; Geng et al., 2007; Ding et

al., 2008; Xu et al., 2008). Researchers at Peking University analyzed the diurnal variations of episodic ground-level O₃ in Beijing from 1982 to 2003, and found that O₃ mixing ratios have sharply increased since 1990s. The O₃ levels often exceeded 200 ppbv (Shao et al., 2006). Tie et al. (2006) used satellite data with a global chemical transport model to characterize the chemical composition over Eastern China from January to December 2007. The results showed that the daily average O₃ mixing ratios in summer in Eastern China including Shanghai was between 40 and 50 ppbv, almost double that in winter. The sensitivity study showed that ground-level O₃ formation was VOC-limited in Eastern China. Ding et al. (2008) reported the O₃ profile over Beijing from 1995 to 2005. A comparison of the data recorded before and after 2000 revealed that ground level O₃ over Beijing had a strong positive trend (approximately 2% per year from 1995 to 2005), indicating worsening photochemical pollution in Beijing. O₃ over Beijing exhibited a common summer maximum and a winter minimum. Examination of meteorological and satellite data suggested that the tropospheric O₃ maximum in June was a result of strong photochemical production, transport of regional pollution, and possibly also more intense burnings of biomass in Central- Eastern China. Trajectory analysis indicated that in summer the regional pollution from the North China Plains, probably mixed with urban plumes from Beijing, played an important role on the high O₃ mixing ratios in the boundary layer. Xu et al. (2008) found the maximum O₃ value shows increase rates of 2.0% yr⁻¹, 2.7% yr⁻¹, 2.4%

yr^{-1} and $2.0\% \text{ yr}^{-1}$ for spring, summer, fall, and winter, respectively, based on data collected at a polluted rural site in the Yangtze River Delta in 1991–2006. The enhanced variability of surface O_3 is mainly caused by an increase of NO_x concentration or emission in the Yangtze Delta region.

2.4 NO_x in the PRD region

Nitrogen oxides ($\text{NO}_x = \text{NO}_2 + \text{NO}$) are mainly formed from combustion processes in stationary (heating, power generation) and in mobile sources (internal combustion engines in vehicles and ships) (Godish, 2003; Harrison, 2007). Nitric oxide (NO) is the key precursor of O_3 (Sillman, 2003). Nitrogen dioxide (NO_2) is an important atmospheric trace gas not only because of its health effects but also because of its critical role in determining O_3 mixing ratios in the troposphere. Annual mean NO_2 concentrations in urban areas throughout the world are generally in the range of $20\text{--}90 \mu\text{g m}^{-3}$ (Forastiere et al., 2005). Urban levels of NO_2 vary depending on the time of the day, the season of the year and meteorological factors. Typical daily patterns include a low background level of NO_2 , upon which is superimposed one or two peaks of higher levels that correspond to rush-hour traffic emissions of NO (Forastiere et al., 2005).

Several studies have reported ambient concentrations of NO_x in the PRD region (Wang et al., 2001a; Wang et al., 2003; Shao et al., 2009). Shao et al. (2009) reported that the ambient concentrations of NO_x in the inland PRD increased

quickly between 1995 and 1996, due to the rapid increase in number of motor vehicles, then slightly decreased from 1996 to 2000 due to stringent NO_x emission control in China. Chan and Yao (2008) reviewed many studies of NO_x in the PRD region and summarized that the annual average NO₂ concentration in Guangzhou was $68 \pm 6.8 \mu\text{gm}^{-3}$ followed by $64 \pm 3.4 \mu\text{gm}^{-3}$ at Tsuen Wan in Hong Kong, $54 \pm 16.2 \mu\text{gm}^{-3}$ in Shenzhen, $46 \pm 13.8 \mu\text{gm}^{-3}$ at Tung Chung in Hong Kong and $13 \pm 2.6 \mu\text{gm}^{-3}$ at Tap Mun in Hong Kong over the period 1999–2005. Large spatial variations of NO₂ in the PRD region suggest that NO₂ is mainly from the local sources. The vehicular population in Guangzhou and Shenzhen has increased by about 10% per year over the last decade. The rapid development of high-rise buildings in these two mega cities also hinders the dispersion of street-level air pollutants (Xie et al., 2003).

Temporal variations of NO_x have also been studied in the PRD region in the recent years. For example, Zheng et al. (2010) displayed the day-of-week variation in the annually-averaged NO_x concentrations. It showed that no significant differences between weekend and weekday NO_x concentrations were observed at the rural site in the northeastern PRD. But there were clear decreases in NO_x concentrations at weekends at the urban, suburban, and coastal sites in the PRD region.

For diurnal variations, Wang et al. (2001) stated that NO exhibited a typical diurnal pattern of non-urban settings at a subtropical coastal site in Hong Kong.

Near zero levels of NO were shown at night due to the titration of NO by O₃ and cessation of photolysis of NO₂ after sunset. After sunrise the median concentration of NO quickly increased to its peak value and then started to decrease at about 10:00.

NO_x also showed an obvious diurnal cycle. It displays higher concentrations in the morning (06:00-09:00) and evening (21:00), with a peak median concentration of about 3 ppbv and a daily minimum of about 1.2 ppbv in the afternoon. Zhang et al. (2008) reported that NO had two peaks at 8:00 and 21:00 in Guangzhou, which was consistent with traffic flow and implied the impact of vehicular emissions. Zheng et al. (2010) pointed out that, at the urban site in the PRD region, the sharp decrease in NO_x in the afternoon can be attributed to a decrease in traffic emissions after the morning traffic peak, strong vertical mixing and photochemical consumption of NO_x. At the rural site at Huizhou in the PRD, no significant trough in the averaged NO_x concentration was found in the afternoon. At the suburban and coastal sites in the PRD, the patterns of NO_x concentrations were intermediate between those for the urban and rural sites.

For the different source contributions to NO_x emissions, Wang et al., (2005) used a nested transport model (STEM-2K1) to analyze the current impacts of NO_x emissions from transportation, industry and power generation on Guangdong air quality. The results showed that the transportation sector is the largest source and accounts for 49.2% of the total anthropogenic emissions. The power and industrial

sectors contribute 27.8% and 20%, respectively. The influence range of the transportation sector to NO_x is large and covers most of the eastern and western Guangdong province.

2.5 Volatile organic compounds (VOCs) in Hong Kong and the inland PRD region

It is well documented that NO_x , VOCs and CO are key O_3 precursors (Cardelino and Chameides, 1995; Sillman, 1999). Nitrogen oxides ($\text{NO}_x = \text{NO}_2 + \text{NO}$) are mainly formed from combustion processes in stationary sources (heating, power generation) and in mobile sources (internal combustion engines in vehicles and ships) (Godish, 2003; Harrison, 2007). VOCs are emitted from both anthropogenic and natural sources. The main anthropogenic sources include motor vehicle emissions, consumer products, various industrial processes, biomass/biofuel combustion, fossil fuel combustion and solvent usage. The most important natural source of VOCs is vegetation. Several hundred hydrocarbons are released to the atmosphere from vegetation sources. Other natural sources include microorganisms, forest fires, animal wastes, and volcanoes (Manahan, 2001).

2.5.1 Ambient VOC levels in the PRD region

A comparison of VOC mixing ratios from various sampling sites in the PRD region is presented in [Table 2.1](#). In addition to the VOC concentration levels, other sampling details are also included.

Numerous studies have been conducted to understand the characteristics of VOCs in Hong Kong (Sin et al., 2000; Lee et al., 2002a; Ho et al., 2004; So and Wang, 2004; Guo et al., 2004a, 2006). Most results showed that toluene was the most abundant aromatic hydrocarbon in the atmosphere in Hong Kong. Sin et al. (2000) observed that the annual average mixing ratios of the measurable VOCs was well within the range of 0.20–5.0 ppbv at Tsuen Wan and Central/Western stations from July 1997 to June 1998. However, individual measurements of the toluene mixing ratio occasionally exceeded 20 ppbv. Guo et al. (2004) further reported that the benzene, toluene, ethylbenzene, and xylenes (BTEX) concentrations were similar at Tsuen Wan and Central/Western stations in 2001. The annual mean concentration of BTEX was found to fall in the range of 0.57–13.27 $\mu\text{g}/\text{m}^3$. Toluene was the most abundant VOC in all the samples, and the maximum daily value was up to 53 $\mu\text{g}/\text{m}^3$. Ho et al. (2004) reported the VOCs levels at PolyU campus (PU), Kwun Tong (KT), and Hok Tsui (HT). Toluene was the most abundant hydrocarbon, followed by benzene in both stations. The concentrations of toluene at PU ranged from 14.4 to 54.3 $\mu\text{g}/\text{m}^3$ in winter and from 11.6 to 39.2 $\mu\text{g}/\text{m}^3$ in summer. KT had the highest toluene concentration in summer with a mean value of 64.3 $\mu\text{g}/\text{m}^3$

Table 2.1 Mixing ratios of selected hydrocarbons in the PRD region

Location	^a Hok Tsui, HK ^a	^b Tai O, HK ^b	^c Central / Western, HK ^c	^c Tsuen Wan, HK ^c	^d Road sites, HKF ^d	^e 43 Chinese cities ^e	^f Guangzhou ^f	^f Dongguan ^f	^g Guangzhou ^g
Sampling periods	3 Mar to 26 Apr , 2001	Aug 2001 to Dec 2002	Jul 1997 to Jun 1998	Jul 1997 to Jun 1998	Jan and Feb, 1998	Jan / Feb, 2001	Sep, 2005	Sep, 2005	Apr, 2005
Sampling methods	Canister	Canister	Canister	Canister	Multi-sorbent tube	Canister	Canister	Canister	Canister
	mean±SD,ppbv (range)	mean±SD,ppbv (range)	mean±SD, ppbv(Cmax)	mean±SD, ppbv(Cmax)	mean±SD,ug/m ³ (Cmax)	range, ppbv	mean±SD,ppbv (range)	mean±SD,ppbv (range)	mean±SD,ppbv
Ethane	2.37±0.51 (1.2-3.39)	2.12±0.99 (0.08-2.01)				3.7-17.0	1.89±0.1 (0.89-3.47)	1.6±0.06 (0.64-2.32)	3.90±1.17
Propane	0.81±0.31 (0.16±1.43)	2.05±2.16 (0.02-12.99)				1.5-20.8	6.79±0.73 (1.3-19.8)	2.46±0.19 (0.48-8.13)	11.29±5.69
i-Butane	0.22±0.11 (0.39±0.49)	0.80±0.93 (0.01-6.05)				0.4-4.6	21.6±0.23 (0.47-6.14)	1.07±0.08 (0.19-3.36)	4.48±2.31
n-Butane	0.33±0.17 (0.05±0.75)	1.64±2.13 (0.01-12.79)				0.6-14.5	3.5±0.36 (0.76-9.77)	1.89±0.17 (0.37-6.5)	6.31±3.21
i-Pentane		0.80±1.44 (0.01-17.25)				0.3-18.8	2.47±0.28 (0.54-8.57)	1.42±0.12 (0.32-4.66)	3.81±1.93
n-Pentane	0.08±0.05 (0.02±0.24)	0.45±0.65 (ND-5.59)				0.2-7.7	1.12±0.13 (0.22-3.83)	0.7±0.1 (0.12-4.95)	1.76±0.87
n-Hexane		0.50±0.67 (ND-4.74)			15.6±15.4 (49.8)	0.1-3.2	0.84±0.92 (0.14-2.25)	0.69±0.09 (0.07-2.98)	1.24±0.59
Ethene	0.50±0.36 (0.10±2.09)	1.67±1.68 (0.03-10.53)				2.1-34.8	3.97±0.42 (0.78-11.1)	3.01±0.27 (0.65-10.7)	8.6±4.28
Propene	0.06±0.05 (0.02±0.21)	0.22±0.29 (0.01-2.18)				0.2-8.2	0.81±0.09 (0.12-2.21)	0.53±0.04 (0.11-1.31)	2.36±1.34
Ethyne	1.40±0.57 (0.42±2.78)	2.77±1.99 (0.08-11.74)				2.9-58.3	4.95±0.48 (1.71-13.4)	4.27±0.41 (1.02-16.7)	9.8±3.95
Isoprene		0.43±0.73 (ND-5.35)				0.04-1.7	1.63±0.17 (0.18-4.46)	0.68±0.12 (0.11-4.74)	0.27±0.14
a-Pinene					0.6±2.2 (12.9)		0.14±0.02 (0.01-0.62)	0.13±0.02 (0.02-0.52)	
Benzene	0.49±0.24 (0.17-1.15)	0.87±0.92 (0.02-10.32)	0.79±0.47 (2.3)	0.90±0.44 (2.2)	26.7±33.0 (128.6)	0.7-10.4	2.05±0.24 (0.65-6.8)	1.26±0.14 (0.27-6.45)	2.75±1.19
Toluene	0.54±0.48 (0.11-1.78)	5.67±7.13 (0.01-48.98)	4.5±3.1 (20)	5.0±2.3 (16)	77.2±74.4 (320.0)	0.4-11.2	5.87±0.74 (0.71-19.6)	6.13±0.81 (0.53-25.3)	10.02±4.69
Ethylbenzene	0.06±0.05 (0.01-0.26)	0.87±1.23 (ND-8.12)	0.45±0.32 (0.93)	0.56±0.42 (2.1)	3.1±6.7 (36.5)	0.1-2.7	1.24±0.17 (0.14-4.6)	1.06±0.17 (0.06-7.45)	1.91±1.04
m/p-Xylene		0.96±1.86 (ND-1.46)	0.91±0.67 (2.5)	0.97±0.562.3 ()	12.1±19.4 (106.0)	0.4-15.3	1.53±0.19 (0.25-4.9)	1.47±0.16 (0.11-6.95)	3.03±1.69

^aWang *et al.*, 2003; ^bGuo *et al.*, 2006 ; ^cSin *et al.*, 2000; ^dChan *et al.*,2002; ^eBarletta *et al.*,2005; ^fBarletta *et al.*, 2008 ; ^g Tang *et al.*, 2007

Guo et al. (2006) observed large variations in the measured non-methane volatile organic compounds (NMVOCs) at a polluted rural/coastal site (Tai O) from August 2001 to December 2002. The total average NMVOC mixing ratio was 25.5 ppbv, in which alkanes accounted for 40%, alkenes 10%, alkynes 11%, aromatics 35% and measured halocarbons (C_2Cl_4 and CH_3Cl) 4%. The most abundantly measured 10 compounds were toluene, ethyne, ethane, propane, ethene, *n*-butane, CH_3Cl , ethylbenzene, benzene and *i*-pentane. These 10 NMHCs accounted for 76% of the total NMVOCs. In particular, toluene alone accounted for 22% of the total NMVOCs.

In other areas of the PRD region, especially Guangzhou, many studies have been carried out in recent years (Wang et al., 2002b, 2008; Chan et al., 2003; Barletta et al., 2005; Chan et al., 2006b; Tang et al., 2007; Barletta et al., 2008a; Liu et al., 2008b; Tang et al., 2008). Chan et al. (2006) performed a VOC study in industrial (T1), industrial-urban (T2), and industrial-suburban (T3) atmospheres of the PRD region in late summer 2000. The sampling sites were throughout Dongguan, Foshan, Guangzhou, Jiangmen, and Zhongshan. Toluene was the most abundant NMHC quantified (T1: 13.5 ± 11.8 ppbv; T2: 11.5 ± 11.6 ppbv; T3: 7.3 ± 5.4 ppbv). Ethane, ethene, ethyne, propane, *n*-butane, *i*-pentane, benzene, and *m*-xylene were the next most abundant VOCs. Tang et al. (2007) reported that toluene, ethyne, propane, and ethene were the most abundant hydrocarbons in Guangzhou (urban site), Panyu (suburban site), and Dinghu mountain (rural site) in April, 2005. For the roadside samples, Guangzhou had

much higher level of propane and butanes, while Qingxi Township, Dongguan, had much higher levels of aromatic hydrocarbons. Barletta et al. (2008) measured NMHCs mixing ratios in Guangzhou and Dongguan in September, 2005. Propane was the most abundant species in Guangzhou, with an average mixing ratio of 6.8 ± 0.7 ppbv, compared to 2.5 ± 0.2 ppbv in Dongguan. In contrast, toluene was the most abundant hydrocarbon in Dongguan (6.1 ± 0.8 ppbv), compared to the value (5.9 ± 0.7 ppbv) in Guangzhou.

When comparing the levels of VOCs in the PRD region with those in other areas around the world, it was found that NMHCs levels in Hong Kong were generally lower or comparable to those of other overseas cities. Guo et al. (2004) reported that the average concentrations of most alkanes and alkenes in Hong Kong in 2001 were generally close to those measured in Europe (Derwent et al., 2000; Borbon et al., 2002), but much lower than those found in Asia and South America (Grosjean et al., 1998b; Morikawa et al., 1998; Barletta et al., 2002). For example, the mean propane concentrations in Mexico City, Santiago, Porto Alegre and Karachi were 10.4, 270.1, 99.4, 80.5 $\mu\text{g}/\text{m}^3$, respectively. In Guo's study, the propane concentration was only 4.21 $\mu\text{g}/\text{m}^3$, which was 20–79 times lower. Tang et al. (2007) concluded that toluene (10.0 ppbv) and *i*-butane (4.5 ppbv) in Guangzhou were at the upper end of the ranges (0.4–11.2 ppbv and 0.4–4.6 ppbv, respectively) in 43 Chinese cities study (Barletta et al., 2005). Mixing ratios of propane, toluene, ethyne, ethene and *i*-butane were higher in Guangzhou than those found in most other Asian cities (So and Wang, 2004;

Chang et al., 2005; Sahu and Lal, 2006), except for Taipei, Taiwan (Wu et al., 2006), and Karachi, Pakistan (Barletta et al., 2002), where the levels of those VOC species were much higher.

2.5.2 Temporal variations of VOCs in the PRD region

Many studies investigated the seasonal and diurnal variations of VOCs in the PRD region, which are controlled by a combination of emission factors, dispersion conditions and chemical mechanisms. The total NMHC levels at urban sites in Hong Kong generally varied with seasons, with high levels in winter and low values in summer (Lee et al., 2002a; Ho et al., 2004; So and Wang, 2004; Guo et al., 2007; Tang et al., 2007; Wang et al., 2008). The higher winter values may be due to the contributions of weaker vertical mixing, slower photochemical reaction, and emissions from the inland PRD under the influence of Asian monsoon system, which brings in highly polluted air masses from the mainland to the sampling sites in winter. While in summer, the Asian monsoon brings in clean oceanic air from the tropics and unstable rainy weather. The rainy weather in the summertime causes a washout effect of pollutants, thus accumulation of VOCs was less than those in the dry winter. In contrast to the urban sites, So and Wang (2004) reported that the roadside site had the highest levels of total NMHCs and alkanes in summer. In particular, compounds such as butane, isobutane and isopentane, mainly emitted from vehicle exhausts, the evaporation of gasoline, and from leaks of liquefied petroleum gas (LPG), all

showed the highest levels at the roadside in summer and the lowest concentrations in winter. As the roadside site was situated near a heavy traffic road and surrounded by tall buildings, the NMHC concentrations at this site were thus dominated by the strength of vehicular emissions and were less affected by the changes in regional-scale air flow patterns, as compared to other sites. The high temperatures in summer could enhance the evaporation of fuel, contributing to a higher level of butane, isobutane, isopentane, and other NMHCs, similar to observations of elevated summertime concentrations of typical fuel components such as butanes and pentanes.

For the diurnal variations of NMHCs, Tang et al. (2007) performed a study on diurnal variation of NMHCs in the PRD in 2005. The measurements revealed that the diurnal patterns of the hydrocarbons differed at different sampling locations. High levels were observed in the morning and evening for most hydrocarbons and total NMHCs in Guangzhou. The two-peak pattern indicates that the major sources of these hydrocarbons were traffic emissions. Wang et al. (2008) reported that the evening concentration peaks of NMHCs in Guangzhou were due to the strong traffic emissions. The late night or early morning peaks of NMHCs in Xinken (suburban) were thought to be the result of advection of plumes from upwind more urbanized.

2.5.3 Source apportionment of VOCs in the PRD region

Several studies on the source apportionments of NMVOCs have been

conducted in Hong Kong (Guo et al., 2004b; Guo et al., 2006; Guo et al., 2007). By using a principal component analysis/absolute principal component scores (PCA/APCS) receptor model, Guo et al. (2004b) indicated that 39% and 48% of the total NMHCs mass concentrations measured at Tsuen Wan and Central & Western originated from vehicle emissions, respectively. 32% and 36.4% of the total NMHCs were emitted from the use of solvent, and 11% and 19.4% were apportioned to the LPG or natural gas leakage, respectively. 5.2% and 9% of the total NMHCs mass concentration were attributed to other industrial, commercial and domestic sources, respectively. Guo et al. (2006) also showed that the regional and local source contributions to ambient NMVOC levels at a polluted rural/coastal site (Tai O) were significantly different due to the differences in local versus regional energy use and industrial activities. For air masses originating in HK, vehicular emissions accounted for approximately 39% of the total NMVOC levels, followed by industrial emissions (35%), gasoline evaporation (14%) and commercial/domestic liquefied petroleum gas/natural gas use (12%). By contrast, for air masses originating from the PRD, the industrial emissions accounted for 43% of the total NMVOC burden, followed by vehicular emissions (32%) and biomass burning (25%).

In the inland PRD, Barletta et al. (2008) reported that vehicular emission appears to be the dominant source of NMHCs measured in Guangzhou, while industrial emissions give a significant contribution to the ambient VOC levels in Dongguan. Liu et al. (2008) performed one source apportionment study by using

a chemical mass balance receptor model in the PRD region in the fall of 2004. The results showed that vehicle exhaust was the largest source of VOCs, contributing to > 50% of ambient VOCs at the three urban sites (Guangzhou, Foshan, and Zhongshan). LPG leakage played an important role, representing 8–16% of emissions at most sites in the PRD. Solvent usage was the biggest emitter of VOCs in Dongguan,(industrial site), contributing 33% of ambient VOCs. Similarly, at Xinken, a non-urban site, the evaporation of solvents and coatings was the largest emission source, accounting for 31% of emissions, probably because it was downwind of Dongguan. Local biomass combustion was a noticeable source of VOCs at Xinken, accounting for 14.3% of emissions.

2.6 Contributions of VOCs to ozone formation

2.6.1 Methodology development in assessing VOC contribution to ozone formation

Photochemical reactions of VOCs are mainly initiated by the OH radical, and the mechanism for each VOC species involved in O₃ formation varies greatly. To assess the reactivity and the contribution to photochemical O₃ formation of individual VOC, a propylene-equivalent concentration method proposed by Chameides et al. (1992) and a maximum incremental reactivity (MIR) method proposed by Carter (1994) are widely used. The calculation of the propylene-equivalent concentration for individual VOC uses the following equation:

$$\text{Propy-equiv}(i) = \text{conc}(i) \times k_{\text{OH}}(i) / k_{\text{OH}}(\text{C}_3\text{H}_6) \quad (2.11)$$

where $\text{propy-equiv}(i)$ is a measure of species i on an OH reactivity-based scale, normalized to the reactivity of propylene, $k_{\text{OH}}(i)$ is the rate constant between species i and OH radical (Atkinson, 1990), and $k_{\text{OH}}(\text{C}_3\text{H}_6)$ is the rate constant between C_3H_6 and OH radical.

MIR is the amount (grams) of O_3 formed per gram of VOC. It is a good indicator for comparing O_3 formation potential (OFP) of individual VOC. The following equation can be used to calculate the contribution to O_3 formation by each VOC under optimal conditions:

$$\text{O}_3 \text{ formation potential } (i) = \text{concentration } (i) \times \text{MIR coefficient } (i) \quad (2.12)$$

MIR coefficients can be found in Carter (1994).

It should be noted that the MIR method is based on a scenario in which O_3 formation is derived under optimum conditions, such as high actinic flux and a scenario with NMHC/ NO_x ratios, which yield a maximum O_3 formation, whereas the propylene-equivalent concentration method simplifies the estimation by solely taking into account the OH reaction rate coefficients and concentrations of a NMHC. However, there is no unique relationship between the competitive reaction rates of a set of organic compounds with hydroxyl radicals and their ability to produce O_3 in atmosphere because the latter depends on the subsequent reaction mechanisms of the products of the OH radical attack. Both methods are used to assess the OFPs simply by summing up the products of measured NMHC amounts and their corresponding MIR and k_{OH} factors, neither of which

considers actual meteorology and transport influence. The OFPs and reactivities assessed by these two methods are not meant to represent actual O₃ concentrations in that area, because it will also be affected by meteorology and transport factors. Nevertheless, these two methods can still be applied as a useful reference of VOC's reactivity under some restricted conditions to identify species with high reactivities (Carter, 1994; Derwent et al., 1998; Chang et al., 2005).

Besides the above two methods widely used to assess the relative contribution of each VOC species to photochemical O₃ formation, the concept of photochemical O₃ creation potential (POCP) is also used, which is developed by Derwent and co-workers to investigate regional scale O₃ formation over periods of up to five days in northwest Europe (e.g. Derwent and Jenkin, 1991; Derwent et al., 1996, 1998). (on a mass basis) of a reference VOC, which is taken to be ethene (Saunders et al., 2003). The POCP for the given VOC '*i*' is defined by Eq. (2.13),

$$\text{POCP}_i = \frac{\text{ozone increment with the } i\text{th VOC}}{\text{ozone increment with the ethene}} \times 100 \quad (2.13)$$

POCPs are available in the literature from earlier studies in Europe by using different versions of MCM (Derwent and Jenkin, 1991; Carter, 1994; Derwent et al., 1996, 2003, 2007a). For example, Derwent et al. (1996) reported that aromatic and olefinic hydrocarbons showed the highest POCP values with halocarbons the lowest by using the POCP index. Among all VOC species, toluene, *n*-butane, ethylene and the xylenes, alone, account for over one third of

the O₃ forming potential of European emissions. When we compared the relative O₃ formation potentials for VOCs as defined by the POCP scale with those predicted by the Maximum Incremental Reactivity (MIR) approach (Carter, 1994), There is a reasonable correlation between POCP and MIR values, which both tend to give similar predictions with regard to the relative importance of different classes of VOC. The MIR scale considers O₃ formation over a much shorter timescale, and therefore places more emphasis on those VOCs which are oxidised rapidly, whereas the POCP approach gives greater resolution to those VOCs of somewhat lower reactivity (Derwent and Jenkin, 1991).

2.6.2 VOC contribution to ozone formation in the PRD region

Studies on the relative contributions of VOCs to photochemical O₃ formation have been carried out around the world using the above mentioned two methods (Grosjean et al., 1998a; Barletta et al., 2002; Guo et al., 2004a; Ho et al., 2004; Chang et al., 2005; Tang et al., 2007). For example, Chang et al. (2005) revealed that toluene, xylene, ethene, and propene had the highest OFP and reactivities in southern Taiwan, and larger benefit margin of O₃ abatement may be obtained by reducing emissions of a group of key species with high OFPs. Guo et al. (2004) concluded that the largest contributors to O₃ formation in Hong Kong, in order of decreasing MIR scale, were formaldehyde, toluene, propene, *m,p*-xylene, acetaldehyde, 1-butene/*i*-butene, isoprene and *n*-butane, suggesting that motor vehicles, gasoline evaporation, use of solvents, leakage of LPG, photochemical

processes and biogenic emissions are sources in the production of O₃. Reaction with OH was dominated by 1-butene/ibutene, followed by formaldehyde, isoprene, propene, toluene, acetaldehyde, *m,p*-xylene and trans-2-butene. Of which, four were alkenes, two aromatics and two aldehydes. Apart from isoprene, the other VOCs were mainly emitted from vehicle exhaust and toluene was also evaporated from gasoline in summer. Therefore, VOCs from vehicles and gasoline evaporation are predominant with respect to reactions with OH radical. So and Wang (2004) demonstrated that isoprene had the highest OH-reactivity and O₃ formation potential at a rural site in Hong Kong, while toluene was the most important contributor to the two parameters at a roadside site. Tang et al. (2007) reported that alkenes and aromatics were the NMHC species highly related to O₃ formation, and hydrocarbons from vehicular emissions and industrial emissions played a dominant role in O₃ pollution in the PRD region. However, it was found that at a remote site (Jianfeng Mountain in Hainan Island) biogenic emission (isoprene) was the major contributor to the O₃ formation. Zheng et al. (2009) reported that the top 10 species, in terms of ozone formation potentials, consisted of isoprene, *m,p*-xylene, toluene, ethylene, propene, *o*-xylene, 1,2,4-trimethylbenzene, 2-methyl-2-butene, 1-butene, and α -pinene. These species contributed only 35.9% to VOCs emissions but accounted for 64.1% of the OFP in the PRD region.

In summary, many studies on the ground-level O₃ and its precursors, *i.e.* NO_x and VOCs have been carried out in Hong Kong and the inland PRD region. The

available data highlight a current situation of severe O₃ pollution in the PRD region. The concentrations of ground-level O₃ in Hong Kong and the inland PRD region generally showed an increasing trend during the last two decades. O₃ pollution episodes, with maximum concentrations >100 ppb, were frequently observed in recent years in the region. Therefore, it is of critical need for a better understanding of the sources of O₃ precursors and O₃ formation mechanisms in the region.

It is evident that the ground-level O₃ concentrations at background sites of Hong Kong might be significantly affected by input of air pollutants from inland PRD region. And the concentrations, generally higher in the inland PRD cities, and source profiles of VOCs, the most important precursors to O₃ formation, displayed significant difference between Hong Kong and the inland PRD cities. Therefore, more efforts and approaches are needed to explore the relationship of air pollution between Hong Kong and the inland PRD. In particular, great attention should be paid to the atmospheric transport from the inland PRD to Hong Kong.

Numeric models are essential tools to meet the above mentioned research needs.

2.7 Model simulation of ozone formation in the atmosphere

Air quality simulation (AQS) models are essential tools for the development of effective strategies to control O₃ pollution in the troposphere. Various

numerical models are available nowadays to simulate O₃ pollution in the atmosphere from the level of box models like observation-based model (OBM), and photochemical trajectory model (PTM) to three-dimensional chemistry and transport models such as the Weather Research and Forecasting-Chemistry mode (WRF-Chem), and the U.S. Environmental Protection Agency's Community Multi-scale Air Quality (CMAQ). One of the most important components in the AQS models is the chemical mechanisms that describe the formation of O₃ from VOCs and NO_x. The chemical mechanisms used in the WRF-chem include CBMZ, CBM4, RACM, and RADM2. The chemical mechanisms used in the CMAQ include CBM4, CB05, and SAPRC-99. All the chemical mechanisms mentioned above are condensed mechanisms. For example, in the carbon-bond mechanism, each volatile organic compound is segregated into one or more bond groups that have similar chemical reactivity (Gery et al., 1989). With surrogate species mechanisms (e.g. SAPRC-99), all VOCs of similar reactivity are grouped together. The rate coefficient of each compound is then set to equal to that of one particular compound (Carter, 1990; Dodge, 2000). In lumped species mechanisms (e.g. RACM), VOCs are grouped by their reactivity with the OH radical. The rate coefficient is determined by taking the mole fraction weighted average of the reaction coefficient of each compound of the lumped group (Stockwell et al., 1990). The condensed chemical mechanisms use parameterizations to describe the general features of O₃ formation, and their sensitivity to emission controls. Hence, it cannot provide information on the roles

of individual VOCs in the formation of O₃ and other secondary oxidants and aerosols. Therefore, other approaches have been developed to describe the complex photochemistry of VOCs as explicitly as possible, leading to a vast number of VOC species and chemical reactions taken into account. A good example is the Master Chemical Mechanism (MCM). The widely used MCM is a near-explicit chemical mechanism describing the detailed degradation of a large number of emitted organic compounds and the resulting generation of O₃ and other secondary pollutants under conditions appropriate to the atmospheric boundary layer (Jenkin et al., 1997). The newly updated MCM v3.1 describes the oxidation of 135 VOCs, which contains around 13,500 reactions involving 5,900 chemical species (<http://mcm.leeds.ac.uk/MCM/home.htm>)

The chemical mechanisms used in the observation-based model and the photochemical trajectory model are CB-VI mechanism and MCM, respectively. Since this study will mainly focus on these two models and mechanisms, a detailed description will be provided in Chapter 3.

2.7.1 Model simulation on the relationship between O₃ and its precursors

Although VOCs and NO_x have been identified as the two key precursors to photochemical O₃ formation, the relationship between O₃ and its precursors is complicated. The VOCs - NO_x chemistry in models is affected by five main factors: the VOC/NO_x ratio; the reactivity of the VOC species; the role of

biogenic hydrocarbons; the extent of photochemical aging; and the severity of the air pollution (Sillman, 1999). For example, the rate of O_3 production ($ppb\ h^{-1}$) as a function of NO_x and VOC concentrations is shown in [Figure 2.1](#) (Sillman, 1999). The isopleth plot shows that the rate of O_3 formation is a nonlinear function of VOC and NO_x concentrations in the atmosphere, depending on the relative concentrations of VOCs and NO_x . When VOC levels are relatively high and NO_x levels are relatively low, the isopleths are oriented horizontally indicating that O_3 production is NO_x -limited and reductions in VOCs have little or no effect on O_3 concentration. Whilst when VOC levels are low and NO_x levels are high, the isopleths are vertical, indicating that O_3 production is VOCs-limited. So the ratio of VOCs to NO_x is an important parameter to evaluate whether the production of O_3 is controlled by NO_x or VOCs: high VOC/ NO_x ratios corresponding to NO_x -limited and low VOC/ NO_x ratios corresponding to VOC-limited. The isopleth plot (Fig. 2.1) illustrates many important features of O_3 - NO_x -VOCs sensitivity but it does not provide a complete understanding of the relationships between O_3 and its precursors (i.e. NO_x or VOCs). In addition to the isopleth plot, the most important feature is the pattern of evolution of an air mass as it moves downwind from emission sources. Typically freshly emitted pollutants are characterized by VOC-sensitive chemistry and evolve towards NO_x -sensitive chemistry as the air mass ages. Cardelino et al. (1992) pointed out that if the 6-9 am VOC/ NO_x ratio in a city centre is less than 10, the O_3 production is VOC-limited, and a

hydrocarbon-based strategy will most effectively reduce O_3 in the urban area. On the other hand, if the ratio is greater than 10, a NO_x - limitation is indicated, and a NO_x -based strategy is needed.

These studies lead into many other modeling works that has been used to assess O_3 precursor sensitivity at different geographic locations. A detailed description is beyond the scope of this thesis. However, as this project is utilizing both OBM and MCM model frameworks, an overview of other applications of these is provided in sections 2.7.2 and 2.7.3 below.

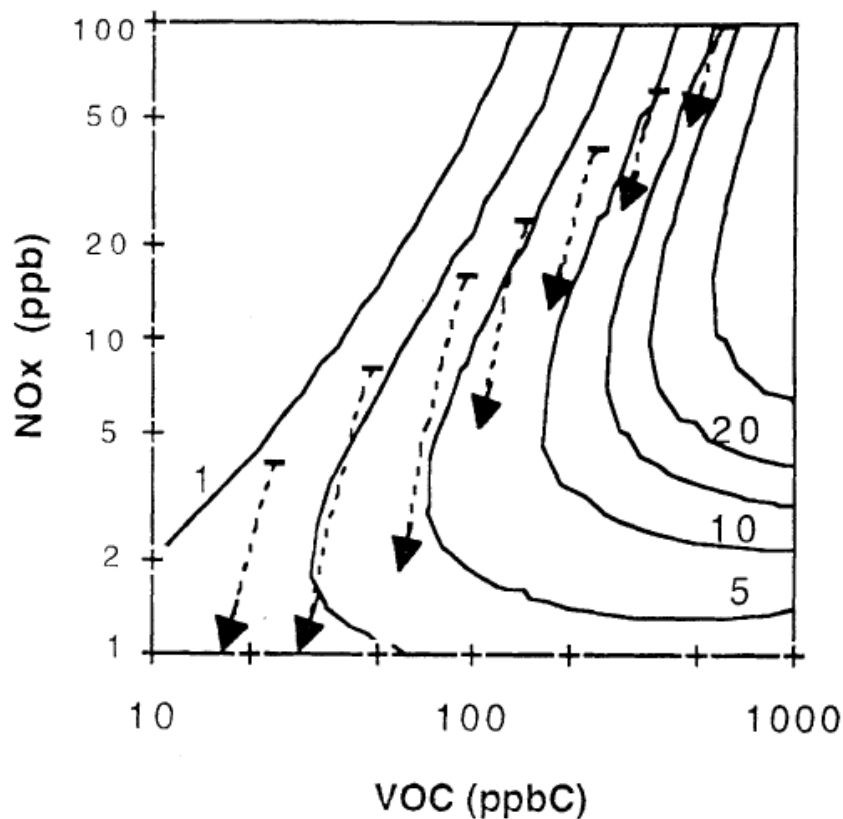


Fig. 2.1. Isopleths giving net rate of O_3 production (ppb/h, solid lines) as a function of VOCs (ppbC) and NO_x (ppb) for mean summer daytime meteorology and clear skies. The solid lines represent production rates of 1, 2.5, 5, 10, 15, 20 and 30 ppb/h. The dashed lines and arrows show the calculated evolution of VOC and NO_x concentrations in a series of air parcels over an 8 h period (9 am-5 pm), each with initial $VOC/NO_x=6$ and speciation typical of urban centers in the US, based on calculated shown in Milford et al. (1994)

2.7.2 Studies undertaken using the observation-based model

The observation-based model (OBM) developed by Cardelino and Chameides (1995) was applied to evaluate the sensitivity of photochemical O₃ production to changes in the concentrations of the precursor compounds in a given area. Briefly, the OBM uses measurements of ambient concentrations of O₃ and its precursors like NO, CO and VOCs along with an algorithm for simulating the photochemical O₃ production and destruction. The major goal of the model is to assess the sensitivity of net O₃ production in an area to changes in the emissions of NO, CO as well as individual and various groups of VOCs without the use of emission inventories and simulation of boundary layer dynamics as in emission-based model (Cardelino and Chameides, 1995, 2000). However, the OBM adopts a number of simplified assumptions. One critical assumption is the neglecting of horizontal transport in solving for the concentrations of the unspecified species. Another assumption is that an O₃ precursor is reduced by a certain amount in the OBM. The critical parameter is the change in O₃ production that occurs between the two cases. The difficulty arises because there are no real-world situations that represent the second case: an O₃ episode in which an O₃ precursor is reduced by a certain amount while all other conditions remain unchanged (Cardelino and Chameides, 1995).

Several studies have been carried out using the OBM (Cardelino and Chameides, 1995, 2000; Shiu et al., 2007; Zhang et al., 2007; Zhang et al., 2008). Cardelino and Chameides (1995) firstly developed the OBM and applied it to the

1990 Atlanta O₃ study data to analyze O₃-precursor relationship. The results suggested that the Atlanta metropolitan area was more sensitive to the reduction of NO_x emissions than to the reduction of anthropogenic hydrocarbon emissions, and a reduction in mobile source emissions would be about twice as effective in reducing O₃ production as a reduction in stationary sources. Further to the above model simulation, Cardelino and Chameides (2000) used OBM to analyze data gathered during the summer of 1995 at three photochemical assessment monitoring sites (i.e. Washington DC, Bronx of New York, and Houston of Texas). The results indicated that natural hydrocarbons (primarily isoprene) represented a significant fraction of the total hydrocarbon reactivity at all three sites and significantly degraded the efficacy of VOC emission reductions as an O₃ mitigation strategy. Shiu et al. (2007) studied photochemical O₃ production in southern Taiwan recently and found that reducing emissions of non-methane hydrocarbons is more effective in controlling O₃ than reducing NO_x. By analyzing some high O₃ episode cases, Zhang et al. (2007) found that the formation of O₃ throughout Hong Kong was limited by VOCs, and high NO concentrations suppressed O₃ production. The reactivity of VOCs was dominated by anthropogenic VOCs, with VOCs from natural or biogenic sources making a minor contribution during autumn in Hong Kong. Of the anthropogenic VOCs, reactive aromatics dominated, of which xylenes and toluene were the most important species. Zhang et al. (2008) demonstrated that total oxidant was of regional scale covering at least the entire PRD. Its relationship with O₃

precursors was highly non-linear. Photochemical production of O₃ was sensitive to VOCs at both the Guangzhou urban site and Xinken downwind rural site.

In the OBM, observed concentrations rather than emission inventories are used to drive the photochemical simulations, and thereby ensure that the calculations are carried out for the proper ratios of NO_x and VOCs. Another big advantage by using the OBM is that the OBM is relative easy and inexpensive to operate. It can be used to analyze a wide array of O₃ episodes and, thus, could prove to be a relatively cost-effective tool for the analysis of O₃-precursor relationships in a given area.

2.7.3 Studies undertaken using the photochemical trajectory model

One of the major functions of the PTM is to determine the relative contribution of each VOC to O₃ formation. The chemical mechanism used in the PTM is the master chemical mechanism (MCM), which is more fundamentally linked to elementary studies of atmospheric chemical reactions. Hence, the PTM allows a more detailed examination of the chemistry and the roles played by individual VOCs in generating O₃ and related secondary pollutants.

The relative contribution of each VOC to photochemical formation of O₃ and other secondary oxidants has been widely simulated in Europe (Derwent et al., 1996, 1998, 2007a; Utembe et al., 2005; Evtugina et al., 2007; Harrison, 2007; Pinho et al., 2009; Walker et al., 2009). Derwent et al. (1996) described the O₃

production from the oxidation of methane and 95 other VOCs in air parcels advected across north-west Europe. They found that aromatic and olefinic hydrocarbons had the highest potential to O₃ formation while halocarbons had the lowest. Evtyugina et al. (2007) simulated the formation of photochemical pollutants in air masses during the sea breeze circulation on Portugal's West Coast in 2001. The simulated concentrations of O₃, HCHO, and isoprene were in good agreement with observed data.

Derwent et al. (2007a) studied the contributions of 248 VOC emission source categories to photochemical O₃ formation. The results indicated that 'road transport—exhaust' was the biggest contributor to O₃ formation, followed by 'solvent and other product usage' sectors and 'extraction and distribution of fossil fuel' sector. The consequences of the large range in POCP values were highlighted for cost-effective VOC emission control strategies across north-west Europe.

Walker et al. (2009) used the PTM to simulate pollutant levels during summertime in Birmingham, UK in 1999. O₃ was well simulated by the PTM with a reasonably good correlation, and about 90% of the modelled afternoon and evening O₃ concentrations were within a factor of two of the measurements. The contribution of local biogenic emissions in the West Midlands to O₃ formation during this period was also assessed and found to be of minor importance.

In view of the more and more application of the OBM and PTM in the world,

the result from the application of the two models has been proved to be useful in developing effective O₃ control strategies. The OBM can be used to identify whether reducing emissions of NO_x or emissions of VOCs would be more effective in decreasing O₃ concentrations. However, The OBM results are based on the observed data in a given site, the result will be relatively site-specific. The PTM using detailed emissions inventories and master chemical mechanism is a regional model, which can be used to identify key VOC species and emission source categories contributing to O₃ formation in the PRD region. Hence, we can investigate the impacts of speciated VOCs on O₃ pollution by utilizing the diagnostic (OBM) and prognostic (MCM) models. The results of the two models can also be compared and validated

In the next chapter, we will describe the methodology used in this study, the detailed description of the OBM and PTM will be included in this part.

Chapter 3

Methodology

3.1 Sampling sites

Field measurements were carried out at two sites, namely Wan Qing Sha (WQS) in Guangzhou, and Tung Chung (TC) in Hong Kong, from 22 October to 1 December, 2007 (Fig. 3.1). The distance between the two sites is about 62 km. WQS (22°43'N, 113°33'E, 2m a.s.l.) is a small town located near the center of the Pearl River Delta (PRD). This small town is surrounded by farmlands and has very few textile and clothing workshops, so the local anthropogenic emissions are not remarkable. The major air pollutants are mainly from the surrounding cities. This site is 50 km to the southeast of the Guangzhou urban center, 40 km southwest of Dongguan, 50 km northwest of Shenzhen, and 25 km northeast of Zhongshan, which is at the geographical centre of the PRD region and downwind of the inland PRD in autumn/winter. The measurement data therefore represents the regional pollution in the inland PRD region. Conversely, since WQS is at the northernmost boundary of the Pearl Estuary and to the northwest of Hong Kong, it is an appropriate site to investigate the influence of the inland PRD region on Hong Kong when northerly wind is prevalent. The measurements were carried out on the rooftop of a 15m high building.

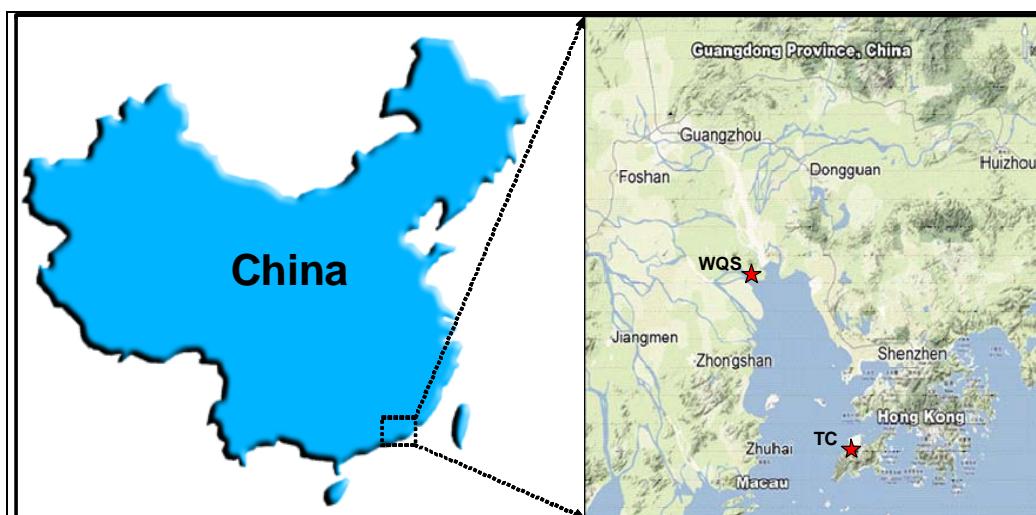


Fig.3.1. Location of the two sampling sites (Tung Chung (TC), Hong Kong and Wan Qing Sha (WQS), Guangzhou)

Tung Chung ($22^{\circ}18'N$, $113^{\circ}56'E$, 5m a.s.l.) is a residential site located on northern Lantau Island, about 3 km south of the Hong Kong International airport at Chek Lap Kok. It is a newly-developed residential town, but adjacent to the highway and to railway lines. It is about 20 km to the southwest of Hong Kong urban center, and 38 km northeast of Macau. In addition to the influence of local emission sources, TC is also affected by polluted continental air masses from the highly industrialized PRD region of mainland China. Thus, this site is capable of monitoring air pollutants transported from the inland PRD region and is suitable for assessing their impact on local air quality. The samples were collected on the rooftop of a building with a height of 15 m.

3.2 Meteorological condition

The PRD region ($21^{\circ}17'-23^{\circ}56'N$, $111^{\circ}59'-115^{\circ}25'E$) is situated on the coast of South China with a total area of $41,700 \text{ km}^2$. The climate in the PRD region is

dominated by the Asian monsoons. One year can be divided into two distinct seasons - wet season and dry season - with the alternation of summer monsoon and winter monsoon. The wet season lasts from around April to October when the summer monsoon is prevailing, including spring and summer seasons. The prevailing wind is from the southeast, south and southwest. It is hot, humid and rainy, with about 90% of the rain falling. The dry season lasts from late October to March when the Asian winter monsoon is dominant, including autumn, winter and early spring. The prevailing wind is from the northeast and north.

3.3 Measurement techniques

3.3.1 Continuous measurements of O₃, CO, SO₂ and NO_x

At TC, O₃, CO, SO₂, NO-NO₂-NO_x and meteorological parameters were measured at a monitoring station operated by the Hong Kong Environmental Protection Department (HKEPD). This station used similar instruments and quality assurance and control protocols to those in the US air-quality monitoring program (<http://epic.epd.gov.hk/ca/uid/airdata>). At WQS, measurement instruments were installed in a room of the building, beneath the rooftop. Ambient air samples were drawn through a 5m long perfluoroalkoxy (PFA) Teflon tube (OD: 12.7 mm; ID: 9.6 mm). The inlet of the sampling tube was located 2 m above the rooftop of the building. The other end of the sampling tube was connected to a PFA manifold with a bypass pump drawing air at a rate of 15 L min⁻¹. The intake of the analyzers for O₃, CO, SO₂ and NO-NO₂-NO_x was

connected to the manifold.

A detailed description of the in-situ measurements of O₃, CO, SO₂, and NO-NO₂-NO_x is given below:

O₃ was measured using a commercial UV photometric instrument (Thermo Environmental Instruments (TEI), model 49C) that had a detection limit of 2 ppbv and a 2-sigma (2-σ) precision of 2 ppbv for a 2-min average. The analyzer was calibrated by a transfer standard (TEI 49PS) prior to the filed studies.

SO₂ was measured by a pulsed UV fluorescence (TEI, model 43S), with a detection limit of 0.06 ppbv and 2-σ precision of 3% for ambient levels of 10 ppbv (2-min average). The uncertainty was estimated to be ~9%. This estimate, however, does not include the possible additional errors caused by the loss of SO₂ in the unheated sampling line and by the interference of atmospheric water vapor.

CO was measured with a gas filter correlation, nondispersive infrared analyzer (Advanced Pollution Instrumentation, Inc., Model 300) with a heated catalytic scrubber (as purchased) to convert CO to carbon dioxide (CO₂) for baseline determination. Zeroing was conducted every 2 h, each lasting 12 min. The 2-min data at the end of each zeroing were taken as the baseline. The detection limit was 30 ppbv for a 2-min average. The 2s precision was about 1% for a level of 500 ppbv (2- min average) and the overall uncertainty was estimated to be 10%.

NO and NO_x were detected with a chemiluminescence NO-NO₂-NO_x

analyzer (Thermo Electron Corporation, Model 42*i* trace level). The analyzer had a detection limit of 0.05 ppbv. the Model 42*i*-TL measures the amount of nitrogen oxides in the air from sub-ppb levels up to 1000 ppb. The Model 42*i*-TL is a single chamber, single photomultiplier tube design that cycles between the NO, NO_x, and zero modes. The addition of the zero mode provides excellent long term stability and extremely low minimum detectable limits.

These analyzers were calibrated daily by injecting scrubbed ambient air (TEI, Model 111) and a span gas mixture. A NIST-traceable standard (Scott-Marrin, Inc.) containing 156.5 ppmv CO ($\pm 2\%$), 15.64 ppmv SO₂ ($\pm 2\%$), and 15.55 ppmv NO ($\pm 2\%$) was diluted using a dynamic calibrator (EnviroNics, Inc., Model 6100). For the O₃, SO₂, NO and NO_x analyzers, a data logger (Environmental Systems Corporation, Model 8816) was used to control the calibrations and to collect data, which were averaged to 1-min values.

In addition to the above chemical measurements, several meteorological parameters were monitored by an integrated sensor suite (Vantage Pro TM & Vantage Pro 2 Plus TM Weather Stations, Davis Instruments). The weather station has two components: The sleekly designed integrated sensor suite, also known as the ISS, and the data-receiving console. The ISS collects weather data such as outdoor temperature, solar radiation, relative humidity, wind speed and direction, and wirelessly transmits its data to the console, which displays the data. To make viewing the data easier, the console is designed with an easy-to-read, 3" x 4 3/8" (7.6 cm x 8.5 cm) screen and a glow-in-the-dark keypad for night

viewing.

3.3.2 Sampling and analysis of carbonyls

Carbonyl samples were collected simultaneously at both sites on the selected days (i.e., 26–27 Oct., 13 Nov., 15–17 Nov., 23 Nov., and 1 Dec. of 2007). These potential high O₃ episode days were selected for carbonyl sampling on the basis of weather prediction and meteorological data analysis, which were usually related to stronger solar radiation, weaker wind speed, and less vertical dilution of air pollution compared to non-O₃ episode days. Silica cartridges impregnated with acidified 2,4-dinitrophenylhydrazine (DNPH) were used for sampling. Air samples were drawn through the cartridge at a flow rate of 0.4–0.5 L min⁻¹ for 150 min; the flow rate through the cartridges was monitored with a rotameter which was calibrated before and after each sampling. An O₃ scrubber was connected to the inlet of the DNPH–silica cartridge to prevent interference from O₃. During each sampling day, a total of four carbonyl samples were collected accordingly.

All cartridges were stored in a refrigerator at 4°C after sampling. The sampled carbonyl cartridges were eluted slowly with 5 ml of acetonitrile into a 5-ml volumetric flask. A 20- μ l aliquot was injected into the high performance liquid chromatography (HPLC) system through an auto-sampler. The operating conditions of the HPLC are shown in Table 3.1. Typically, C1–C8 carbonyl compounds can be measured effectively by this technique with a detection limit

of ~0.2 ppbv. Since the sampling periods ranged from 2 to 3 h, cubic spline interpolation was used to derive hourly carbonyl concentrations for modeling purpose. Cubic spline interpolation is a useful technique to interpolate between known data points due to its stable and smooth characteristics. As an interpolation method, this method tends to derive the unknown values with the help of the known ones and tries to interpolate the values as closer to the original ones as possible.

Table 3.1 Gradient separation of C₁ – C₉ aldehyde and ketone derivatives

Column	Nava-Pak C18 3.9 ×150 mm
Moblie phase	A: Water/Acetonitrile/ Tetrahydrofuran 60/30/10
Gradient	B: Water/Acetonitrile 40/60
Flow rate	100% A for 2 min then a linear gradient from 100% A to 100% B in 18 min, 100% B for 4min
Injection volume	20μL
Detection	Absorbance at 360 nm

3.3.3 Sampling and analysis of NMHCs

Ambient VOC samples were collected using cleaned and evacuated 2-L electro-polished stainless steel canisters on the same days as those for carbonyls. A flow-controlling device was used to collect 1-h integrated samples. At the two sampling sites, hourly NMHC samples were collected from 6 a.m. to 6 p.m. at WQS and from 7 a.m. to 6 p.m. at TC, respectively. A total of 104 and 96 NMHC samples were collected at WQS and TC, respectively.

The samples were analyzed by an Entech model 7100 pre-concentrator

(Entech Instruments Inc., California, USA) coupled with a gas chromatography–mass selective detector (GC-MSD, Agilent 5973N). An HP-1 capillary column (60 m × 0.32 mm × 1.0 μ m; Agilent Technology, USA) was used with helium as carrier gas. The GC oven temperature was initially programmed at –50°C, holding for 3 min, increasing to 10°C at 15°C min⁻¹, then to 120°C at 5°C min⁻¹, then to 250°C at 10°C min⁻¹, and holding for 10 min. The MSD was operated in selected ion mode with electron impact ionization.

3.3.4 Quality control and quality assurance for VOC and carbonyl analyses

Before sampling, all canisters were cleaned at least five times by repeatedly filling and evacuating humidified pure nitrogen gas. In order to check whether there was any contamination in the canister, we filled the evacuated canisters with pure N₂ and stored them in the laboratory for at least 24 hours. These canisters were then checked by the same VOC analytical method to ensure that all the target compounds were not found or were under the method detection limit (MDL). In addition, duplicate samples were regularly collected to check the precision and reliability of the sampling and analytical methods.

NMHCs were identified by their retention times and their mass spectra. The quantification of target VOCs was accomplished using multi-point external calibration curves. The calibration curves were updated every day and were prepared using 1 ppmv standard calibration gases (TO-14 gases, Spectra Gases

Inc.) at five different diluted concentrations plus humidified zero air (0–40 ppbv).

The detection limits were 3 pptv.

Identification and quantification of carbonyl compounds were based on retention times and peak areas of the corresponding calibration standards, respectively. The instrument was calibrated using five standard concentrations covering the concentrations of interest for ambient air. There were good linear relationships ($R^2 > 0.998$) between the concentrations and responses for all carbonyls identified. Cartridge collection efficiency was determined with two cartridges in series; over 98% of carbonyl compounds were found in the first cartridge. Relative percent differences for duplicate analysis were within 10%.

3.4 Backward air mass trajectories

To identify the origin and transport pathways of the air masses arriving at the study sites, the respective backward trajectories were calculated by the trajectory model NOAA-HYSPLIT4.8 (Draxler and Rolph, 2003) for 1 hour intervals. The hourly output data of Weather Research and Forecasting (WRF) model was used to drive the model. The WRF model is a new generation of medium-scale weather forecast model and assimilation system. It is non-hydrostatic, with two dynamic cores (ARW and NMM), two vertical coordinates (eulerian height coordinate and eulerian mass coordinate) as well as many different choices for physical parameterizations to represent processes, and is designed to be a flexible, state-of-the-art, and portable code that is efficient in a massively parallel

computing environment. Simulations and real-time forecasting tests have indicated that the WRF model has a good performance in all kinds of weather forecasts, and has broad application prospects. In this study, WRF was run in two nested domains with grid spacings of 36km and 12 km, respectively. The finest domain covers the south-east China. Grid nudging was adopted in the outmost domain to minimize integration errors. More details of the model description can be found in Jiang et al. (2008). WRF simulation was hourly conducted for arrival times at WQS of 0000, 0300, 0600, 0900, 1200, 1500, 1800 and 2100 h during the periods of 12 – 17 November, 2007, which is at three-hourly resolution for the entire sampling campaign.

3.5. Observation- based model (OBM)

3.5.1 Model description

The observation-based model developed by Cardelino and Chameides (1995) uses ambient concentrations of O₃ and its precursors (e. g. NO, CO and VOCs), and meteorological data measured as a function of time at a given location as input for a coupled set of photochemical box models that simulate photochemical O₃ production and destruction, and to explore the O₃-precursor relationships.

To calculate the photochemical O₃ production, two base simulations of OBM need to be conducted. The first simulation adopts the concentrations of specified species such as O₃, NO, CO and the primary VOC functional groups to calculate the concentrations of the unspecified species and the integrated source functions

by integrating a coupled set of different equations of the following form:

$$\frac{\partial C_j}{\partial t} = P_j - L_j - D(t)(C_j - C_j^{FT}) \quad (3.1)$$

where C_j is the concentration of the j^{th} unspecified species, and P_j and L_j are the photochemical production and destruction rates of species j , respectively; C_j^{FT} is the free tropospheric concentration of species j ; and $D(t)$ is the mixing height variation. In all cases, the initial concentrations of the unspecified species are assumed to be zero.

In the first simulation, the time-dependent source function $\Sigma_i(t)$ for the specified species is obtained by solving equations of the following form:

$$\Sigma_j(t) = \left[\frac{\partial C_j}{\partial t} \right]_{obs} - P_j + L_j + D(t)(C_j - C_j^{FT}) \quad (3.2)$$

where C_j is the concentration of the j^{th} specified species, and $[\partial C_j / \partial t]_{obs}$ is the observed local time derivative in C_j . This source function, $\Sigma_j(t)$ (in unit of ppb hr⁻¹), in fact represents the combined effects of emissions at the site, horizontal transport to the measurement site, and the horizontal transport away from the measurement site.

After the source functions are determined, the second base case simulation is conducted by solving equations of the following form:

$$\frac{\partial C_j}{\partial t} = P_j - L_j + \Sigma_j - D(t)(C_j - C_j^{FT}) \quad (3.3)$$

With the source function, Σ_j , is given by the solutions obtained from Equation 3.2 from the first simulation.

The second base case simulation not only gives an internal check on the accuracy of the source function calculated in the first simulation, but also

determines the O₃-forming potential at the monitoring site (i.e., P^s_{O₃-NO}, which is the integration of model-calculated rates of O₃ production and NO destruction).

The major goal of the model is to assess the sensitivity of O₃ photochemical production in an area to changes in the precursor compounds, i.e. Relative Incremental Reactivity (RIR), defined as the percent change in O₃ production per percent change in precursor sources, giving a relative measure of the effectiveness of reducing the emissions of one compound or group of compounds over that of another compound or group of compounds. The RIR for precursor X at site “S” is given by

$$\text{RIR}^s(X) = \frac{P_{\text{O}_3\text{-NO}}^s(X) - P_{\text{O}_3\text{-NO}}^s(X - \Delta X)}{\frac{\Delta S(X)}{S(X)}} \quad (3.4)$$

Where superscript “s” is used to denote the specific site where the measurements were made; X is used to represent the relevant precursor (i.e. HC_i, NO, or CO); S (X) is the integrated amount of species X (ppbv) emitted or transported to the measurement site that results in the concentration of X at the site; ΔX is the change in the concentration of X caused by a hypothetical change in S (X); and P^s_{O₃-NO} (HC_i, NO, O₃, CO) is defined as the O₃-forming potential, that is the net amount of O₃ formed and NO consumed over a period.

Since the production of O₃ is related to the concentration of O₃ at the site, and the concentration of a precursor is essentially linearly related to its emissions, RIR can be used to assess the effect of a given emission reduction on O₃ concentrations at a site without detailed knowledge of the emissions (Cardelino

and Chameides, 1995).

Internal tests can be carried out to determine whether an application of the OBM to a given dataset is appropriate or not. One test is to assess the consistency of the RIRs across multiple days. If the standard error of the mean for the time-averaged RIRs defined in the OBM is relatively small, the calculated RIRs will be more likely to be robust (Cardelino and Chameides, 1995).

3.5.2 The chemical mechanism (Carbon-Bond IV mechanism)

The chemical mechanism used in the OBM is the Carbon-Bond IV mechanism. It is a lumped structure chemical mechanism, containing 33 species or lumped carbon-bond groups and 81 reactions. These 33 compounds include odd oxygen species (O, O(¹D), and O₃); odd-hydrogen species (OH, HO₂, and H₂O₂); odd-nitrogen species (NO, NO₂, NO₃, N₂O₅, HNO₂, HNO₃, and HO₂NO₂); CO and water vapor (H₂O); and 18 functional groups. The functional groups contain PAR (paraffin), which is used to represent the chemistry of alkanes and most of the alkyl groups found in other organics; the carbon bond surrogate OLE (olefin), which contains two carbon atoms, is used to represent the carbon-carbon double bonds that are found in 1-alkenes; a third surrogate, ALD2 (aldehydes), which also contains two carbon atoms, is used to represent the -CHO group and adjacent carbon atom in acetaldehyde and higher aldehydes. It is also used to represent 2-alkenes since these species react very rapidly in the atmosphere to produce aldehyde products; the surrogate TOL is a seven-carbon species used to

categorize monoalkylbenzene structures, and its chemistry is based on the reactions of toluene; XYL is an eight carbon surrogate used to represent dialkylbenzenes and trialkylbenzenes, and its chemistry is based on *m*-xylene; formaldehyde is treated explicitly because formaldehyde is highly reactive and its oxidation chemistry is sufficiently different from that of other carbonyl species; ethene is also treated explicitly because it reacts significantly slower than other alkenes, it is a large fraction of hydrocarbon emissions, and it yields a high fraction of formaldehyde; isoprene is the third and final organic represented explicitly because its reactions with free radicals are much faster, and it forms a prominent part of biogenic emissions in rural areas.

3.6 The photochemical trajectory model

3.6.1 Model description

The PTM is a ground level Lagrangian box model, simulating complex chemical reactions within a well mixed boundary layer air parcel, which extends from the Earth's surface up to the top of a diurnally varying boundary layer. The boundary layer height is made to vary from 300 m at night to a maximum of 1200m during the daytime, based on radio sounding results obtained in the PRD region during the October 2004 sampling campaign (Fan et al., 2008). The horizontal dimensions of the air parcel are 10 × 10 km. When the air parcel moves through the pre-located trajectory, it picks up emissions of anthropogenic and biogenic VOCs, CO, NO_x, SO₂. In this box model, the secondary compounds

and their precursors react among themselves according to the defined chemical mechanism (i.e. MCM).

The chemical development of the species, i , in the air parcel, in terms of its change rate of concentration in molecule $\text{cm}^{-3} \text{s}^{-1}$, is described by a series of differential equations of the following equation (3.5):

$$\frac{dC_i}{dt} = P_i - L_i \times C_i - \frac{V_i C_i}{h} + \frac{E_i}{h} - (C_i - B_i) \frac{1}{h} \frac{dh}{dt} \quad (3.5)$$

where C_i is the species concentration in the air parcel, P_i the instantaneous production from photochemistry, $L_i \times C_i$ the instantaneous loss rate by photochemistry, V_i the species-dependent dry deposition velocity, h the time-dependent boundary layer depth, E_i the local emission rate from pollution sources, and B_i the background concentration of the species persisting aloft from the previous evening.

3.6.2 Master chemical mechanism

The chemical mechanism employed in the photochemical trajectory model is master chemical mechanism (MCM), which is a near-explicit chemical mechanism describing the detailed degradation of a large number of emitted organic compounds and the resulting generation of O_3 and other secondary pollutants under conditions appropriate to the atmospheric boundary layer (Jenkin et al., 1997). The MCM v3.1 describes the oxidation of 139 non-methane VOCs, which contains around 13,500 reactions involving 5,900 chemical species. The MCM can be accessed via the University of Leeds website

<http://mcm.leeds.ac.uk/MCM>).

The MCM consists of a number of identifiable and separate elements:

1. the inorganic chemical reactions of the simple atoms and radicals containing oxygen, hydrogen, nitrogen and sulphur, and those of CO, employing rate coefficient taken from the evaluations of Atkinson et al. (1992, 1996).

2. The photolysis reactions of the photochemically labile inorganic species and of a large number of organic oxygenate. The latter category consists of simple carbonyl compounds such as aldehydes and ketones, and also many other complex carbonyl compounds, organic hydroperoxides and nitrates which are generated as degradation products.

3. The time dependence of the photolysis rates is described by calculating the instantaneous solar zenith angle, Z , and using the following equation to estimate the photolysis rate, J , for a particular photochemical process:

$$J=l*(\cos Z)^m \exp(-n \sec Z) \quad (3.6)$$

The coefficients l , m and n were calculated for each process by fitting the J values to the appropriate functions of the zenith angle (Z)

4. The atmospheric degradation of 139 VOCs. Extended MCM v3.1 describes the degradation of 22 alkanes including methane, 20 alkenes (including 2 dienes and 2 monoterpenes), 1 alkyne, 18 aromatics, 10 aldehydes, 10 ketones, 19 alcohols and glycols, 8 esters, 9 ethers and

glycoethers, 3 carboxylic acids, 2 hydrobromocarbons, 3 other oxygenated VOCs and 15 chlorinated hydrocarbons. The complete list of the VOC species is available on the website of the University of Leeds. Kinetic and mechanistic data relevant to the tropospheric degradation of VOCs, and the production of secondary pollutants, have previously been used to define a protocol which underpinned the construction of a near-explicit MCM (Atkinson, 1997; Jenkin et al., 1997; Atkinson and Arey, 2003).

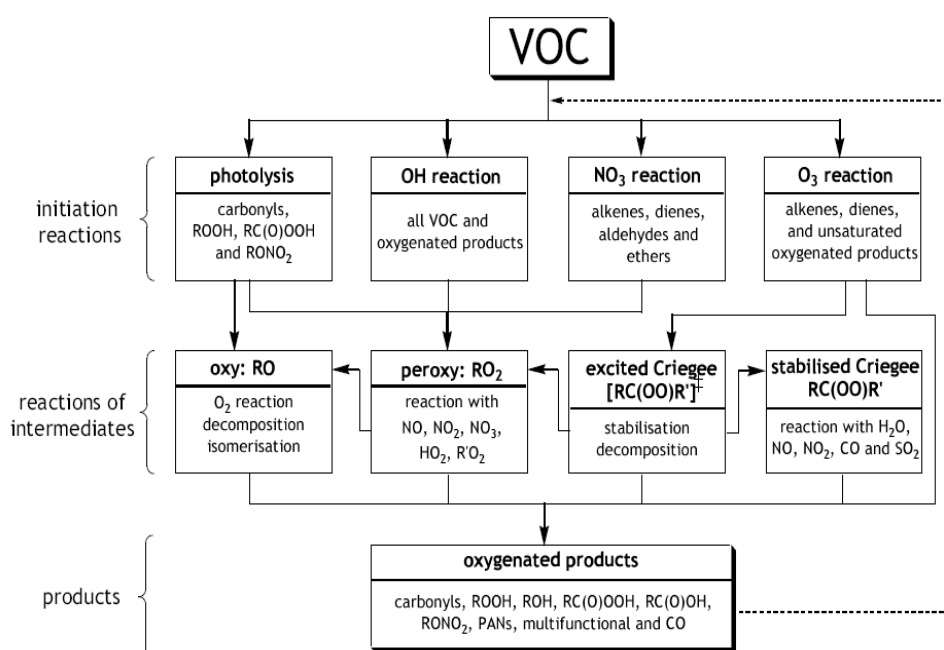


Fig.3.2. Flow chart indicating the major reactions, intermediate classes and product classes considered in the MCM protocol

The flow chart summarises the main types of reaction considered and classes of organic intermediate and product which are potentially generated (Fig.3.2). The chemistry of a given VOC is thus developed within this framework, based on a predefined set of rules (i.e. the protocol). The flow chart essentially

represents the degradation of the given VOC into a set of ‘first generation products’, which are themselves further degraded within the same general framework. This process is continued until the chemistry either yields CO₂, or until an organic product or radical is generated for which the subsequent chemistry is already represented in the mechanism (Saunders et al., 2003). It is known that the rigorous application of a series of rules can lead to an unmanageably large number of reactions, particularly for larger VOCs. The idea of a fully explicit mechanism is therefore impractical, and a degree of simplification is required even for so called explicit mechanisms. Mechanism simplification has been achieved in several ways, for example, by limiting the proliferation of the chemistry related to minor reaction pathways through disregarding OH reaction channels of low probability, and simplifying the treatment of the degradation of a number of product classes deemed to be ‘minor’. In addition, a substantial reduction is achieved through parameterizing the representation of the permutation (i.e. self and cross) reactions of organic peroxy radicals. A fully explicit inclusion of these reactions alone for the 902 peroxy radicals generated in MCMv3 would require approximately 400, 000 reactions (assuming a single channel in each case). The parameterization used in the MCM requires only one reaction for each peroxy radical, with up to three channels in each case.

3.6.3 Photochemical ozone creation potential

In the PTM model, an index, the photochemical O₃ creation potential (POCP),

is used to describe the relative contribution of each VOC to O₃ formation at the regional scale. The concept of POCPs was initially developed to determine the role of individual VOCs in O₃ formation in north-west Europe (Derwent and Jenkin, 1991), and previous versions of the MCM have been applied to calculation of POCP values (Derwent et al., 1996, 1998). The POCP for a particular VOC is determined by quantifying the effect of a small incremental increase in its emission on O₃ formation along the trajectory, relative to that resulting from an identical increase in the emission (on a mass basis) of a reference VOC, which is taken to be ethene (Saunders et al., 2003). Ethene is a suitable VOC species to normalize the POCP values because it is one of the most important O₃ precursors with medium reactivity towards hydroxyl radical, and its chemical degradation processes are also well-defined. The POCP for the given VOC '*i*' is defined by Eq. (3.7),

$$\text{POCP}_i = \frac{\text{ozone increment with the } i\text{th VOC}}{\text{ozone increment with the ethene}} \times 100 \quad (3.7)$$

POCPs are available in the literature from earlier studies in Europe by using different versions of MCM (Derwent and Jenkin, 1991; Carter, 1994; Derwent et al., 1996, 2003, 2007a).

In the next chapter, we will report the results obtained in this project.

Chapter 4

Concurrent observation of air pollutants at two sites in the Pearl River Delta

4.1 Introduction

The Pearl River Delta (PRD) region on the coast of Southern China has become one of the world's fastest growing industrial areas in recent years. The PRD region consists of nine cities within Guangdong Province, namely Guangzhou, Shenzhen, Zhuhai, Dongguan, Zhongshan, Foshan, Jiangmen, Huizhou and Zhaoqing (usually these nine cities are considered to comprise the inland PRD region), plus Hong Kong and Macau Special Administrative Regions. A consequence of the rapid development is the sacrifice of environmental quality. Ozone (O₃) pollution has been one of the major problems facing the environmental society in the PRD region. Photochemical O₃ has been studied in Southern China for over a decade (Chan et al., 1998a, 1998b; Wang et al., 1998; Wang and Kwok, 2003; Wang et al., 2003). Lam et al. (1998) analyzed the behaviour of background surface O₃ measured at a coastal site in Hong Kong. Chan et al. (1998a, b) compared background and urban O₃ in Hong Kong. They focused on seasonal variations of O₃ and related the observed trends to the large-scale Asian monsoon circulation. Low O₃ during summer was attributed to the inflow of maritime air, whereas abundant O₃ in autumn-winter was due to the outflow of polluted continental air. Wang et al. (1998) found that the local-scale

re-circulation was an important mechanism in transporting O₃ to a rural/coastal monitoring site near Hong Kong. The temporal variability and emission patterns related to photochemical smog episodes in Hong Kong were also reported by Wang et al. (2003) and Wang and Kwok (2003).

In addition, many O₃ episodes were analyzed in combination with the meteorological conditions in Hong Kong using numerical simulations (Lee et al., 2002; Wang and Kwok, 2003; Lam et al., 2005; Huang et al., 2006; Lee and Savtchenko, 2006; Wang et al., 2006). These studies suggested the importance of regional transport from the inland PRD region. Lee and Savtchenko (2006) found that air pollution in Hong Kong was correlated with that in the inland PRD region in 2003 and 2004. Huang et al. (2006) surveyed 54 O₃ episodes that occurred over Hong Kong during 2000–2004 and found that O₃ episodes were dominated by regional transport when a tropical cyclone/typhoon was located over the Northwestern Pacific or the South China Sea to the east or southeast and when an anticyclone appeared over mainland China to the north. Sensitivity studies even revealed that, in some O₃ episodes, 40–90% of the ambient O₃ at urban and rural areas of Hong Kong was attributed to horizontal transport (Lam et al., 2005; Wang et al., 2006). However, all of these studies were carried out within Hong Kong. The relative contributions of local photochemical formation and regional transport to O₃ episodes in Hong Kong are not fully understood. Furthermore, the causes of O₃ episodes in the inland PRD, which was considered as a major reason for O₃ episodes in Hong Kong, remain unclear, though some

studies have been undertaken inside the inland PRD region (Zhang et al., 1999, 2008). Therefore, in order to improve our understanding of the correlation between air pollution in Hong Kong and the inland PRD region, simultaneous measurements of O₃ and its precursors (i.e. volatile organic compounds and nitrogen oxides) were conducted at two sites in October–December, 2007 (autumn is the period that O₃ episodes are often observed) (Guo et al., 2009).

Volatile organic compounds (VOCs) and nitrogen oxides (NO_x) are important precursors of tropospheric O₃. Studies have shown that the formation of O₃ in the PRD region is limited by VOCs (So and Wang, 2004; Zhang et al., 2007; Zhang et al., 2008; Cheng et al., 2009). A number of studies have been conducted to understand the spatial and temporal characteristics of VOCs in the inland PRD region (Chan et al., 2006a; Tang et al., 2007; Barletta et al., 2008b; Liu et al., 2008b) and in the Hong Kong area (Sin et al., 2000; Lee et al., 2002a; Guo et al., 2004a, 2007; So and Wang, 2004; Zhang et al., 2007). The regional and local source contributions to ambient VOCs in Hong Kong have been studied by measurements at a rural/coastal site near Hong Kong (Wang et al., 2005a; Guo et al., 2006). These previous studies mainly focused on the speciation, spatial and temporal variations, source characterization and identification of VOCs either in Hong Kong or in the inland PRD. To better understand the relationship of VOCs between inland PRD and Hong Kong during O₃ episodes, and the photochemistry of VOCs in the formation of O₃, it is necessary to undertake concurrent field measurements in these two different areas (Guo et al., 2009).

In this chapter, we present the measurement data of the main air pollutants simultaneously collected between 22 October and 1 December 2007 at two sampling sites which are located in the inland PRD region (WQS) and in Hong Kong (TC), respectively (detailed sampling information can be found in Chapter 3: Methodology). We firstly describe the general climate conditions at WQS and TC, and then the temporal variations of trace gases at the two sites are discussed. Finally, we discuss the influence of regional transport on these study areas by examining the relationship between selected VOC species ratios and the age of air masses, and by analyzing their backward trajectories.

4.2 General climate conditions

The mean sea level pressure and wind field on 1000 hPa for East Asia over the whole sampling period are shown in Fig. 4.1. The figure was made using NCEP FNL (final) data with a horizontal resolution of $1^{\circ}\times 1^{\circ}$ (<http://dss.ucar.edu/datasets/ds083.2/>). It shows that there was an intensive high-pressure system over Northern China, while Hong Kong and the inland PRD region were in front of the high pressure ridge. Due to the influence of the high-pressure system, the prevailing synoptic winds in Hong Kong and the inland PRD region were from the northeast.

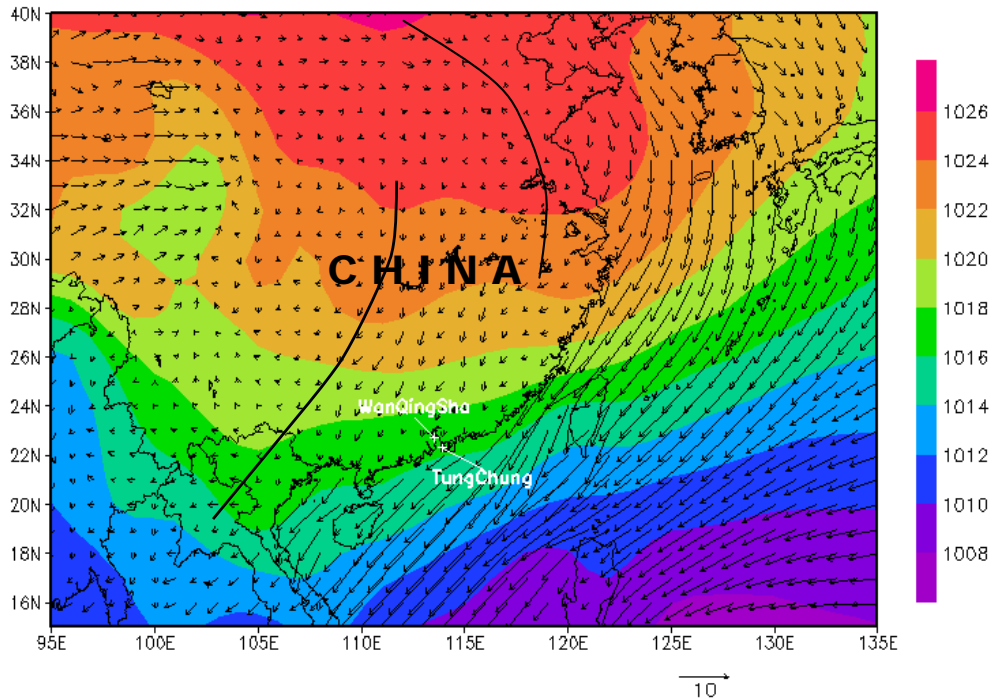


Fig.4.1. Mean sea level pressure and wind field on 1000 hPa between 22 October and 1 December 2007

Statistical analysis of the ground meteorological observation data suggests that the wind speed at the coastal TC site ($1.95 \pm 0.06 \text{ms}^{-1}$) was higher than that at the inland WQS site ($1.32 \pm 0.08 \text{ms}^{-1}$), and the average wind direction was 97° (degrees azimuth, 0° means North) at TC and 57° at WQS (Table 4.1). The differences in wind speed and wind direction at the two sites implied that the air masses of the two sites may have had different transport pathways. In contrast, no statistical differences were found for temperature and relative humidity at the two sites, respectively (Table 4.1).

Table 4.1. Statistics of meteorological parameters at the TC and WQS sites

Sites	Average		Max value		Min value		95% confidence interval	
	TC	WQS	TC	WQS	TC	WQS	TC	WQS
Temperature (°C)	21.8	21.9	31.6	31.5	11.0	12.6	±0.21	±0.24
Wind speed (m s ⁻¹)	1.95	1.32	5.3	5.1	0.4	0.0	±0.06	±0.08
Wind direction (°)	96.8	57.4	-	-	-	-	-	-
Relative humidity (%)	65.6	66.3	97.0	96.0	18.0	26.2	±0.97	±1.12
Solar radiation (W m ⁻²)	665*	585*	789	721	-	-	±15.6	±15.6

* Average of the daily maximum solar radiation

4.3 Temporal variations of trace gases at WQS and TC

4.3.1 Day-to-day variations

Time series of hourly concentrations of O₃, NO, CO, SO₂, and meteorological parameters at WQS and TC are shown in [Figs. 4.2 and 4.3](#), respectively. An O₃ episode day was defined as a day when the highest hourly average O₃ concentration exceeded 80 ppbv (i.e., China's Grade II standard). At WQS, two pollution events characteristic of high O₃ levels were observed, namely, between the 23 – 30 October and 09 – 17 November. High O₃ concentrations (>120 ppbv) were observed in most of the days during the two events. However, the primary pollutants, i.e., NO, SO₂ and CO, did not show the same temporal pattern as O₃. For example, the SO₂ and CO concentrations were high on some episode days (e.g., 25 October and 15 – 16 November), but low on other days (e.g., 23 – 24 October). [Table 4.2](#) shows some meteorological parameters on the O₃ episode days in comparison with the selected normal days from October to November 2007.

During the two pollution events and on the selected normal days, the maximum temperature ranged from 25.8°C to 31.5°C and 19.0°C to 21.4°C, and the average wind speeds were 0.8 and 2.4 ms⁻¹, respectively. The results indicate that meteorological conditions including high temperature, intense solar radiation, and low wind speed are favorable for photochemical O₃ formation, which has been demonstrated in many previous studies (Cooper et al., 2001; Wang et al., 2001b).

Table 4.2. Meteorological parameters during O₃ episode events and the selected normal days

	Date	Maximum O ₃ (ppbv)	Maximum temperature (°C)	Wind speed (m/s)	Maximum solar radiation (w/m ²)
Two O ₃ events (Days with max O ₃ >80ppbv)	23-30 Oct	132 ± 24 (89-168)*	29 ± 0.95 (25.8-31.55)	0.93 ± 0.72 (0.01-3.29)	650 ± 58 (575-721)
	07-17 Nov	157 ± 25 (103-182)	27.55 ± 0.92 (26.63-29.05)	0.62 ± 0.60 (0.01-3.15)	581 ± 107 (304-664)
The normal days (O ₃ < 80 ppbv)	31 Oct	36 ± 14	21.07 ± 0.26	1.83 ± 1.06	345 ± 269
	- 2 Nov	(21-54)	(20.84-21.44)	(0.01-4.41)	(131-715)
	25-28 Nov	58 ± 7 (51-68)	20.85 ± 2.07 (19.05-22.97)	2.96 ± 1.38 (0.05-5.13)	456 ± 176 (303-645)

* Mean±95% confidence interval (min - max)

At TC, the concentrations of SO₂, CO, and O₃ were lower than those at WQS. The results show that the air pollution in Guangzhou was more serious than in Hong Kong. The peak O₃ concentrations exceeded the Hong Kong Air Quality Objective of 122 ppbv on 26 October (139 ppbv) and 10 November (123 ppbv) during the study period. The meteorological conditions in Hong Kong were more complicated than in Guangzhou. The winds showed a complex pattern due to land-sea breezes and topography effects and were roughly from the northeast or northwest during the daytime and then switched to the southeast at night.

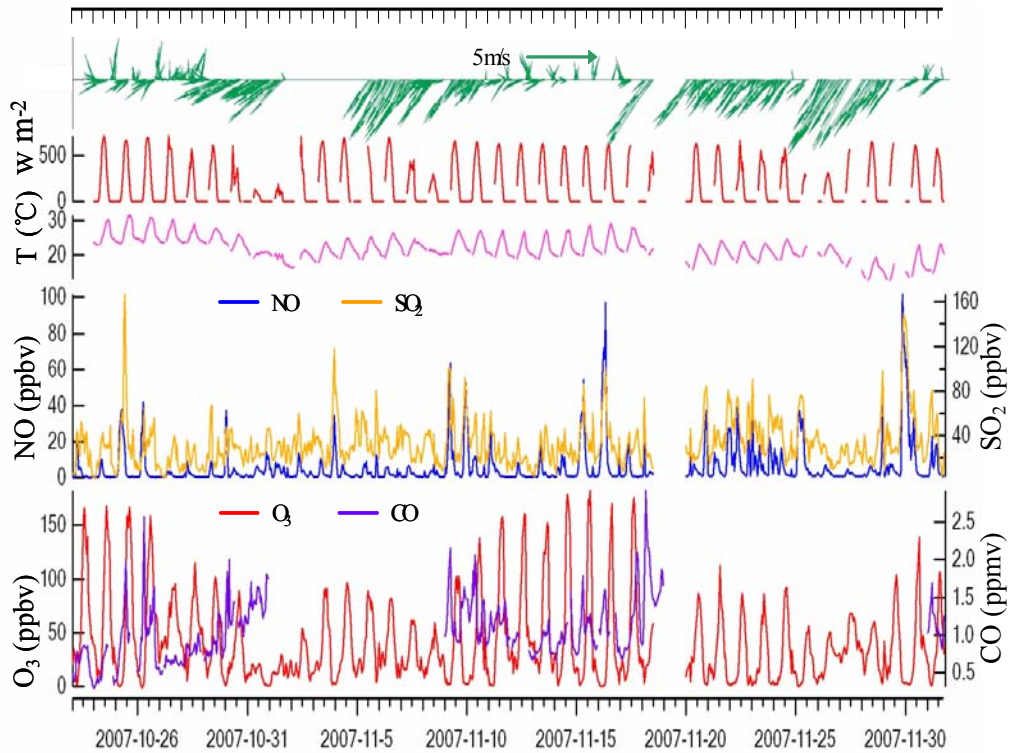


Fig.4.2. Time series of O₃, CO, NO, SO₂, temperature, wind speed and direction and solar radiation measured at WQS from 23 October to 01 December, 2007

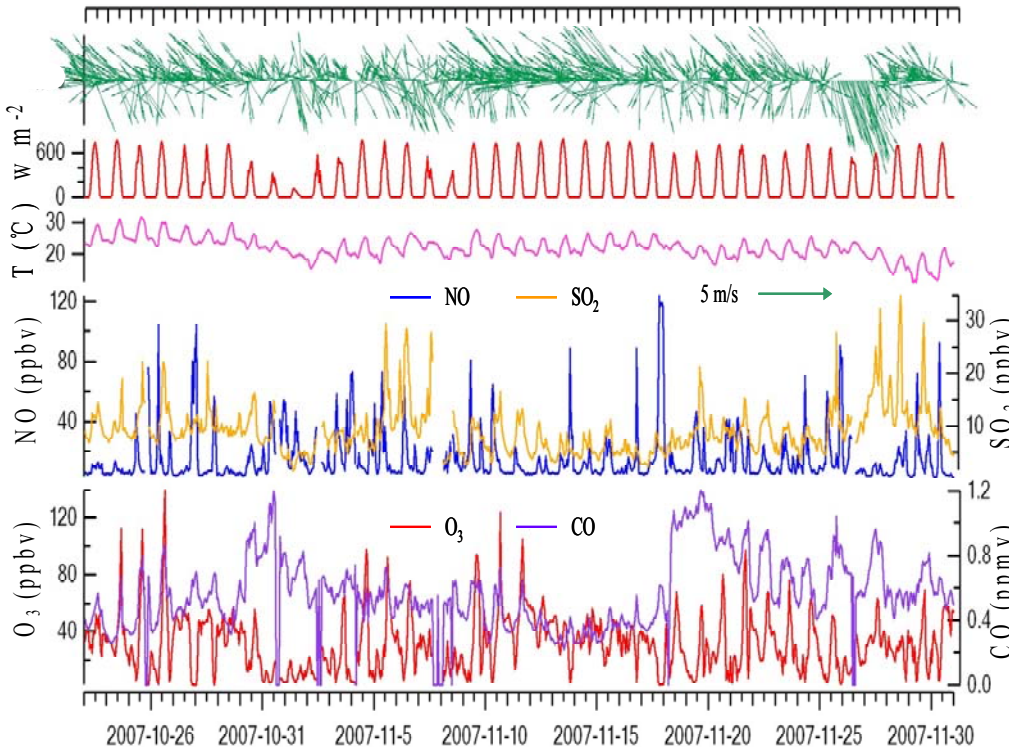


Fig.4.3. Time series of O₃, CO, NO, SO₂, temperature, wind speed and direction, and solar radiation measured at TC from 23 October to 01 December, 2007.

Increased O₃ levels (>100 ppbv) were observed with light northeastern winds. A distinct feature during the sampling periods was that O₃ and CO values were positively correlated on some days and negatively correlated on other days. For example, between 31 October and 2 November, CO concentration dramatically increased while O₃ concentration had a decreasing trend. Meteorological analysis indicated an intense northeast monsoon and a rain band over southern China due to a high-pressure system moving toward eastern China, which brought cool and rainy weather to Hong Kong. This continental airstream brought high CO concentration from inland to Hong Kong with low O₃ concentration due to the precipitation and the decrease in temperature and solar radiation (Guo et al., 2009). When the intense northerly monsoons were over, resulting in elevated temperature and solar radiation and a stable boundary layer, the photochemical reaction strengthened and the O₃ level increased rapidly, such as on 10–11 November. In addition, due to the stable boundary layer and lower surface wind, the dispersion of primary air pollutants was reduced, resulting in elevated levels of NO, SO₂, and CO. This implies that the elevated O₃ levels may be dominantly affected by local production.

4.3.2 Diurnal variations

By analyzing the diurnal variations of air pollutants, information about the contributions of emissions and chemical and physical processes to a diurnal cycle can be obtained. [Fig.4.4](#) shows the mean diurnal variations of trace gases, total

NMHCs (8-day average), and wind fields at WQS and TC between 23 October and 1 December. A clear diurnal shift in wind direction was found at TC: the winds were southeasterly at night and then became more northerly with increased speeds during the daytime. However, the mean winds at WQS basically reflected the large-scale air flow from the northeast, with increased speeds in the morning and decreased speeds in the afternoon and at night. In general, O₃ showed a daily peak in the afternoon (14:00-16:00) and had relatively low concentrations at night at both sites (Fig. 4.4), which is a typical diurnal profile for O₃ at surface sites (Wang et al., 1998, 2003). However, different features were also observed at the two sites. Firstly, the maximum O₃ level was much higher and the diurnal change was much faster at WQS than at TC, suggesting more significant photochemical production of O₃ at WQS than that at TC. Secondly, the O₃ concentration began to increase in the early morning (about 07:00) at WQS, whereas there was a low trough in early morning at TC followed by enhanced O₃ beginning at about 09:00, likely due to high concentrations of NO in the morning which titrated some O₃. Thirdly, the O₃ concentrations at nighttime at TC (27±4 ppbv) were higher than those measured at WQS (18±3 ppbv), which was probably attributed to the constant transport of O₃ to TC by southeasterly flows from the South China Sea where O₃ was consumed less (Wang et al., 1998, 2003). This speculation was based on the fact that wind direction was from the southeast in the evening when the O₃ level was higher at TC than that at WQS. Furthermore, early studies found that O₃ levels gradually increased from the east

to the west of Hong Kong when the South China Sea is downwind of Western Hong Kong (So and Wang, 2003). The average diurnal O_3 difference (the mean daytime minus nighttime concentration) was 8 ± 4 ppbv and 41 ± 6 ppbv at TC and WQS, respectively (Table 4.3).

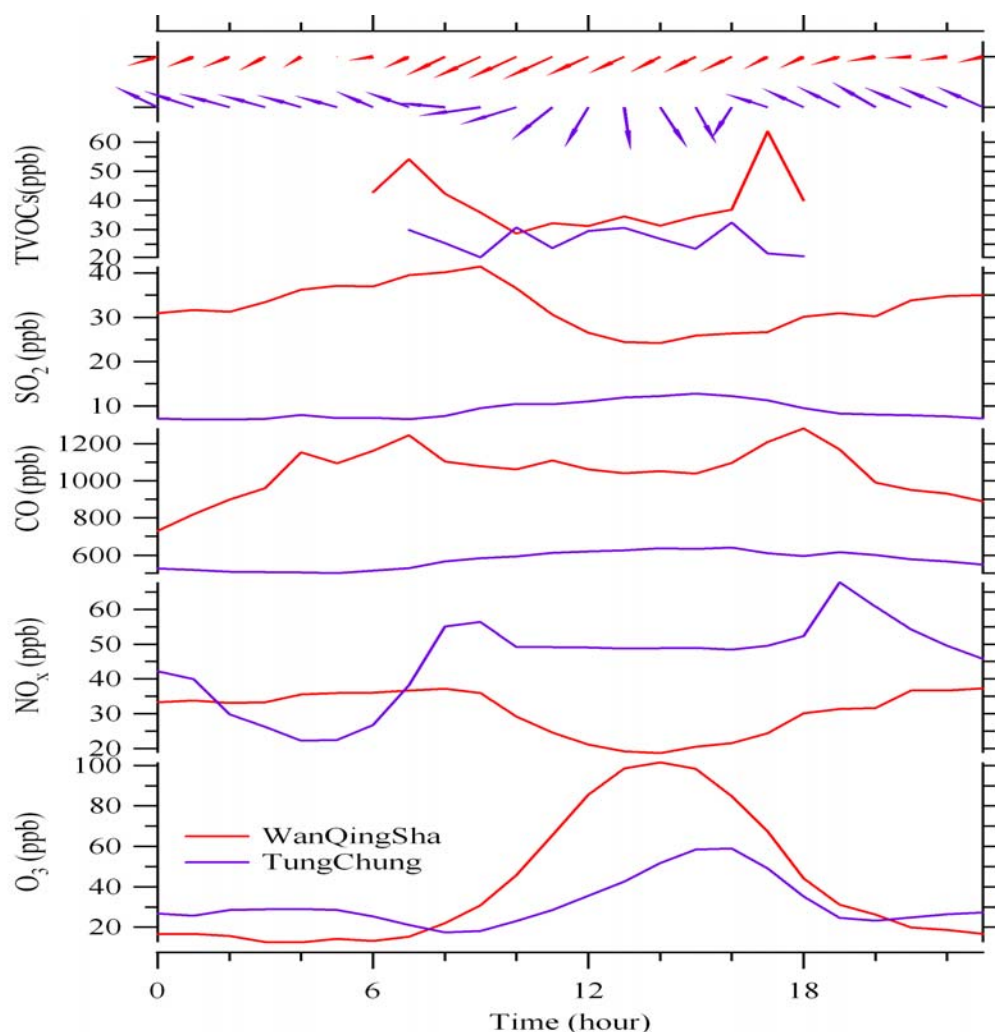


Fig.4.4. Mean diurnal variations of trace gases and total NMHCs, other trace gases and wind fields between 23 October to 1 December (total NMHCs were averaged using all VOC samples from 8 sampling days)

The diurnal variation of NO_x at the TC site showed a typical urban profile (obvious bimodal structure) with peaks at about 09:00 and 19:00, respectively (Fig. 4.4). This observation is consistent with the traffic pattern of Hong Kong.

However, much weaker NO_x peaks were found at WQS as it was a rural site. As observed at many rural and coastal sites, reduced mid-daytime concentrations of NO_x were found at both TC and WQS, which can be explained by high photochemical conversion and elevated vertical turbulence dilution. The diurnal patterns of SO₂ and CO at the TC site were almost exactly the same, with a small and broad peak in the afternoon indicating the contribution of regional transport to SO₂ and CO in Hong Kong by northerly winds. By contrast to TC, at the WQS site CO had an obvious bimodal structure profile, and SO₂ had a high morning peak and a low afternoon concentration. The diurnal variation of total NMHCs at WQS showed two major peaks, namely in early morning and in late afternoon; at TC the peaks were much weaker and were not statistically different from the troughs. These observations show that O₃ production is even more acute in the Hong Kong area than in the inland PRD region.

Table 4.3 Mean concentrations of trace gases at daytime and nighttime and the diurnal difference

Units: ppbv	Daytime*		Nighttime**		Daytime – Nighttime	
	TC	WQS	TC	WQS	TC	WQS
O ₃	35 ± 3	59 ± 7	27 ± 4	18 ± 3	8 ± 4	41 ± 6
NO _x	48 ± 4	27 ± 3	42 ± 5	34 ± 5	6 ± 6	-7 ± 5
CO	601 ± 62	1118 ± 115	545 ± 55	951 ± 160	58 ± 33	163 ± 100
SO ₂	10 ± 1	32 ± 3	7 ± 1	33 ± 5	3 ± 1	-2 ± 6

* From 06:00 to 18:00

** From 19:00 to 05:00

4.4 Characteristics of air masses in inland PRD and Hong Kong

CO can be considered as an air pollution transport indicator due to its relatively long lifetime (~ 2 months). The poor correlation of CO measured at TC vs. WQS ($R^2=0.16$, $p<0.05$) implies that the transport of air masses between Hong Kong and the inland PRD region during this study period may not be significant, or that local source influences are a dominant factor (Fig. 4.5).

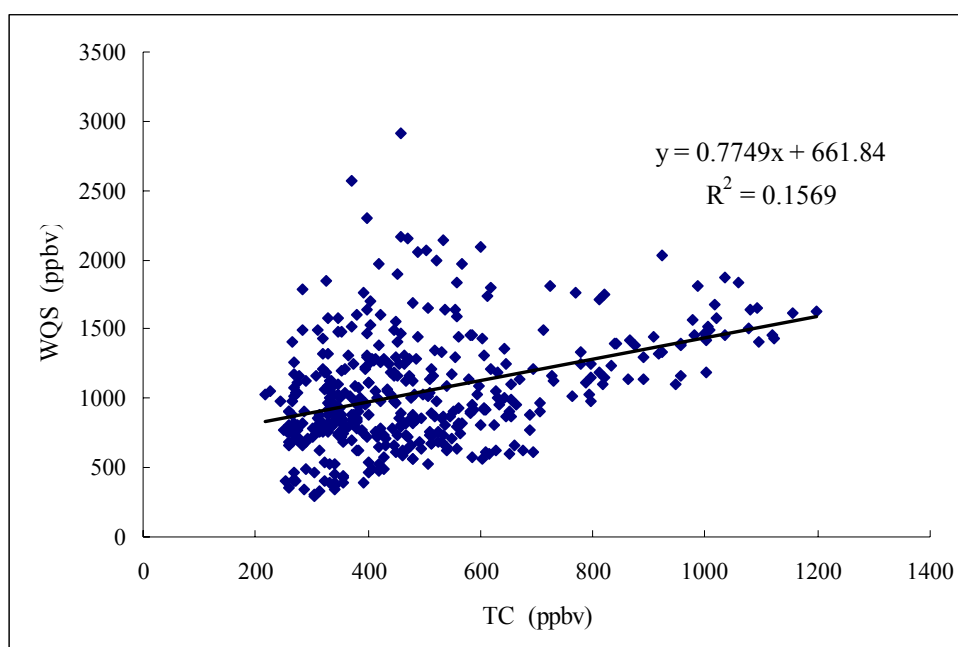


Fig.4.5. A scatter plot of CO measured at TC vs. WQS

The concentration ratios of SO_2 to NO_x and of CO to NO_x can provide signatures of the air masses arriving at each site. In this study, the SO_2/NO_x ratio was found to be 0.25 ± 0.01 ppbv/ppbv at TC and 1.26 ± 0.06 ppbv/ppbv at WQS, whereas the CO/NO_x ratio was 15.8 ± 0.5 ppbv/ppbv at TC and 52.0 ± 3.8 ppbv/ppbv at WQS. That is, the SO_2/NO_x and CO/NO_x ratios at WQS were much

higher than those at TC ($p < 0.001$). This is because the air masses from mainland China are laden with relatively abundant CO and SO₂ while the air masses in Hong Kong have high NO_x levels (Kok et al., 1997; Wang et al., 2001b; Wang et al., 2005a). Compared to previous studies, the SO₂/NO_x and CO/NO_x ratios at WQS (1.26 and 52.0, respectively) were 3–4 times higher than the values reported in upwind Guangzhou urban areas (0.4 and 11.9, respectively) (Zhang, 1998a; Wang et al., 2005b). The higher ratios were probably caused by the lower NO_x level due to photochemical conversion at this rural site.

The potential influence of local and regional air masses on the TC site can be therefore evaluated by SO₂/NO_x and CO/NO_x ratios. The SO₂/NO_x ratios at nine Hong Kong urban air quality monitoring stations were further investigated during the same period as this study. The ratio from October to December 2007 ranged from 0.12 to 0.29 (data from HKEPD website, <http://www.epd.gov.hk>), suggesting that the air masses at TC (SO₂/NO_x ratio: 0.25) had similar chemical characteristics to that in Hong Kong urban areas. Similarly, we investigated the CO/NO_x ratios at Hong Kong urban air quality monitoring stations during the same period as well. Data at two stations were available, namely Tsuen Wan and Yuen Long, with ratios of 14.6 ± 0.7 and 20.6 ± 0.6 ppbv/ppbv, respectively, which were similar to the value at TC (15.8 ppbv/ppbv). Hence, both the SO₂/NO_x and CO/NO_x ratios suggest that the air masses at TC were mainly impacted by Hong Kong local emissions, in particular, the emissions of NO_x, and that there does not appear to have been a significant temporal change in these ratios during this

decade for autumn values.

The ratios of VOCs with different photochemical lifetimes are useful tools to examine the atmospheric processes of air masses, including atmospheric transport and photochemical aging. Due to different lifetimes of two given VOC species, their ratio may change during the course of air mass transport. Using the ratio of a more reactive VOC to a less reactive VOC, a higher ratio indicates relatively little photochemical processing of the air mass and major impact from local emissions. On the other hand, a lower ratio is reflective of more aged VOC mixes and thus presumably that the VOCs were emitted from more distant sources. Comparisons of the ratios among sites can be used to estimate the relative ages of air parcels and help provide evidence of transport histories. Moreover, this ratio analysis can further indicate whether the site is dominantly affected by pollutants from local or regional sources. In this study, we compared the ratios of *m, p*-xylene/ethylbenzene and *i*-butane/propane at the two sites as a measure of atmospheric processing in different air masses (So and Wang, 2004; Guo et al., 2007). *m, p*-Xylene and ethylbenzene are mainly emitted from vehicles and solvent usage, whereas *i*butane and propane have an origin of liquefied petroleum gas emission (Guo et al., 2007). *m, p*-Xylene is more reactive than ethylbenzene, with lifetimes about 1 and 2 days, respectively; *i*-butane also has a shorter lifetime than propane, with lifetimes of about 6 and 12 days, respectively. [Figure 4.6](#) shows the scatter plots of (a) *m, p*-xylene to ethylbenzene and (b) *i*-butane to propane at TC and WQS. Clearly, TC had

higher slopes than WQS for both VOC ratios, with an *m, p*-xylene/ ethylbenzene ratio of 1.07 (versus 0.91 at WQS), and an *i*-butane/propane ratio of 0.38 (versus 0.26 at WQS). The results suggested that the air masses at WQS were more aged than that at TC, reflecting the higher importance of regional transport at the WQS site.

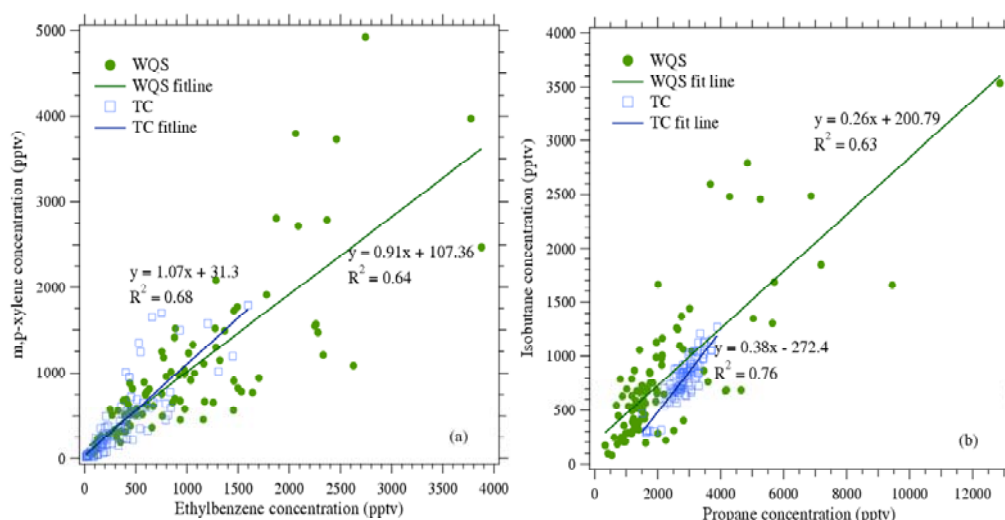


Fig.4.6. Scatter plots of (a) *m, p*-xylene to ethylbenzene (b) *i*-butane to propane at TC and WQS during the VOC sampling period.

4.5 Air mass classification with trajectories

To further investigate the regional transport of air pollutants, back trajectories were used to examine the typical air masses arriving at TC and WQS during this study period. From 25 October to 1 December, a total of 304 back trajectories (8 tracks per day) were calculated at each site, and then they were classified by using cluster analysis, which is a relatively objective method to investigate different transport patterns of air masses (Stohl, 1998). In this work, we

classified the trajectories into 3 groups at both sites by using the Hierarchical Clustering Method as shown in Fig. 4.7. The typical air mass patterns at TC and WQS were similar: the first trajectory was along the Eastern China coast (Track1); the second originated from inland China (Track 2), passing over Fujian and Jiangxi provinces; and the third (Track 3) was also from inland China, but more northerly (over Jiangxi province) and with much higher transport speeds than Track 2. The proportion of air masses associated with each track and the corresponding concentrations of air pollutants are shown in Table 4.4. At TC, the air masses were mainly from Track 1 (44%), followed by Track 3 (39%) and Track 2 (17%). By comparison, the air masses arriving at WQS were mainly from Track 2 (41%), then Track 3 (34%) and Track 1 (25%). The trajectory results confirm that the air masses arriving at the two sites were of different origins.

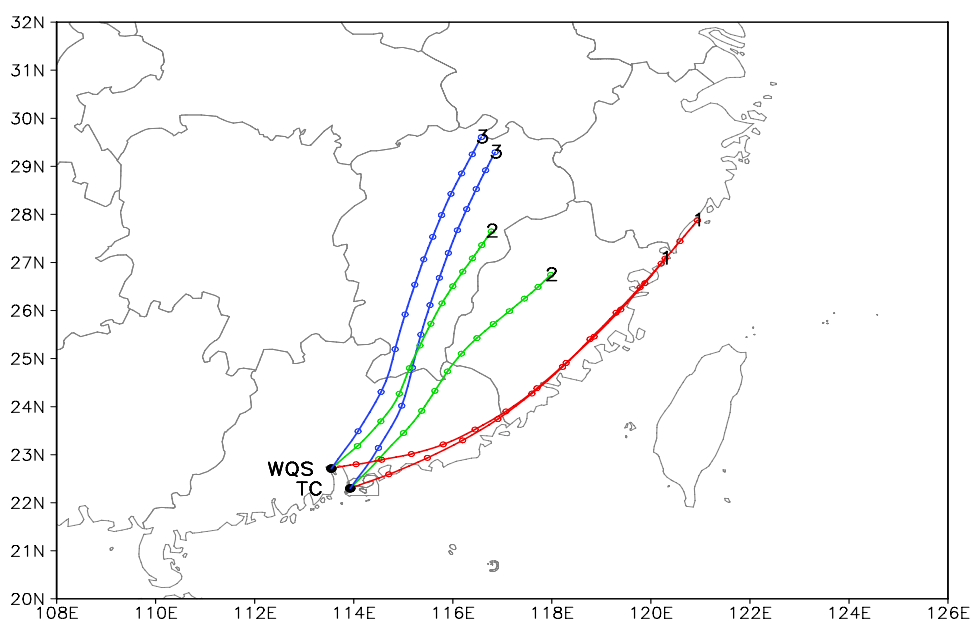


Fig.4.7. Three typical back trajectories for each site at the 200 m height level.

As anticipated at TC, air masses from Track 1 had the lowest concentrations for primary pollutants (i.e. NO_x , CO, SO_2), and those from Track 3 had the highest concentrations of trace gases ($p < 0.01$). In contrast, the mean O_3 concentration for Track 1 (35 ± 3 ppbv) was significantly higher than that for Track 3 (27 ± 3 ppbv) ($p < 0.01$). Inspecting the corresponding times of the Track 1 and Track 3 air masses, we found that the transport pathways of air masses were mainly dominated by Track 3 when the northerly monsoons were elevated, while Track 1 air masses were generally observed under fine weather conditions, i.e. with stronger solar radiation. At WQS, Track 2 air masses had the highest concentrations of NO_x (37 ± 4 ppbv) and SO_2 (38 ± 4 ppbv), which were significantly higher than the concentrations of Track 3 ($p < 0.05$). The higher NO_x and SO_2 concentrations were most likely caused by chimney emissions of the power plant in Humen town of Dongguan, because Track 2 passes over the power plant area. As was the case with TC, the air masses from Track 1 (i.e. the coastline) had the lowest concentrations of CO (894 ± 64 ppbv) compared to Tracks 2 and 3 ($p < 0.001$), and the CO concentrations from Track 2 and Track 3 had no obvious difference ($p = 0.26$), indicating strong transport influences of CO from Eastern China regions. For O_3 , there were no statistical differences among the three tracks, further suggesting that O_3 levels were dominantly affected by local production and/or sub-regional transport.

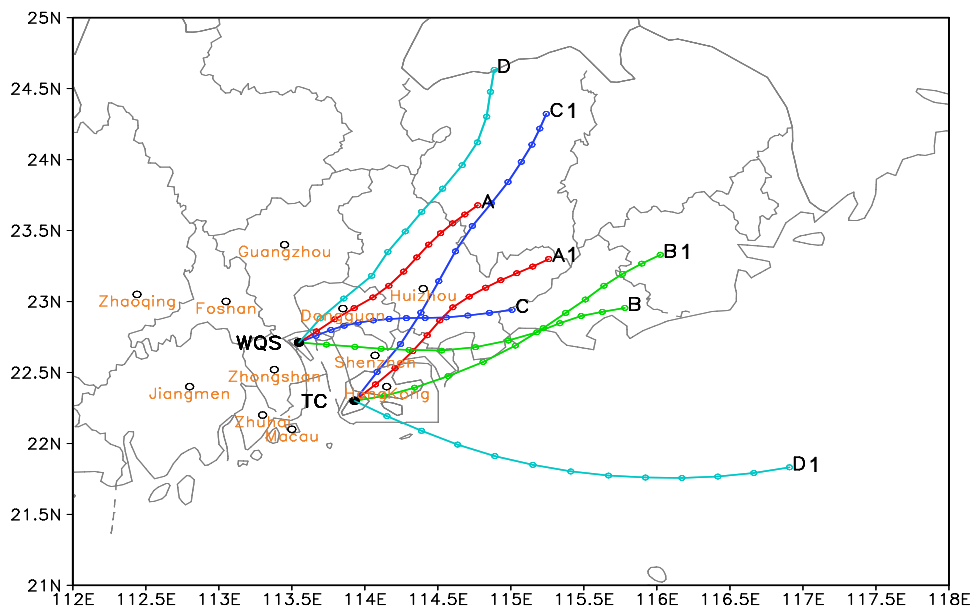


Fig.4.8. Four typical back trajectories for each site at the 50 m height level during the VOC sampling period.

In contrast to the trace gases CO , SO_2 , NO_x and O_3 , the NMHCs were manually monitored for 8 sampling days within the study period. All samples were found to originate from Track 1 and Track 2, and no samples were observed from Track 3. Furthermore, because of relatively small sample size there was no statistical difference in NMHC concentration between the two tracks at both sites ($p > 0.05$). In order to obtain a more detailed signature of NMHCs in different air masses, a much finer back trajectory analysis was conducted to better understand the influence of regional transport on NMHCs. Nine-km resolution WRF output data were used in the HYSPLIT model, and 12-hour back trajectories at a 50m height level were calculated for each hour during the VOC sampling period at both sites. Four groups of air masses were identified at each site, namely, Tracks

A1, B1, C1, D1 at TC, and tracks A, B, C, D at WQS, respectively (Fig. 4.8). The corresponding concentrations of NMHCs for each track were calculated as well (Table 4.5).

At the TC site, the air masses from Track C1 (passing over the inland region) had a higher total NMHC concentration than air masses from Tracks B1 and D1 ($p < 0.05$), which originated from the coast and the South China Sea, respectively, suggesting the significant influence of emission from the inland PRD region (mainly the northeastern part, i.e. Huizhou and Shenzhen) on NMHC levels at TC (Table 4.5). Further inspection of the anthropogenic NMHCs (i.e. alkenes, alkanes and aromatics) shows that the concentrations of alkanes for Track C1 were much higher than for Tracks B1 and D1, mainly due to the contribution of 2-methylpentane, 3-methylpentane, n-hexane, and methylcyclopentane, with mean concentrations 4–6 times those for Tracks B1 and D1. In contrast, the total NMHC concentration for Track A1 (27.8 ± 6.5 ppbv) was similar to that for Tracks B1 and D1, although Track A1 also originated from the inland region. Its value was between the levels for Track C1 (42.6 ± 12.7 ppbv) and Tracks B1 (23.2 ± 3.2 ppbv) and D1 (22.6 ± 2.1 ppbv), perhaps due to the fact that the air masses from Track A1 were intersected by air masses from the inland region and the Southern China coast. However, the concentration of alkenes for Track A1 (4.9 ± 0.6 ppbv) was significantly higher than that for Tracks B1 (3.9 ± 0.2 ppbv) and D1 (3.5 ± 0.6 ppbv).

Table 4.4. Proportion of air masses associated with each track and the corresponding concentrations of trace gases.

	Track A (1)		Track B (1)		Track C (1)		Track D (1)	
	TC	WQS	TC	WQS	TC	WQS	TC	WQS
Proportion (%)	18	55	65	9	11	24	6	12
Total NMHCs (ppbv)	27.8 ± 6.5	42.5 ± 9.2	23.2 ± 3.2	22.2 ± 7.5	42.6 ± 12.7	42.6 ± 15.1	22.6 ± 2.1	30.8 ± 6.3
Alkene (ppbv)	4.9 ± 0.6	8.2 ± 0.7	3.9 ± 0.2	5.8 ± 0.8	3.8 ± 0.8	7.7 ± 1.6	3.5 ± 0.6	8.3 ± 1.3
Alkane (ppbv)	15.6 ± 3.3	15.8 ± 1.8	14.5 ± 2.0	12.5 ± 6.1	30 ± 10.7	17.6 ± 6.1	15.3 ± 2.0	14.5 ± 3.5
Aromatic (ppbv)	6.5 ± 3.2	18.3 ± 8.7	4.0 ± 1.3	3.6 ± 1.1	6.7 ± 2.2	17.0 ± 8.5	3.7 ± 0.7	7.7 ± 2.3

*Mean ± 95% confidence interval

Table 4.5 Proportion of each air mass associated with each track and the corresponding concentrations of NMHCs during the VOC sampling period

	Track 1		Track 2		Track 3	
	TC	WQS	TC	WQS	TC	WQS
Proportion (%)	44	25	17	41	39	34
O ₃ (ppbv)	35 ± 3*	47 ± 11	31 ± 7	37 ± 7	27 ± 3	35 ± 5
NO _x (ppbv)	40 ± 5	30 ± 5	48 ± 7	37 ± 4	49 ± 4	25 ± 4
CO (ppbv)	470 ± 30	894 ± 64	648 ± 45	1232 ± 113	680 ± 37	1351 ± 153
SO ₂ (ppbv)	8 ± 1	27 ± 4	9 ± 1	38 ± 4	11 ± 1	31 ± 3
Total NMHCs (ppbv)	22 ± 5	40 ± 9	30 ± 15	30 ± 5	-	-

At the WQS site the concentrations of total NMHCs, alkanes, alkenes and aromatics in Track A were similar to those in Track C (both over Dongguan and Huizhou). The concentrations of total NMHCs for these two tracks were significantly higher than those for Track B ($p < 0.05$), which came along the coast and passed over the north of Shenzhen, indicating the influence of Dongguan and Huizhou on the WQS site. Further inspection found that the higher total NMHCs in Tracks A and C were mainly attributed to the higher aromatic concentrations. For example, the mean concentrations of toluene, ethylbenzene, *m/p*-xylene, and *o*-xylene for Track C were 3-6 times those for Track B. This result also confirms that Dongguan made a significant contribution to aromatics at WQS.

4.6 Summary

This Chapter presents the measurement data of O₃ and its precursors, i.e., CO, NO_x, and VOCs, simultaneously monitored at two sites in Hong Kong (TC) and Guangzhou (WQS) from October 23 to December 1, 2007. Thirteen O₃ episode days (>120 ppbv) were observed at WQS and only on 2 days at TC during the sampling period. O₃ episodes usually occurred when weather systems were relatively stable. Analysis of the synoptic weather conditions and variations of air pollutants indicated that high O₃ levels were mainly attributed to local photochemical production. However, significant differences in diurnal variations of air pollutants were also observed at the two sites, indicating different local and regional contributions. In particular, O₃ episodes were stronger and more

frequent at WQS than TC. Diurnal variations of O₃ showed higher nighttime levels of O₃ at TC than at WQS as well as more photochemical activity at WQS than TC.

Various air pollutant ratios (SO₂/NO_x, CO/NO_x, *m*, *p*-xylene/ethylbenzene, *i*-butane/propane) suggested that air masses arriving at TC were mainly affected by local emissions superimposed by regional transport, whereas the air at WQS was highly influenced by regional emissions and was therefore more aged. Indeed, backward trajectory analysis showed that air masses arriving at these two sites had different transport pathways. This finding was corroborated by higher wind speeds and different wind directions at TC than WQS. The back trajectories showed that air masses arriving at WQS were mainly affected by inland China, including Dongguan and Huizhou, whereas air masses arriving at TC were primarily from the East China Coast, which brought lower levels of pollutants to Hong Kong.

Chapter 5

Observation based model (OBM) evaluation on the relationship between ozone and its precursors

5.1 Introduction

Photochemical smog, characterized by high concentrations of ozone (O_3) and fine particles, is of great concern in the urban areas, in particular megacities and city clusters like the Pearl River Delta (PRD) (Chameides et al., 1992; Wang et al., 1998, 2001a; Wang and Kwok, 2003; Zhang et al., 2008). O_3 is not directly emitted into the atmosphere but is a photochemical product via a series of complex chemical reactions among volatile organic compounds (VOCs) and nitrogen oxides (NO_x) in the presence of sunlight. Although VOCs and NO_x have been confirmed as the key precursors of O_3 , the development of an effective strategy for reducing O_3 pollution in megacities is still problematic due to the nonlinear dependency of O_3 formation on NO_x and VOCs (Cardelino and Chameides, 1995; Sillman, 1999). A number of VOC groups, including alkenes, aromatics, and carbonyls, participate in the photochemical formation of O_3 . However, different VOC species react at different rates and with different reaction mechanisms. They are also emitted into the atmosphere at different mass emission rates depending on the local and regional industries, land use, and biogenic sources. Because of this, each VOC species has a different reactive potential with respect to O_3 formation. Several studies have explained that

photochemical O₃ formation is focusing on a few key VOC species with high reactivities, such as toluene, *m,p*-xylene, and isoprene (Carter, 1994; So and Wang, 2004; Chang et al., 2005).

Observation-based model (OBM), which uses measurements of ambient concentrations of O₃ and its precursors as input, is a useful tool to simulate O₃ photochemical production and destruction and to explore the ozone– precursor relationships. Several studies have been carried out using OBMs (Cardelino and Chameides, 1995; Shiu et al., 2007; Zhang et al., 2007; Zhang et al., 2008). For example, Cardelino and Chameides (1995) applied the OBM to analyze ozone–precursor relationships using the 1990 Atlanta O₃ study data. Shiu et al. (2007) studied photochemical O₃ production in southern Taiwan and found that reducing emissions of non-methane hydrocarbons (NMHCs) is more effective in controlling O₃ than reducing NO_x. By analyzing some high O₃ episode cases, Zhang et al. (2007) found that the formation of O₃ throughout Hong Kong was limited by VOCs, especially reactive aromatics, and high NO concentrations suppressed O₃ production. Recently, it was reported that photochemical production of O₃ was sensitive to VOCs at an urban site in Guangzhou and a rural site, Xinken, downwind of Guangzhou (Zhang et al., 2008). Although the latter two studies provide a view of ozone–precursor relationships using an OBM in Hong Kong and the inland PRD region, respectively, some limitations still remain. For example, it is well known that some carbonyl species, including formaldehyde, are abundant in the atmosphere due to various sources. These

carbonyls usually have relatively high photochemical reactivities (Atkinson, 1990; Carter, 1994). However, in the previous OBM studies, the contribution of carbonyls to O₃ formation was either not considered or, if considered, it was only discussed using approximate simulated carbonyl concentrations, principally due to the lack of field measurement data of carbonyls (Cardelino and Chameides, 2000; Zhang et al., 2007; Zhang et al., 2008). Moreover, previous modeling simulations were mainly based on limited daily VOC samples (five to six samples per day), although during the O₃ episode events, the concentrations of O₃ precursors, i.e., VOCs and NO_x, varied significantly with time. Hence, inadequate VOC samples collected daily for model simulation input could significantly affect the model output (Zhang et al., 2007). Most importantly, since the previous two studies were not conducted at the same time (one in 2002 and the other in 2004), the relationship of O₃ pollution between the inland PRD and Hong Kong remains unclear. Given that source emissions and source profiles of O₃ precursors in the inland PRD and Hong Kong have changed significantly due to rapid urbanization and industrialization in mainland China and implementation of control measures in Hong Kong in more recent years (Streets et al., 2006; Government, 2008; HKEPD, 2009), the contributions of VOCs and NO_x to the formation of O₃ in this region could vary significantly. As such, simultaneous measurement data of O₃ and its precursors (i.e., VOCs and NO_x) in the inland PRD and Hong Kong are urgently needed in order to improve our

understanding of the interaction between O₃ pollution in Hong Kong and the inland PRD region.

In this study, a high-quality database of O₃ and O₃ precursors was generated, on the basis of VOC samples collected concurrently in Guangzhou of the inland PRD and Hong Kong, from 23 October to 1 December 2007. Though the measurements are limited during one particular month, leaving an incomplete picture of ongoing photochemistry throughout the year, this study period represents a significant season when the prevailing autumn/winter monsoons bring polluted inland air masses to the downwind sampling sites and photochemical O₃ episode days are most frequently observed in this region.

Table 5.1. Daily maximum 1-h O₃ (ppbv) on eight O₃ episode days at WQS, and an O₃ episode day and a near-O₃ episode day at TC during VOCs sampling days

	26-Oct	27-Oct	13-Nov	15-Nov	16-Nov	17-Nov	23-Nov	1-Dec
WQS	158	91	152	182	170	176	86	109
TC	139						76	

In this chapter, we focus on O₃ episode days during the VOC sampling periods. Eight O₃ episodes encountered at WQS and an O₃ episode day and a near-O₃ episode day observed at TC during the VOC sampling campaign (Table 5.1). We first illustrate the diurnal variations of O₃ and its precursors observed at the two sampling sites during the O₃ episode days, and then the measurement data are applied in an OBM for the assessment of the ozone-precursor relationships. Thirdly, we evaluate the effect of carbonyls on O₃ photochemical production in the PRD region. Finally, we will identify the relative effects of

VOC species on O₃ formation.

5.2 Diurnal variations of O₃ and its precursors

Diurnal variations of O₃ and its precursors can provide valuable information on the interplay of emissions, chemical, and physical processes in a daily cycle (Wang et al., 2001a). Fig.5.1 shows the diurnal variations of O₃, NO, CO, and TVOCs on O₃ episode days at WQS and TC, respectively. In general, O₃ precursors exhibited different diurnal variations at WQS and TC.

At WQS, the O₃ concentrations showed typically rural diurnal variations, exhibiting broad maxima in the afternoons, with minima at nights and in the early mornings. Despite a similar trend of O₃ during the eight episode days, there were obvious day-to-day variations. For example, the O₃ concentrations showed broader maximum values on 27 October and 13 November compared to other O₃ episode days. The time when the maximum values appeared was delayed about 2 or 3 h on these two days (appeared at 1700 – 1800), though the peak O₃ concentrations were almost observed at 1400 – 1500 on other O₃ episode days. Such a feature indicated that the increased O₃ on 27 October and 13 November may be related to atmospheric transport of O₃ originating from elsewhere, as opposed to the predominately local O₃ production during other episode days. This was further confirmed by the diurnal patterns of primary pollutants and backward trajectories discussed later. At TC, the O₃ peaks were observed at ~1600, suggesting the impact of regional transport as well. Comparing the

diurnal patterns of O₃, TC showed a narrower peak in the afternoon than at WQS,

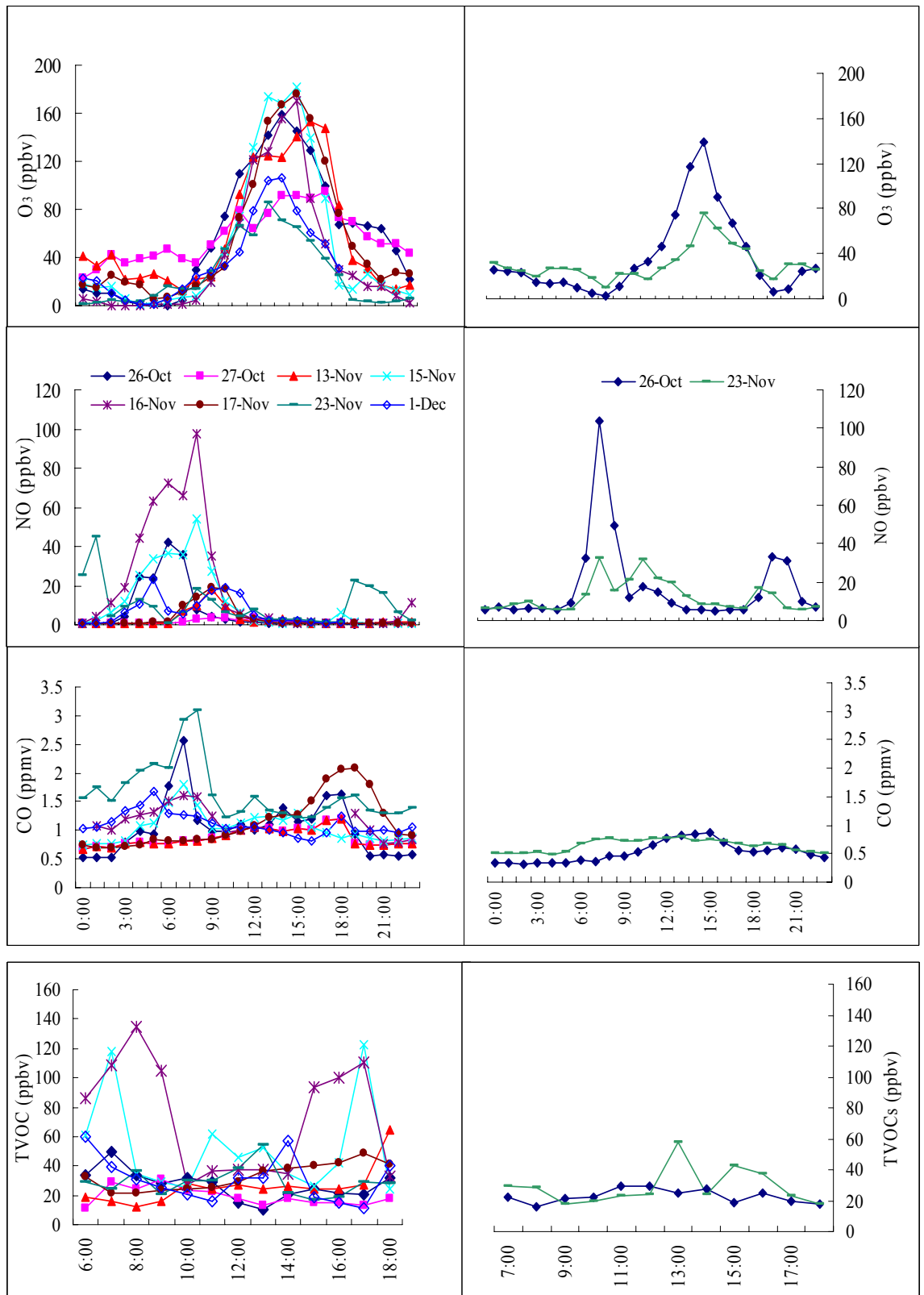


Fig.5.1. Diurnal variations of O₃, NO, CO, and TVOC on O₃ episode days at WQS and TC

reflecting that the impact of regional transport was more significant at WQS than at TC. The much lower O₃ levels during morning hours (700 – 900) and in the evening (1900 – 2100) coincided with very high levels of NO, indicating strong titration of O₃ by freshly emitted NO at TC.

At WQS, except for on 27 October and 13 November, NO concentrations quickly increased to peak values after sunrise and then rapidly decreased to near zero in the afternoon and evening due to being consumed in the photochemical reactions, deposition, and cessation of photolysis of NO₂ after sunset. The pattern is consistent with those observed in the southeastern US and Cape D' Aguilar, Hong Kong (Kleinman et al., 1994; Wang et al., 2001a). At TC, NO showed two peaks on O₃ episode days, featuring a typical urban diurnal pattern (Chameides et al., 1992; Wang et al., 2001a). The first peak appeared through rush hours in the early morning (700 – 900). The other appeared around late evening and early night (1800 – 2100).

Different from the flat patterns observed on 27 October and 13 November, CO displayed high concentrations in early morning and late afternoon and low concentrations in the afternoon on other O₃ episode days at WQS. The first peak appeared in the morning (700 – 900), and the second appeared in late afternoon (1700 – 1900). This pattern was similar to those observed in urban areas such as Nanjing in China and Bangkok Metropolitan in Thailand (Zhang and Kim Oanh, 2002; Tu et al., 2007). The lower CO concentrations in early afternoon were likely due to photochemical consumption, vertical dilution, and a lower traffic

fleet volume. The CO diurnal pattern at TC differed from that at WQS. The CO concentrations on the two episode days did not show large diurnal variations, reflecting the impact of regional transport.

Peak values of the average TVOC concentrations were observed in the morning and in late afternoon on most of the O₃ episode days at WQS. At noon, the decrease in the TVOC concentrations was probably due to the increased reaction with OH radicals, increased mixing height of the planetary boundary layer, and less emission of VOCs. At TC, the diurnal variations of TVOCs did not show a distinct pattern on 26 October, but two peaks were seen in the afternoon on 23 November, perhaps attributed to the regional transport of air masses on 26 October and local emissions with high TVOC concentrations during noontime on 23 November.

In summary, the diurnal variations of O₃ and its precursors, i.e., NO, CO, and TVOC, showed different features on 27 October and 13 November from those on other O₃ episode days at WQS. On these two days, the O₃ concentrations showed broader maximum, whereas NO, CO, and TVOCs did not exhibit distinct urban diurnal patterns, which were observed for the other O₃ episode days. This suggests that O₃ and its precursors on the two days mainly originated from atmospheric transport, contrary to the predominantly local O₃ production on other O₃ episode days. At TC, the diurnal variations of O₃ and its precursors suggested that the influence of local emission/ production and regional transport on the levels of different trace gases was different. NO showed two peaks on O₃

episode days, attributed to local emissions, while the diurnal variations of CO concentrations implied the impact of regional transport.

5.3 Observation-based model (OBM)

At a certain site, the ground-level O₃ may be either produced locally via photochemical processes and/or result from atmospheric transport of O₃ produced elsewhere. The OBM calculates only the locally produced O₃ such that the derived relative incremental reactivity (RIR) functions refer to local O₃ production. Significant limitation will not occur with the OBM when local production dominates the total observed O₃ increment. However, the application of the OBM may be limited when the derived local production is significantly smaller than the observed O₃ increment, under which scenario an important contribution of regional transport may exist. Therefore, by balancing the net O₃ production calculated by the OBM and actual O₃ increment, the relative contributions of local photochemical O₃ production and regional transport of O₃ can be determined (Cardelino and Chameides, 1995; Zhang et al., 2007).

An internal test was first used to confirm that the application of the OBM to this study is appropriate. At WQS, the standard error (SE) of the mean for the day averaged RIRs are relatively small for the relevant O₃ precursor. Here, the SE for TVOC is 0.0010, for NO is 0.0077, and for CO is 0.0002, suggesting that the calculated RIRs are robust.

5.3.1 Hourly primary production of carbonyls

Carbonyls are direct precursors of O₃ through peroxy radical reactions (HO₂ and RO₂) and RC(O)O₂, which arise from the oxidation of CO and VOCs by hydroxyl radicals (OH), nitrate radicals (NO₃), halogen atoms, and O₃ (Atkinson, 1990; Lary and Shallcross, 2000). Carbonyls such as formaldehyde have both primary sources, i.e., automotive exhaust and biomass burning, and secondary formation by the photooxidation of NMHCs, both natural and man-made (Penkett, 1988). While the distinction between primary and secondary carbonyls is not important in an emission-based model (EBM), which calculates concentrations from emissions, it is of critical importance in the OBM where observations of primary carbonyls are used to drive the simulation. Although the refined carbon bond 4 mechanism splits the carbonyls into primary and secondary function groups in the OBM, previous OBM studies did not consider the contribution of carbonyls to O₃ formation or used approximately simulated concentrations of carbonyls to estimate the contribution. In previous studies, the carbonyls were not split into primary and secondary function groups, mainly due to the lack of field measurement data (Cardelino and Chameides, 1995, 2000; Zhang et al., 2007; Zhang et al., 2008). Therefore, the net O₃ production could be significantly underestimated. Here, we studied the effect of carbonyl compounds on O₃ formation by inputting the observed primary carbonyl values into the OBM. As formaldehyde, acetaldehyde, and acetone were the major species among the measured carbonyls at WQS and TC, only these three carbonyls were

included in this study.

The measured concentrations of carbonyls include both primary and secondary source contributions. Only the fraction of primary carbonyls needs to be considered as input for the OBM calculations, and the concentrations of secondary carbonyls, produced via photochemical reactions of hydrocarbons, are calculated in the OBM as a function of time by integrating the appropriate continuity equations. Hence, it is essential to fractionate the primary carbonyls in the measured values so that we could estimate the relative contribution of primary carbonyls to photochemical O₃ formation. Here, we use a simple and new method to fractionate the measured carbonyls. Using CO as a tracer, the correlations between CO and these carbonyls in roadside and/or tunnel samples were calculated. In this way, the ratio of an individual carbonyl to CO, i.e., $\mu = [HCHO]_T/CO$, can be obtained. Here, $[HCHO]_T$ is the concentration of carbonyls emitted from primary sources, i.e., vehicular exhaust.

In the atmosphere, formaldehyde, acetaldehyde, and acetone are mainly emitted from traffic (T) and generated in photochemical reactions (P). Therefore, the ambient concentration of formaldehyde, for example, can be described by the following equation:

$$[HCHO] = [HCHO]_T + [HCHO]_P \quad (5.1)$$

By introducing the carbonyl/CO ratio μ ($\mu = [HCHO]_T/[CO]$, primary sources) into Eq. (5.1), the photochemical fraction was given by:

$$\frac{[HCHO]_P}{[HCHO]} = 1 - \mu \frac{[CO]}{[HCHO]} \quad (5.2)$$

where $[HCHO]$ and $[CO]$ are the formaldehyde and CO concentrations measured in ambient air. Equations 5.1 and 5.2 also apply to acetaldehyde and acetone.

To obtain the μ value, we considered two methods for the estimation. (1) Using the ambient air samples: In the ambient air, carbonyls originate from primary and secondary sources, while CO totally comes from primary sources. In the urban area such as Hong Kong, it is reasonable to assume that both primary carbonyls and CO share the same source, i.e., vehicular exhaust. The μ values were obtained by averaging the minimum ratios of each individual carbonyl to CO every day. At WQS, the average μ values for formaldehyde, acetaldehyde, and acetone were 0.0079 ± 0.0017 , 0.0032 ± 0.0012 , and 0.0023 ± 0.0011 (mean \pm 95% C.I.), respectively. At TC, the average μ values for formaldehyde, acetaldehyde, and acetone were 0.0074 ± 0.0013 , 0.0029 ± 0.0005 , and 0.004 ± 0.001 , respectively. (2) Using the tunnel samples: Carbonyls and CO were measured simultaneously at Shing Mun Tunnel, Tsuan Wan in 2003 and 2004 (unpublished data). As the source of carbonyls and CO in the tunnel was almost exclusively vehicular exhaust, the μ values can be simply obtained by averaging the ratios of an individual carbonyl to CO in each sample. The average μ value for formaldehyde, acetaldehyde, and acetone was 0.0086 ± 0.001 , 0.0024 ± 0.0003 , and 0.001 ± 0.0004 , respectively. By comparing the two methods, the μ values were comparable except for acetone. Among the three carbonyls, acetone has the longest lifetimes for removal by photolysis and OH reaction,

approximately 40 and 20 days in the atmosphere, respectively (Atkinson, 2000). Hence, the effect of acetone concentration on O₃ formation is relatively small compared to formaldehyde and acetaldehyde. The difference of the two μ values for acetone/CO would not significantly influence the final results.

We used the minimum [HCHO]/[CO] ratio of the ambient air samples as the μ value in the analysis. Thus, the hourly concentrations of the primary carbonyl, HCHO, can be determined from Eq. 5.3 below:

$$[\text{HCHO}]_{\text{T}} = \mu \times [\text{CO}] \quad (5.3)$$

where the μ value for formaldehyde was 0.0079 at WQS and 0.0074 at TC. Equation 5.3 also applies to acetaldehyde and acetone. To further confirm the μ values, we calculated the fraction of photochemical carbonyl productions at both sites by Eq. 5.2. The proportions of secondary carbonyl production were ~20 – 30% in the early morning and ~70 – 85% at noon. These values agreed well with those reported for Beijing and Rome (Possanzini et al., 2002; Pang and Mu, 2006).

5.3.2 OBM-calculated net O₃ production with and without carbonyls

[Fig.5.2](#) shows the OBM-calculated net O₃ production and observed O₃ increment at WQS for the eight O₃ episode days, both with and without carbonyl input. The observed O₃ increment is defined here as the difference between the peak O₃ concentration and the early morning O₃ concentration. In general, the net

O₃ production calculated by the OBM agreed better with the observed O₃ increment after hourly carbonyl concentrations were included. Especially for three of the eight O₃ episode days (i.e., 26 October, 16 November, and 23 November), the net O₃ production calculated by the OBM was readily comparable to the observed O₃ increment. The percentage difference between the model-derived O₃ production and observed O₃ increment ((observed O₃ increment – net O₃ production)/ observed O₃ increment) was 13% on 26 October, 8% on 16 November, and 18% on 23 November, respectively. The results indicated that a significant portion of O₃ observed at WQS could be explained by photochemical production on the three days. This is consistent with the observed diurnal patterns of O₃ on these days, which showed a relatively sharp peak in early afternoon (Fig. 5.1).

However, there was a big difference between the net O₃ production calculated by the OBM and the observed O₃ increment on 27 October and 13 November, respectively (Fig. 5.2). On 27 October, the OBM-calculated net O₃ concentration (114 ppbv) is much higher than the observed O₃ increment (44 ppbv), probably due to the fact that locally photochemically formed O₃ concentrations at WQS were diluted by clean marine air from the South China Sea. Indeed, on that day, the prevailing wind switched from northeasterly to southeasterly. In contrast, on 13 November, the OBM-calculated net O₃ concentration was significantly less than the observed O₃ increment ($\Delta O_3=162$ ppbv), indicating that the transport of O₃ produced elsewhere to WQS may play

an important role. To further investigate the contribution of regional transport to O_3 formation, backward trajectory was used to determine the possible transport pathways of air masses. The back trajectories were calculated using NOAA-HYSPLIT4.8 model for 3-h intervals, driven by the hourly output data of weather research and forecasting model. More details of the model description can be found in chapter 3 in this thesis. Twelve-hour backward air masses for both sites (WQS and TC) were obtained at the ending point of 200 m above sea level (Fig. 5.3). As shown in Fig. 5.3, the air masses arrived at WQS mainly passed over South China Sea on 27 October and Dongguan city (an important industrial center in PRD) on 13 November, respectively. The backward trajectory results confirmed the above speculation on the basis of OBM simulations. The results are also consistent with the findings derived from the diurnal variations of O_3 and its precursors (see Fig. 5.1).

Furthermore, the OBM-calculated net O_3 concentrations were still lower than the observed O_3 increments on 15 November, 17 November, and 1 December, even though the carbonyl concentrations were included. On the basis of the observed diurnal patterns of O_3 on these days, O_3 was likely generated by local photochemical reactions. In other words, the difference between the model-derived O_3 concentration and the observed O_3 increment is not attributed to regional transport on these days. The potential attributes to the difference might be due to high HONO concentrations on these days, which were not measured for input of the OBM model. Similarly to carbonyls, HONO at high

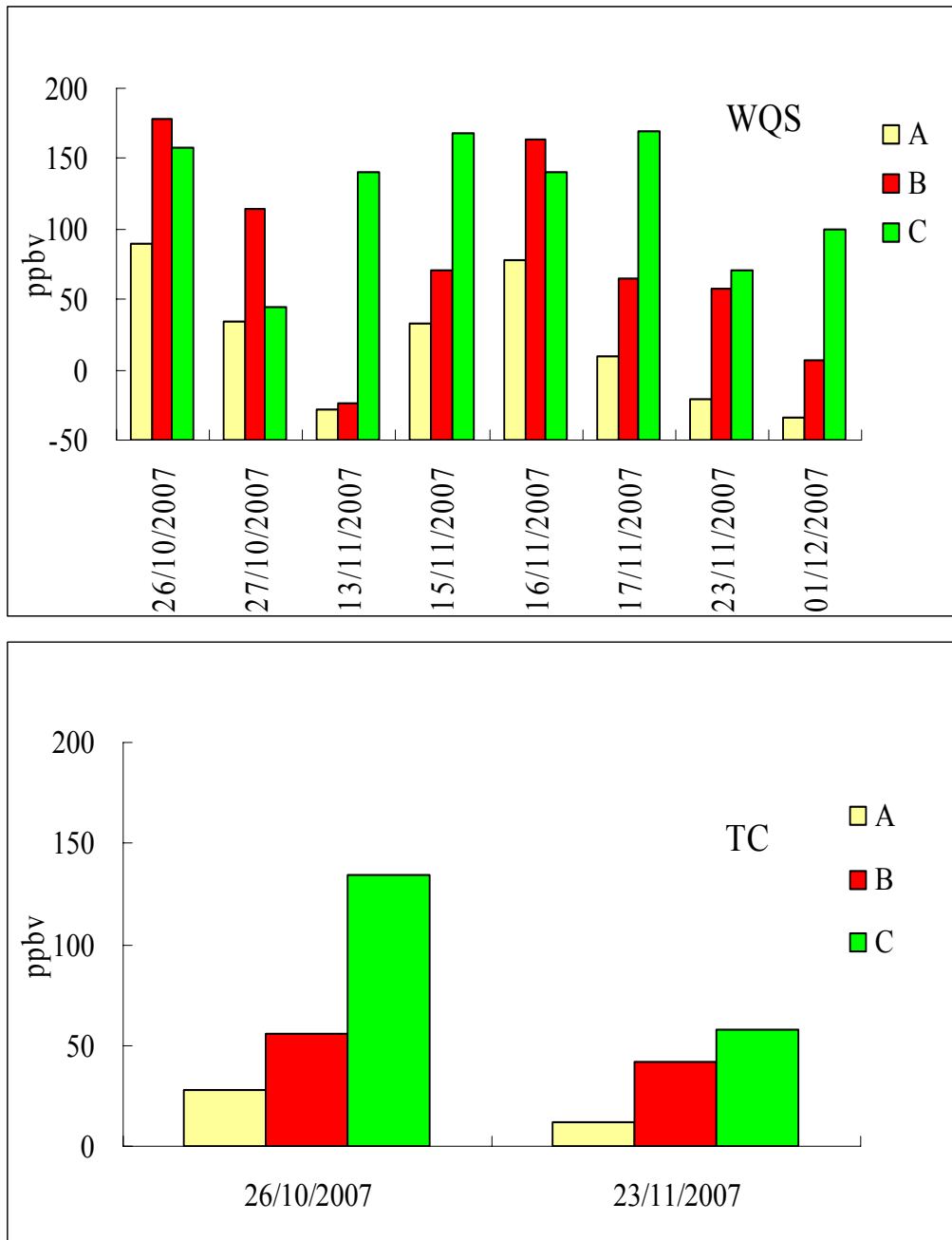


Fig.5.2. Comparison of net photochemical O₃ production calculated by the OBM with the observed O₃ increments at WQS (top) and TC (bottom). A represents OBM derived values without carbonyls; B represents OBM derived with carbonyls; C represents observed increment.

levels makes a significant contribution to photochemical O₃ formation. On the other hand, when carbonyls were excluded from the OBM, the agreement between the modeled net O₃ production and the observed O₃ increment significantly deteriorated, suggesting that carbonyls were important VOCs in O₃ photochemical production. For example, on 15 November, the agreement between the modeled net O₃ production and the observed O₃ increment improved by 23% after the hourly primary carbonyl concentrations were included in the model. At TC of Hong Kong, only one O₃ episode day (26 October; peak value, 139 ppbv) and one near-O₃ episode day (23 November; peak value, 75 ppbv) were encountered during the campaign. The percentage difference between the model-derived O₃ production with carbonyls and the observed O₃ increment were 58% on 26 October and 24% on 23 November, respectively. The results indicated that regional transport likely made a significant contribution to the observed O₃ concentration on 26 October, whereas local O₃ production was dominant on 23 November. These speculations were confirmed by the backward trajectory results (Fig. 5.3), which showed that most air masses particularly those at noon originated from the inland PRD on 26 October, whereas air masses on 23 November mainly passed over Hong Kong. The findings are also consistent with the field observations described above (Fig. 5.2).

One of the major motivations for this concurrent two-site experiment was to study the interaction of air masses between the two sampling sites. The backward trajectory results suggest that air masses at WQS may not have impact on the air

at TC, while the air masses at WQS passed over TC before arrival on some days, as shown in Fig. 5.3. A more detailed analysis using backward particle release simulation on a multi-day O₃ episode event observed on 9 – 17 November was illustrated in Guo et al. (2009).

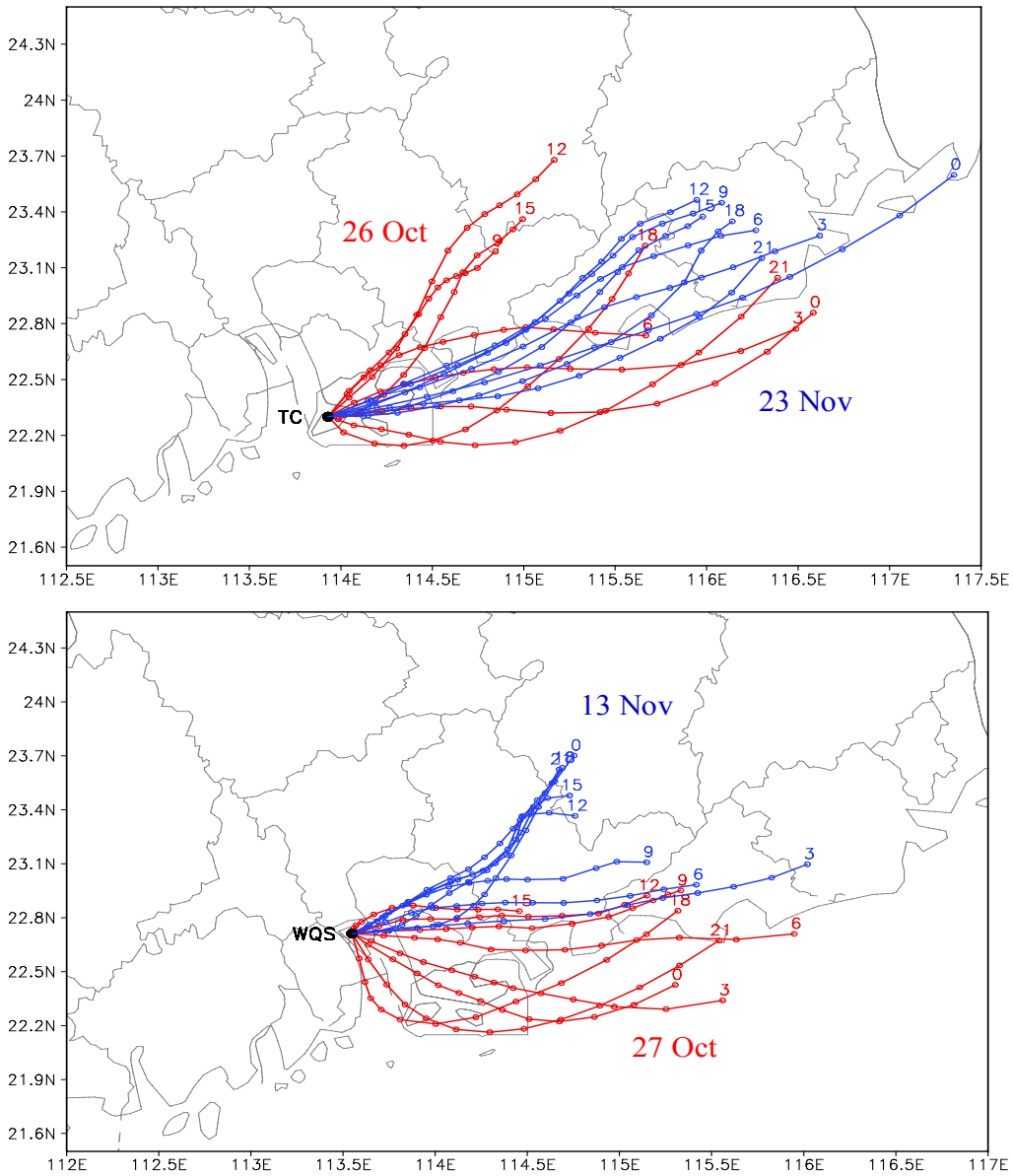
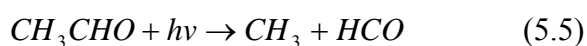


Fig.5.3. Back trajectories of air masses with 3 hours interval arrived at WQS (27 Oct and 13 Nov) and TC (26 Oct and 23 Nov)

As shown in chapter 4 in this thesis (Fig.4.2 and Fig.4.3), there was severe multi-day O₃ pollution at WQS with daily maximum O₃ levels exceeding 100 ppbv for 9 days. However, at the TC site, the O₃ episodes were only observed on the first three days (i.e., 9–11 November). Briefly, the results from the particle release simulations showed that at the TC site, there was more inland transport on the first several days, particularly from the nearby Shenzhen urban area, and then the transport pathway of the air masses turned more easterly from the inland to the coast. Under such situations, TC became downwind of the Hong Kong urban area, whereas the WQS site was consistently downwind of Dongguan and Huizhou. Hence, with the condition of strong solar radiation, high anthropogenic emissions from this area (i.e., Dongguan, Shenzhen and Huizhou) caused high photochemical pollution for the entire period at WQS and the first three days at TC, suggesting that the cross-boundary transport of air pollution from the PRD region, particularly from eastern PRD, could play a significantly important role in the photochemical pollution in western Hong Kong in autumn.

5.3.3 Impact of carbonyls on HO₂ and P_{O₃-NO}

The photolysis of HCHO and CH₃CHO in the atmosphere is an important primary source of HO₂ radicals via the following reactions (Atkinson, 1990):



The effects of carbonyls on HO₂ and P_{O₃-NO} can be illustrated by comparing the simulated HO₂ and P_{O₃-NO} with carbonyl included to the case without carbonyl input. The difference between the cases with and without carbonyls can be interpreted as the carbonyl contribution. As O₃ episodes were observed simultaneously on 26 October at WQS and TC, the corresponding chemistry involved in this O₃ episode was compared to highlight the similarities and differences of HO₂ and P_{O₃-NO} between the two sites.

As shown in [Fig. 5.4](#), adding carbonyls leads to a larger increment in both simulated HO₂ concentrations and P_{O₃-NO}. In fact, the P_{O₃-NO} peak increased by 64% at WQS and 47% at TC, and the HO₂ peak increased by 43% at WQS and 39% at TC, respectively. The results highlight the importance of carbonyls in the photochemistry in this region. When we compared simulated HO₂ concentrations and P_{O₃-NO} at WQS with those at TC, it is clear that WQS had a higher HO₂ level and a higher P_{O₃-NO} production rate, suggesting that local photochemical O₃ production was more significant at WQS than that at TC.

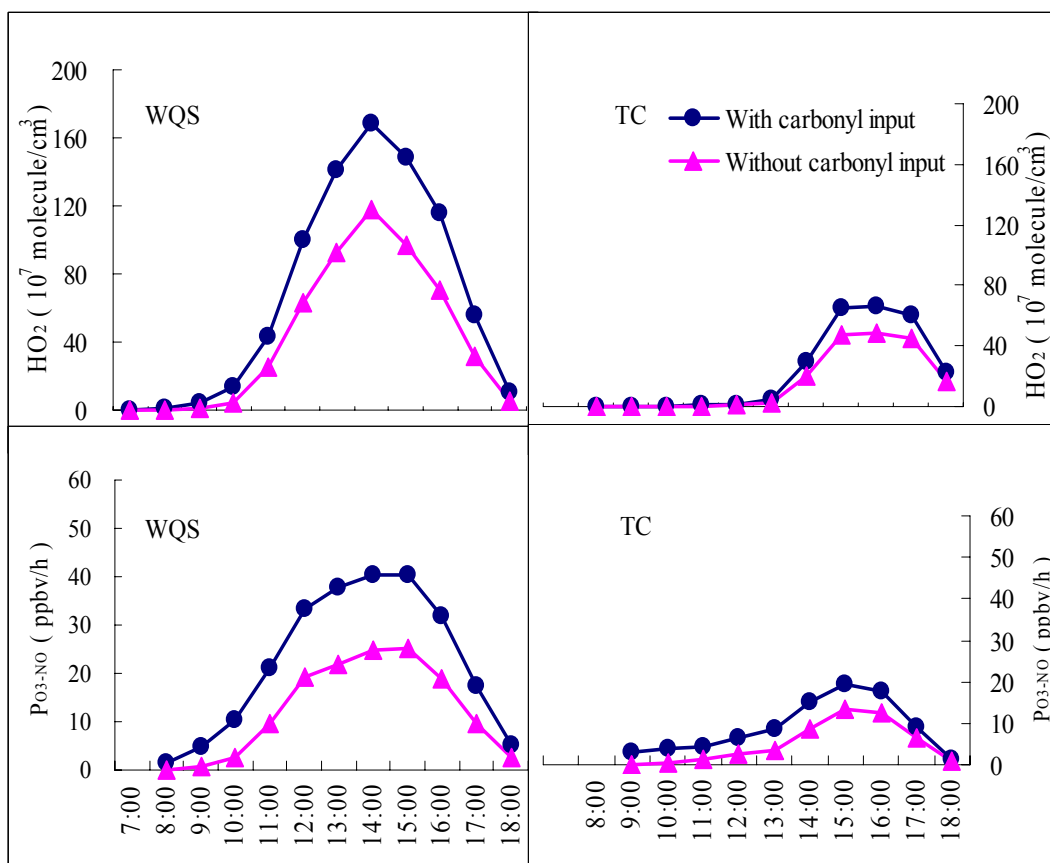


Fig. 5.4. Model simulated HO₂ and P_{O₃-NO} with and without carbonyl input on 26 October at WQS (left) and TC (right)

5.4 Ozone–precursor relationships

Data of the eight episode days at WQS and two days at TC were used to calculate the sensitivity of O₃ production to changes in the precursor concentrations, i.e., RIR. The O₃ precursors were divided into four major groups: anthropogenic hydrocarbons (AHC) including primary carbonyls, biogenic hydrocarbons (BHC, defined as isoprene and pinenes), NO, and CO. Figure 5.5 shows the RIRs for O₃ precursors at the two sites during O₃ episodes. It was found that O₃ production was VOC-limited at both sites. AHC groups showed the highest RIRs, meaning that the AHC was the most important group in O₃

production, while the RIRs of BHC and CO were positive but small. On all episode days at both sites, except for 17 November, NO was negatively correlated with O₃ production, indicating that reducing NO at both sites would lead to an increase in O₃ production. This result is consistent with those observed by other studies in Guangzhou and Hong Kong (Zhang et al. 2007; Zhang et al. 2008). It is interesting to note that at TC, the RIRs for O₃ precursors on 26 October were much smaller than those on 23 November, even though the observed O₃ concentrations on 26 October (maximum value, 139 ppbv) were much higher than those on 23 November (maximum, 75 ppbv), reflecting the fact that reducing O₃ pollution through reduction of VOC emissions on 23 November would be more effective than on 26 October. This gave further evidence that regional transport of O₃ played an important role on 26 October and local O₃ production was dominant on 23 November.

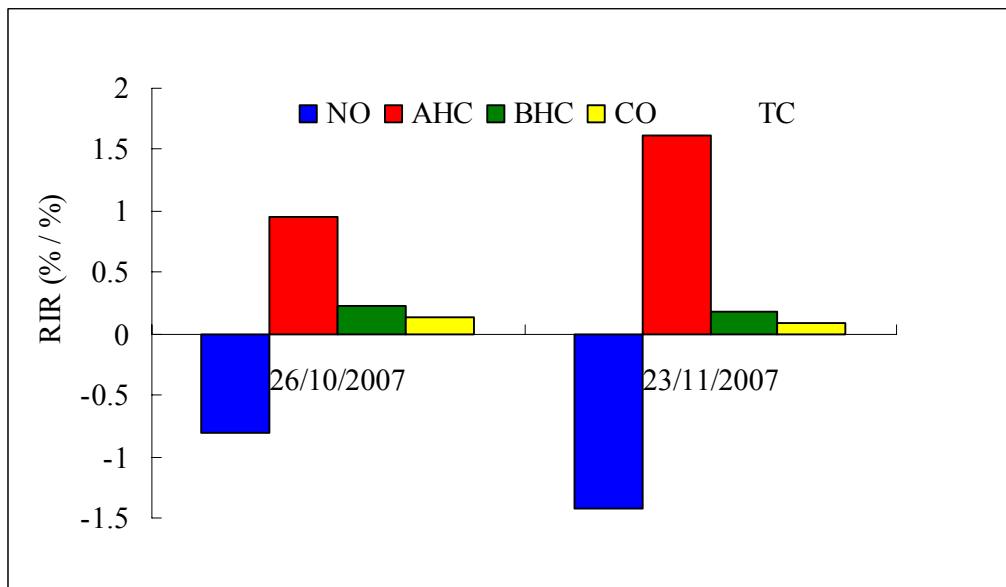
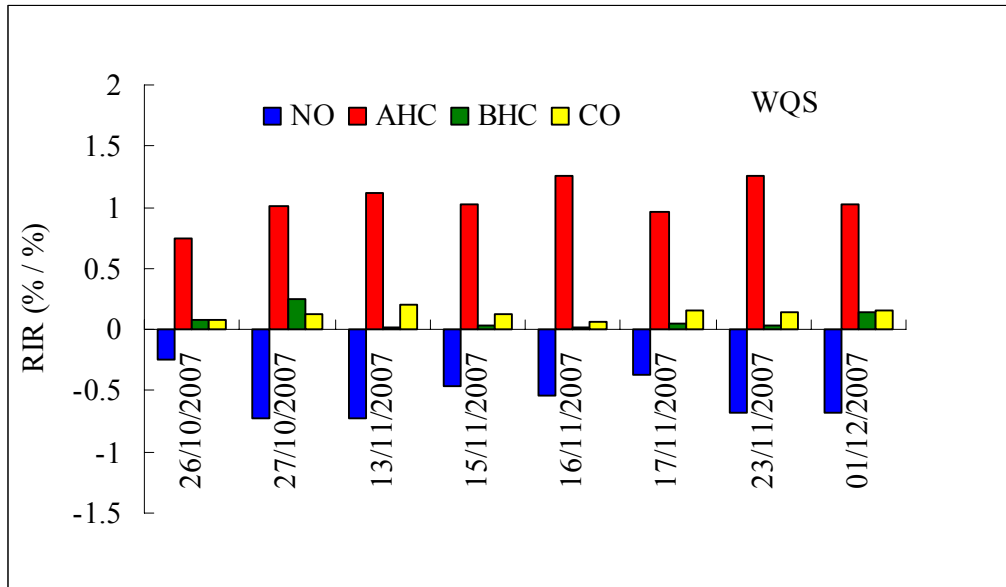


Fig. 5.5. RIRs for O₃ precursors at WQS and TC.

5.5 The relative effects of VOC species on O₃ formation

To further investigate the relative importance of various VOC species in the control of O₃ formation, contributions of individual VOCs were calculated using the RIR in the OBM on the basis of carbon bond IV mechanism. Figure 5.6 shows the top 12 VOC species with the highest RIR at TC and WQS, respectively. Though a total of 60 VOC species were identified at WQS and TC, the summed RIR of the top 12 compounds accounted for 89% of the total RIR (VOCs) at WQS and 85% at TC, respectively, reflecting that local photochemical O₃ formation can be mainly attributed to a small number of VOC species. At WQS, primary formaldehyde had the highest RIR among all the VOC species and aromatic compounds such as *m,p*-xylene, toluene, and *o*-xylene also showed high RIR, while at TC, primary formaldehyde, acetaldehyde, isoprene, *m,p*-xylene, ethene, 1-butene, and toluene were the dominant precursors with high RIR values. These results are consistent with previous studies which found that aromatics were the main contributors in Taiwan and PRD region (Chang et al., 2005; Zhang et al., 2007; Zhang et al., 2008). However, alkanes including propane, butanes, and alkenes, which are associated with liquefied petroleum gas leakage, made a significant contribution to O₃ production in Mexico City and Santiago (Blake and Rowland, 1995; Chen et al., 2001). The relatively higher RIR of aromatics and lower RIR of C₂ - C₃ olefins at WQS compared to those at TC suggested that the control strategies on O₃ between the inland PRD and Hong

Kong should be different.

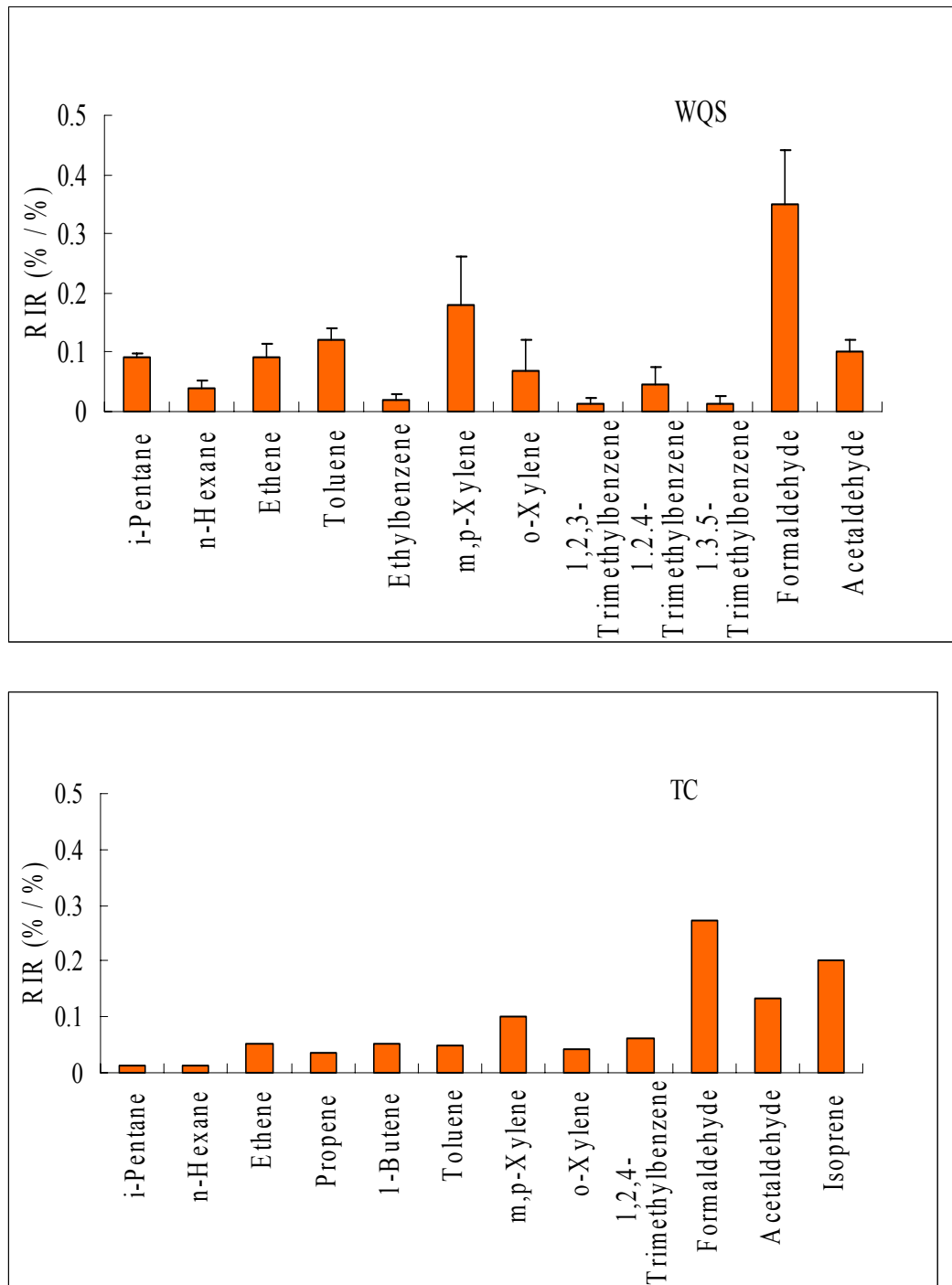


Fig.5.6. Average RIR values for individual VOC species at WQS and TC

To investigate sources in the two areas of the PRD region, a principle component analysis (PCA) was performed. The PCA analysis was performed by using SPSS statistical software packages. The principle of PCA is to transform the original set of variables into a smaller set of linear combinations that account for most of the variance of the original set. In general, varimax rotation is applied to the components to make the results clearer (Guo et al., 2004, 2007).

23 species out of the 61 measured VOCs were chosen for PCA analysis since they were the key species responsible for the O₃ formation and were typical tracers of various emission sources. Tables 5.2 and 5.3 showed the PCA results for WQS and TC, respectively. Six factors were extracted from the classified data at both sites. At WQS, the first factor (F1) was associated with solvent usage, as toluene, *o*-xylene, ethylbenzene, *m/p*-xylene, and trimethylbenzenes are all main components of solvent usage (Borbon et al., 2002). The pollutants in F2 were associated with petrochemical industry but not related to LPG usage. Because not only propane, n-butane, and iso-butane have high factor loadings in F2, n-heptane and n-hexane also have high factor loadings in F2. In F3, high factor loadings of ethane, ethene, benzene indicated the existence of combustion sources such as vehicular emissions and/or biomass/biofuel burning. Given that this site was a rural site, biomass/biofuel burning was likely dominated in the F3. *n/i* - Pentanes are known to be tracers of gasoline evaporation (Morikawa et al., 1998), so F4 was associated with gasoline evaporation. F5 was related to biogenic emissions with high factor loading for isoprene. Primary formaldehyde

and acetaldehyde are highly correlated with the sixth factor (F6), indicating the contribution of vehicle emission.

Table 5.2 PCA results for selected NMHCs and CO at WQS

	F1	F2	F3	F4	F5	F6
Formaldehyde						0.95
Acetaldehyde						0.83
Propane		0.90				
<i>n</i> -Butane		0.89				
<i>i</i> -Butane		0.91				
<i>n</i> -Pentane				0.81		
<i>i</i> -Pentane				0.93		
<i>n</i> -Hexane		0.87				
<i>n</i> -Heptane		0.57				
Ethene			0.82			
Propene		0.58				
<i>1,3</i> -Butadiene		0.74				
Isoprene					0.88	
Ethyne			0.71			
Benzene		0.47	0.66			
Toluene	0.65					
<i>o</i> -xylene	0.98					
Ethylbenzene	0.96					
<i>m/p</i> -Xylene	0.99					
<i>1,2,3</i> -Trimethylbenzene	0.97					
<i>1,2,4</i> -Trimethylbenzene	0.97					
<i>1,3,5</i> -Trimethylbenzene	0.88					
% of variance	34.41	19.28	8.76	7.43	6.02	5.36
Cumulative %	34.41	53.69	62.44	69.87	75.89	81.25
Source	Solvent usage	Petrochemical industry	Biomass/biofuel emission	Gasoline evaporation	Biogenic emission	Vehicular emission

Table 5.3 PCA results for selected NMHCs and CO at TC

	F1	F2	F3	F4	F5
Formaldehyde		0.92			
Acetaldehyde		0.83			
Propane				0.93	
<i>n</i> -Butane				0.76	
<i>i</i> -Butane				0.89	
<i>n</i> -Pentane			0.80		
<i>i</i> -Pentane			0.64		
<i>n</i> -Hexane			0.75		
<i>n</i> -Heptane	0.87				
Ethene		0.74			
Propene		0.73			
<i>1,3</i> -Butadiene		0.55			
Isoprene					0.87
Benzene	0.68				
Toluene	0.88				
<i>o</i> -Xylene	0.83				
Ethylbenzene	0.40				
<i>m/p</i> -Xylene	0.82				
<i>1,2,3</i> -trimethylbenzene		0.81			
<i>1,2,4</i> -trimethylbenzene		0.92			
<i>1,3,5</i> -trimethylbenzene		0.65			
% of variance	31.21	28.54	12.45	11.69	6.54
Cumulative %	31.21	59.75	72.20	83.89	90.43
Source	Solvent usage	Vehicular emission	Gasoline evaporation	LPG usage	Biogenic emission

At TC, high factor loadings of benzene, toluene, *o*-xylene, ethylbenzene, and *m/p*-xylene in F1 indicated solvent usage. The VOC species associated with F2 were likely vehicular emissions because primary formaldehyde and acetaldehyde, 1,2,3-trimethylbenzene, 1,2,4-trimethylbenzene, and 1,3,5-trimethylbenzene had high factor loadings in F2. The pollutants associated with F3 were predominant of gasoline evaporation due to high factor loadings of *n*-butane and *n* / *i* – pentanes. In F4, high factor loadings were found for propane, *n*-butane, and isobutene. These compounds are mainly from the use of LPG. It is no doubt that F5 was associated with biogenic emissions.

The PCA results indicated that *m,p*-xylene, toluene, and *o*-xylene were mainly emitted from the evaporation of solvent usage at WQS, consistent with a previous study conducted at Xinken of Guangzhou (Zhang et al., 2008), whereas at TC, the sources of aromatics such as 1,2,4-trimethylbenzene, and C2 – C3 olefins were likely attributed to vehicular emission. Other aromatics like *o*-xylene, ethylbenzene, and *m/p*-xylene are mainly from solvent usage.

Overall, combining the PCA results with the OBM simulations, it was found that solvent usage and vehicular emission were the major sources of reactive VOCs at WQS, while vehicular emissions, solvent usage and biogenic emissions made significant contributions to reactive VOCs at TC. Therefore, by controlling the VOC emissions from solvent usage and vehicular emissions, the photochemical O₃ pollution in the study region would be significantly reduced.

5.6 Summary

This chapter focuses on O₃ episode days during the VOC sampling periods at two sites in Hong Kong (TC) and Guangzhou (WQS) from October 23 to December 1, 2007. Eight O₃ episodes encountered at WQS and an O₃ episode day and a near-O₃ episode day observed at TC during the VOC sampling campaign. The results indicate that O₃ pollution at WQS was more serious than that at TC. The high O₃ concentrations in this region were attributed to local photochemical formation and/or regional transport.

An OBM was developed to assess the ozone-precursor relationships as well as determine the relative contributions of different VOC species, particularly carbonyls, to photochemical O₃ production. The net O₃ production derived from the OBM agreed better with the observed O₃ increment after hourly carbonyl concentrations were included. When adding carbonyls to the OBM, the derived P_{O₃-NO} peak increased by 64% and 47%, and the HO₂ peak increased by 43% and 39% at WQS and TC, respectively. These results highlight the importance of carbonyls in the photochemistry in this region.

The OBM-derived RIRs support O₃ production being VOC-limited at WQS and TC, respectively. The AHC group showed the highest RIR, while BHC and CO showed positive but small RIRs. NO was negatively correlated with O₃ production, indicating that reducing NO would lead to an increase in O₃ production. Among the VOC species, primary formaldehyde had the highest RIR. Aromatics such as *m,p*-xylene, toluene, and *o*-xylene also showed high RIR at

WQS. Primary formaldehyde, acetaldehyde, isoprene, *m,p*-xylene, ethene, 1-butene, and toluene were the dominant precursors with high RIR at TC. The summed RIR of the top 12 compounds accounted for 89% of the total RIR (VOC) at WQS and 85% at TC, respectively, suggesting that local photochemical O₃ formation was mainly attributed to a small number of VOC species. The results from OBM and PCA analyses suggest that controlling the VOC emissions from solvent usage and vehicular emissions would likely reduce the photochemical O₃ pollution in the PRD region.

Chapter 6

Photochemical trajectory modeling of ozone (O₃) formation in the PRD region

6.1 Introduction

In chapter 5, we used an observation-based model (OBM) to investigate the O₃-precursor relationships, and the relative contribution of individual volatile organic compound (VOC) species to O₃ formation in the PRD region. The results showed that O₃ formation was VOC-limited at a rural site (WQS) in Guangzhou, and a suburban site (TC) in Hong Kong. Among the VOC species, primary formaldehyde, *m,p*-xylene, toluene, and *o*-xylene had the highest contribution to O₃ formation at WQS. Primary formaldehyde, acetaldehyde, isoprene, *m,p*-xylene, ethene, 1-butene, and toluene were the dominant precursors to O₃ at TC. Since the OBM uses observed concentrations to simulate the O₃ formation at WQS and TC, the results will be relatively site-specific. On the other hand, as the OBM is a diagnostic rather than prognostic, it should be viewed as a supplement, rather than a substitute, to more sophisticated emission-based models. To evaluate the OBM results, and deeply understand which specific VOCs contribute most to O₃ formation in the PRD region, a photochemical trajectory model will be used to simulate the photochemical O₃ formation in the PRD region in this chapter.

It is well documented that ground level O₃ formation is caused by reactions

of the key precursors of VOCs and nitrogen oxides (NO_x) in the presence of sunlight (Sillman, 1999). Most previous studies have shown that O_3 production is VOC-limited in the PRD region (Zhang et al., 2007; Zhang et al., 2008; Cheng et al., 2009). For example, Zhang et al. (2007) found that the formation of O_3 throughout Hong Kong was limited by VOCs, and high NO concentrations suppressed O_3 production. The reactivity of VOCs was dominated by anthropogenic VOCs. Of the anthropogenic VOCs, reactive aromatics dominated, of which xylenes and toluene were the most important species. Zhang et al. (2008) reported that photochemical O_3 production was sensitive to VOCs at an urban site in Guangzhou and a rural site, Xinken, downwind of Guangzhou. Hence a greater understanding of which specific VOCs contribute most to O_3 formation in the region is important for developing effective control strategies. VOCs as a group include many hundreds of species, and each one reacts at different rate and with a different reaction mechanism. For example, the initial reaction rates of VOCs with the OH radical vary by factors of 10,000, and their different molecular structures of VOCs mean that they possess intrinsically different potentials for photochemical O_3 formation. Furthermore, they are also emitted into the atmosphere at different mass emission rates, depending on the local and regional industries, land-use and biogenic sources. Hence, the relative contribution of VOCs to the photochemical O_3 formation varies from one compound to another (Atkinson, 1990; Carter, 1994) and from region to region (Derwent et al., 1996; Chang et al., 2005; Cheng et al., 2009).

To understand regional O₃ pollution and develop effective strategies to control O₃ formation, computer modeling using detailed descriptions of the chemical degradation mechanism, emission inventories, and meteorological conditions has been effectively employed (Utembe et al., 2005; Derwent et al., 2007a). A photochemical trajectory model (PTM), using the Master Chemical Mechanism (MCM), has been used to simulate photochemical O₃ formation and other secondary oxidant generation in Europe (Derwent et al., 1996, 1998; Evtyugina et al., 2007; Pinho et al., 2009). An index, the photochemical ozone creation potential (POCP), was developed to determine the contribution of each VOC to the regional O₃ formation in north-west Europe. The POCP for a particular VOC is determined by quantifying the effect of a small incremental increase in its emission on O₃ formation along the trajectory, relative to that resulting from an identical increase in the emission (on a mass basis) of a reference VOC, which is taken to be ethene (Saunders et al., 2003). Ethene is a suitable VOC species to normalize the POCP values because it is one of the most important O₃ precursors with medium reactivity towards hydroxyl radical, and its chemical degradation processes are also well-defined. POCPs are available in the literature from earlier studies in Europe (Derwent and Jenkin, 1991; Carter, 1994; Derwent et al., 1996, 2003). For example, Derwent et al. (1996) described the O₃ production from the oxidation of methane and 95 other VOCs in air parcels advected across north-west Europe. Aromatic and olefinic hydrocarbons showed the highest POCP values, and halocarbons showed the lowest. Complimentary

work in the USA by Carter (1990) defined maximum incremental reactivity (MIR) as the amount of O₃ (grams) formed per gram of VOC emitted in an urban area. This work also showed that aromatics and alkenes had the highest MIR values. Although regional VOC and NO_x emissions vary significantly, recently available observations and emissions inventory data coupled with the local meteorology in the PRD region have enabled the development of a detailed chemical model to assess O₃ formation in the region. For example, a number of intensive field sampling campaigns of air pollutants including O₃ and its precursors, and laboratory experiments of emission profiles of VOC sources have been conducted in the PRD region in recent years (Wang et al., 1998; Wang and Kwok, 2003; Liu et al., 2008; Zhang et al., 2008; Guo et al., 2009; Zheng et al., 2010). A detailed emission inventory of air pollutants in Asia including the study region has been developed by Streets et al. (2003) initially for the Transport and Chemical Evolution over the Pacific (TRACE-P) mission undertaken in 2000, and updated by Zhang et al. (2009) for the Intercontinental Chemical Transport Experiment – Phase B (INTEX-B) conducted in 2006. Zheng et al. (2009) recently developed a highly resolved temporal and spatial PRD regional emission inventory for 2006 with the use of newly available domestic emission factors and local activity data. These measurement data and emission inventories provide a solid base to this study for the development of a detailed chemical model in the PRD region.

A comprehensive field measurement campaign was simultaneously carried

out at a non-urban site in inland PRD (WQS) and an urban site (TC) in Hong Kong from October to December 2007, in order to better understand the photochemical smog problem in this region. Using this data set, the causes of a multi-day O₃ episode were analyzed in detail (Jiang et al., 2010). In addition, the spatiotemporal variability of O₃ pollution and the impact of regional transport were overviewed (Guo et al., 2009), and the seasonal profiles and annual trends of halocarbons were examined (Zhang et al., 2010).

In this study, a photochemical trajectory model - employing the most updated version of a near-explicit photochemical mechanism (extended MCM v3.1) describing the oxidation of methane and 139 non-methane VOCs - was developed to simulate the formation of photochemical pollutants observed at the WQS rural site in Guangzhou during a photochemical pollution episode between 12 and 17 November, 2007. The PTM was applied under a near-realistic situation in south-east China under anticyclone conditions. We aimed to identify which VOC species, and hence which emission source categories, are likely to contribute most to regional scale O₃ formation in south-east China.

In this chapter, we firstly compare the simulated and observed pollutant mixing ratios at WQS, and then we simulate the reactivity of individual VOCs by calculating their individual POCP. Finally, we identify which VOC species and emission source categories were likely to contribute most to regional scale O₃ formation in the PRD region, with the aim of assisting local management strategies and comparing with other regional air sheds.

6.2 Photochemical trajectory model (PTM)

6.2.1 Model description

The detailed description of the model has been included in the chapter 3, i.e., methodology part. The transport process within the PTM is defined using backward trajectory path analysis. In this study, the respective backward trajectories over a 72-hr period arriving at WQS, Tung Chung (TC), and Central/Western (C/W) were calculated using NOAA-HYSPLIT4.8 (Draxler and Rolph, 2003) for 1 hour intervals at the ending point of 200m above sea level. The hourly output data of the Weather Research and Forecasting (WRF) model was used to drive the model. WRF was run in two nested domains with grid spacings of 36km and 12km. The finest domain covers south-east China. Grid nudging was adopted in the outmost domain to minimize integration errors. More details of the model description can be found in Jiang et al. (2008). WRF simulation was conducted for air parcel arrival times at the three sites of 0000, 0300, 0600, 0900, 1200, 1500, 1800 and 2100 hr during the period of 12–17 November 2007, with three-hour resolution for the entire sampling campaign.

6.2.2 Master chemical mechanism

The chemical mechanism employed in the photochemical trajectory model is an extended version of the MCMv3.1, which is a near-explicit chemical mechanism describing the detailed degradation of a large number of emitted

organic compounds and the resulting generation of O₃ and other secondary pollutants under conditions appropriate to the atmospheric boundary layer (Jenkin et al., 1997). It currently describes the oxidation of methane and 139 non-methane VOCs, which contains around 13,500 reactions involving 5,900 chemical species. The MCM can be accessed via the University of Leeds website (<http://mcm.leeds.ac.uk/MCM>).

The system of differential equations in the model is integrated with a variable order Gear's method within the FACSIMILE software suite (Curtis and Sweetenham, 1987). The initial mixing ratios for the majority of VOC species in the model are set to 0.5 ppb and for a small number of species, initial mixing ratios are set up for typical autumn conditions associated with photochemical pollution episodes in South-east China, as follows: O₃ (20 ppbv), NO₂ (20 ppbv), CO (600 ppbv), methane (1.79 ppm), ethane (4.0 ppbv), propane (3.5 ppbv), ethene (3.5 ppbv), propene (0.6 ppbv), ethyne (4.5 ppbv), toluene (5.0 ppbv), *m,p*-xylene (2.5 ppbv), formaldehyde (5.0 ppbv) (Guo et al., 2004c, 2007; Barletta et al., 2005; Wang et al., 2008). In order to evaluate the impact of initial VOC mixing ratios on the model simulation results, a sensitivity test of the PTM model was carried out by setting up the initial mixing ratios of the majority of VOC species (except those listed above) to each of the following values: 0.0 ppbv, 0.25 ppbv, 0.5 ppbv, 0.75 ppbv, and 1 ppbv, respectively. The percentage variation of the simulated O₃ concentration concentrations was approximately 0.5-1.1% among the five different initial concentrations, indicating that the

variations in the initial modeled VOC concentrations have no significant influence on simulated results.

6.2.3 Emission inventories

The anthropogenic emission inventory employed in this study was got from the website http://www.cgrer.uiowa.edu/EMISSION_DATA_new/index_16.html, which is the INTEX-B inventory of 2006 (Zhang et al., 2009) . It is one of the most comprehensive and updated analyses of anthropogenic emissions in south-east China. The INTEX-B inventory, with a resolution of $0.5^{\circ} \times 0.5^{\circ}$ and unit of ton/year, includes six major source categories: power plants, industry, residential biofuel, residential fossil fuel, residential non-combustion, and transportation.

The biogenic VOC (BVOC) emissions used in this study are calculated from the Model of Emissions of Gases and Aerosols from Nature (MEGAN v2.04), which is defined as the MEGAN emission inventory (Guenther et al., 2006). MEGAN is a global biogenic emission model, and is designed for both global and regional emission modeling with a global coverage of about 1 km^2 spatial resolution. Only emissions of isoprene, α -pinene and β -pinene obtained from the MEGAN were used in the PTM as these three species accounted for the majority of the total BVOC emission in the region.

In addition to the above emission inventories, a 2006-based PRD emission inventory ($21^{\circ}27'47''$ - $23^{\circ}56'13''$ N and $111^{\circ}59'50''$ - $115^{\circ}24'48''$ E, exclusive of

Hong Kong and Macau) developed by Zheng et al. (2009) and an emission inventory for Hong Kong compiled by Hong Kong Environmental Protection Department (HKEPD) were also used in this study. The two emission inventories for the year of 2006, with a high resolution of 3×3 km, were compiled with newly available domestic emission factors and local activity data. These two inventories include six major categories i.e. power plants, industry, mobile sources, VOC product-related sources, biogenic sources and biomass burning.

For the target area, the allocation of total VOC emissions from a source to each VOC is obtained by applying a source profile database to each source category. The speciation profiles for each source category were drawn from two major information sources: a source profile database including vehicle exhaust, gasoline vapor, paint, asphalt, industrial and residential coal burning, biomass burning, and the petrochemical industry (Liu et al., 2008a), and the USEPA SPECIATE 4.2 database (USEPA, 2008, <http://www.epa.gov/ttn/chief/software/speciate/>, a database of total organic compounds' profiles for a variety of sources). The overall emission amount of each VOC in this study is thus obtained by multiplying the species profile of a specific source category by the total VOC emission for the same source category, and summing the emissions of the specific VOC from the major source categories. To couple with the master chemical mechanism, the anthropogenic VOC emissions from each source category were allocated to the 139 VOC species, which accounted for $93 \pm 5\%$ of the total emissions, taking into

consideration that some emitted chemical species do not appear in the chemical mechanism (MCM v3.1).

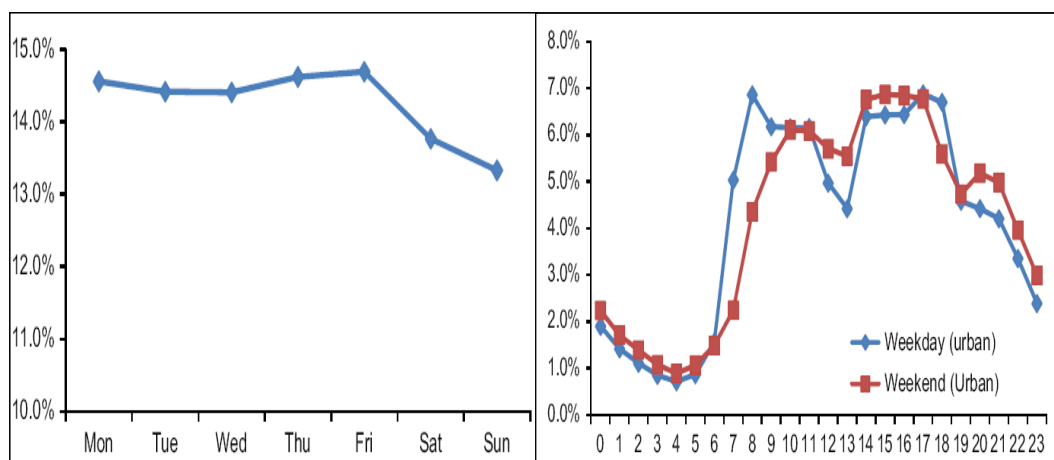


Fig 6.1. Weekly profile of on-road sources

Fig 6.2. Diurnal profile of on-road sources

A literature review was undertaken to determine the temporal variations of each source category of the INTEX-B inventory in the PRD region (Liu et al., 2008a; Zheng et al., 2009). For example, the temporal variations applied to the emissions of anthropogenic VOCs and NO_x were identified in the PRD region by Zheng et al. (2009). In that study, temporal variations including monthly, weekly, and diurnal patterns were investigated for power plant, industrial and on-road mobile sources. Figs. 6.1 and 6.2 illustrate the weekly and diurnal variations of on-road mobile source emissions based on traffic flows in the PRD region. For the weekly variations, it showed that there were no obvious variations of traffic flows during the weekdays except Monday and Friday when slightly higher traffic flows were observed. Significant decreases of traffic flows were found on weekends. For the diurnal variations, two traffic peaks were observed in the

morning (7:00-9:00) and evening (17:00-18:00) on both weekdays and weekends.

For the biogenic VOC emissions, the seasonal and diurnal variations of biogenic VOCs used in the PTM were mainly obtained from Tsui et al. (2009) in Hong Kong. Estimated BVOC emissions were the highest in July due to high temperature and strong solar radiation; and the lowest in February as a result of relatively low temperature and weak sun light (Fig.6.3). For the diurnal variations of isoprene, its emission is mainly affected by sunlight and temperature. Hence its emission only occurs at daytime hours (Fig.6.4). on the other hand, total monoterpene emissions are temperature dependent but independent of light. Therefore, emissions of these compounds were estimated to occur throughout the daytime hours at steady rates (Tsui et al., 2009).

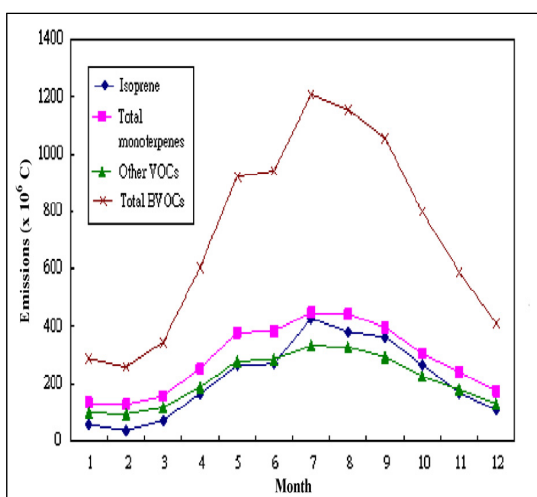


Fig.6.3.Monthly variations of estimated BVOC emission

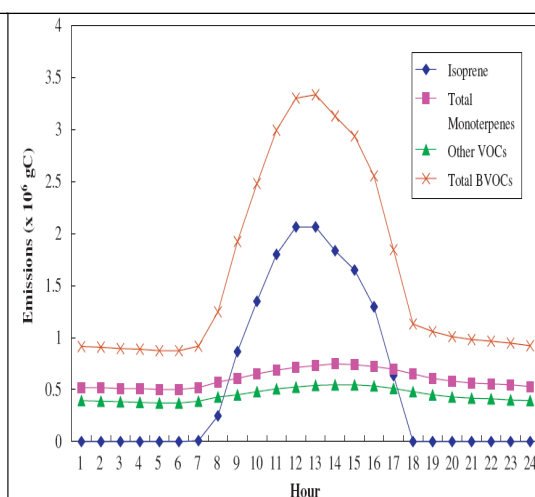


Fig.6.4.Diurnal variations of estimated BVOC emission

6.2.4 Meteorological and air quality data used in the PTM

The main observational data used to evaluate model performance were taken

at WQS in Guangzhou (Fig.1). Details about the site are described in the Chapter 3 (Methodology).

To further evaluate model performance, measured data from urban Hong Kong air quality monitoring stations were also used (<http://epic.epd.gov.hk/ca/uid/airdata>). The selected stations are TC and C/W. TC (22°18'N, 113°56'E) is a residential site located on northern Lantau Island of Hong Kong, which is a newly-developed residential town. The C/W station (22°17'N, 114°08'E) is located at the northwest of Hong Kong Island and represents a typical Hong Kong urban site, which is influenced by residential and traffic emission sources.

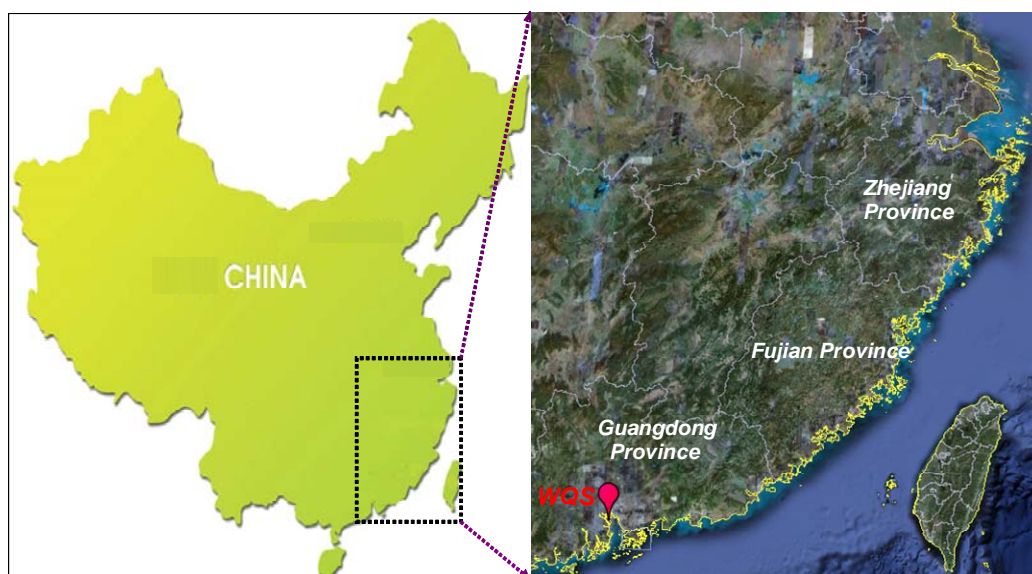


Fig.6.5. Location of sampling site in Guangzhou, China (WQS).

6.3 Comparison of simulated and observed data

To evaluate the model performance, the simulated pollutant mixing ratios

were compared with those observed at WQS (Fig. 6.6). The simulated NO_x showed reasonable agreement with the observed values on most of the days except on the 15 and 16 November ($R^2=0.44$). The observed peak NO_x mixing ratios in the morning (i.e. 8 a.m.) were 108 ppbv and 128 ppbv on the 15 and 16 November, respectively, while the simulated NO_x mixing ratios at 8 a.m. were only 51 ppbv and 63 ppbv, respectively. The difference may be attributed to chimney emissions of upwind power plants in Humen town of Dongguan, where the air masses had passed over in these two days, and/or the high vertical gradient of NO_x due to the fact that the PTM assumes that pollutants are completely mixed in the vertical direction. Another important factor for the difference may be related to the uncertainties in the 2006-based PRD emission inventory, which showed that there was medium to high uncertainty for the NO_x emission and high uncertainty for VOC and CO emissions (Zheng et al., 2009).

For O₃, the model simulated the diurnal variations very well, and the correlation coefficient (R^2) of simulated values with observed O₃ mixing ratios was 0.80 ($p < 0.05$), indicating that together the PTM and combination of boundary layer trajectories, precursor emissions and chemical processing provided a reasonable description of O₃ formation in the PRD region. However, the simulated mixing ratios were generally higher than the observed values during the sampling periods with peak value differences ranging from 0.9 to 16%, especially in the afternoon, the simulated O₃ mixing ratios did not decline as rapidly as the observed O₃ values. The overestimation of the simulated mixing

ratios might be partially due to the fact that no horizontal dispersion was considered in this model.

The model simulation was based on the combination of the 2006-based PRD emission inventory (3×3 km), MEGAN emission inventory and the INTEX-B inventory (0.5° × 0.5°). The simulation results using highly resolved 3×3 km emission inventory were closer to the observed data than those only based on the INTEX-B and MEGAN emission inventories (here $R^2 = 0.02$, $p = 0.31$ for NO_x , $R^2=0.78$, $p < 0.05$ for O_3). The large difference of predicted NO_x mixing ratios between different horizontal grid resolutions indicates that different resolutions of precursor emissions have a significant impact on model simulations.

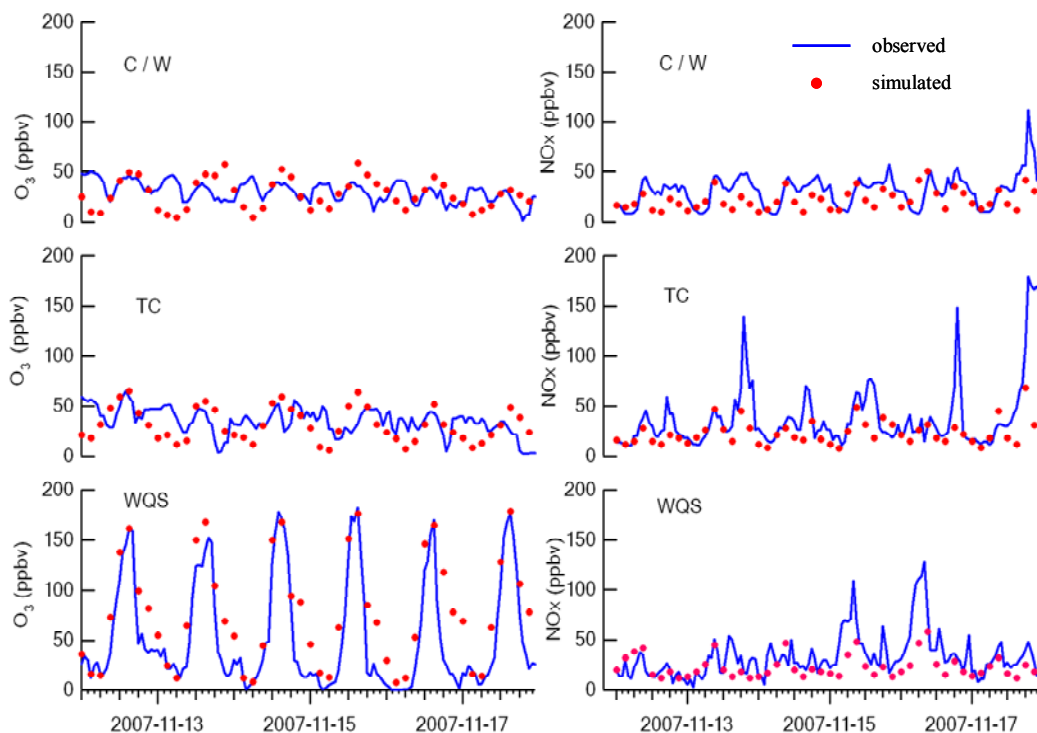


Fig.6.6. Comparison of simulated (red dots) and observed (blue lines) O_3 and NO_x concentrations at WQS, TC, and C/W from November 12-17, 2007.

To further evaluate the performance of the PTM, comparison of the simulated O₃ and NO_x with measured data at other locations (i.e. TC and C/W) in the PRD region during the 12-17th of November was conducted. The model simulation was generally able to capture the diurnal O₃ variations and exhibited good agreement with measurements. For example, the correlation coefficient (R²) of simulated values with observed O₃ mixing ratios was 0.68 ($p < 0.05$) and 0.59 ($p < 0.05$) at C/W and TC, respectively (Fig. 6.6). During the period, the weather conditions showed a typical phenomenon which is common in the autumn season. Namely, the weather is sunny, and the sky is cloudless, and air mass movements from both North China and South China Sea are weak, which leads to a fairly stable weather system. In response to the common meteorological conditions in Hong Kong, the observed O₃ mixing ratios generally remained at a low level of about 40 ppbv at the two sites between 12 and 17 November, 2007.

In summary, the above results indicated that the PTM can provide a reasonable description of O₃ formation in both O₃ episode and non- O₃ episode days in the PRD region. It should be noted that an exact agreement between simulated and observed mixing ratios is unrealistic because of the absence of vertical and horizontal dispersion in the PTM. However, the model simulation results can guide control strategies for photochemical oxidants under typical meteorological conditions with elevated O₃ mixing ratios over PRD region.

6.4 Contribution of individual VOCs to O₃ formation

6.4.1 The base case model experiment to calculate the POCP values

Fig. 6.7 shows the backward trajectories of air parcels whose arrival time at WQS was 3 p.m. from 12 to 17 November, 2007. On all days the air masses originated from Zhejiang province and passed through Fujian province including Fuzhou, except for 12 November when the air mass crossed Jiangxi province including Shangrao. The air mass then passed over Guangdong province including Huizhou, Shenzhen and Dongguan, and eventually arrived at WQS on all days. Almost all the air masses had similar pathways to the receptor site during the photochemical pollution episode days when a relatively high-pressure system was formed in south-east China, corresponding to an anticyclonic flow structure over the region. This was accompanied by successive days of high temperatures (around 27 °C), long hours of sunshine, weak wind speed (lower than 1.0 m s⁻¹) and nearly cloudless skies, favorable to the formation of photochemical smog (Fig.6.8). These meteorological features have been frequently associated with elevated O₃ mixing ratios in the PRD region (Wang et al., 1998; Wang and Kwok, 2003; Lam et al., 2005).

As a typical case for studying regional scale O₃ formation, a backward trajectory from 13 November (3 p.m. arrival time at WQS) was selected to determine the contribution of each VOC to the photochemical O₃ formation. This

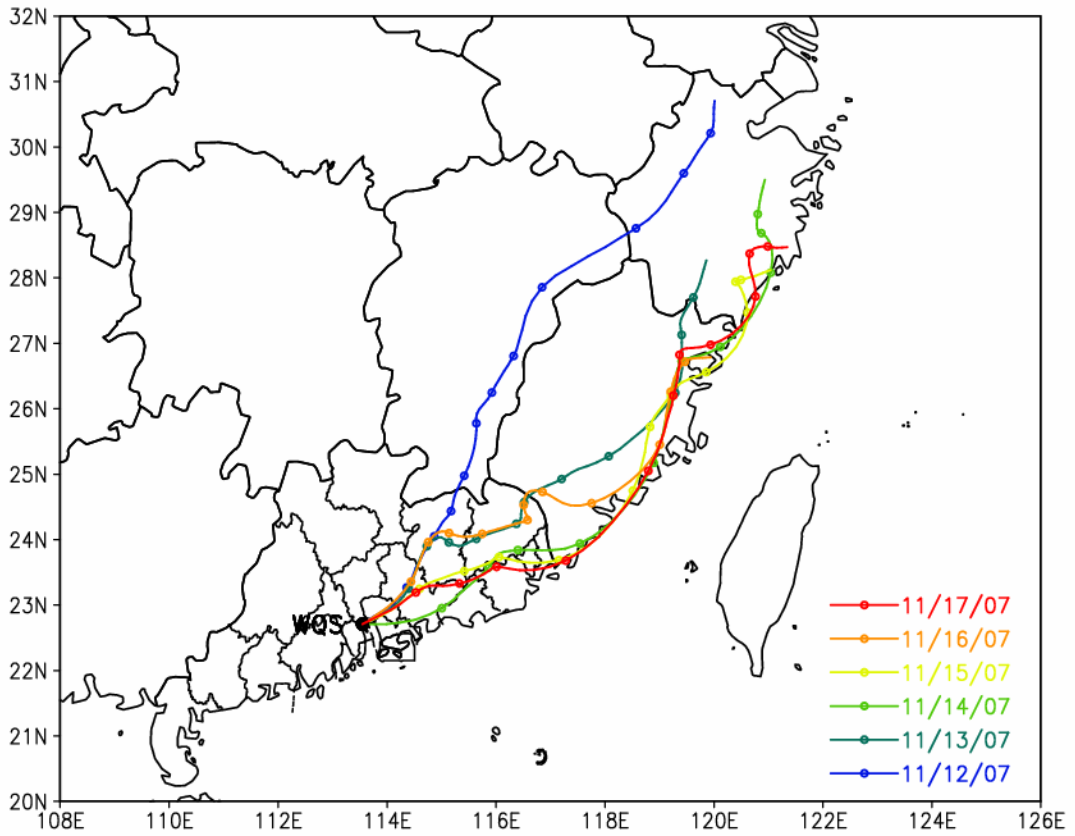


Fig.6.7. Backward trajectories of air parcels whose arrival time at WQS was 3 p.m. from 12-17 November, 2007.

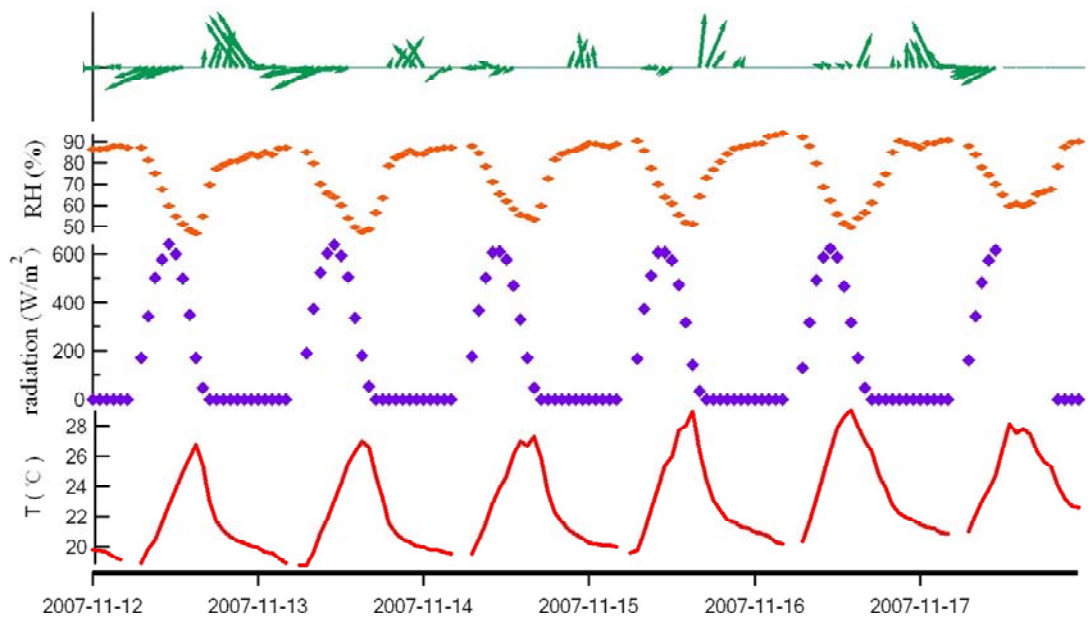


Fig.6.8. Temporal variations of meteorological parameters at WQS between 12 and 17 November, 2007.

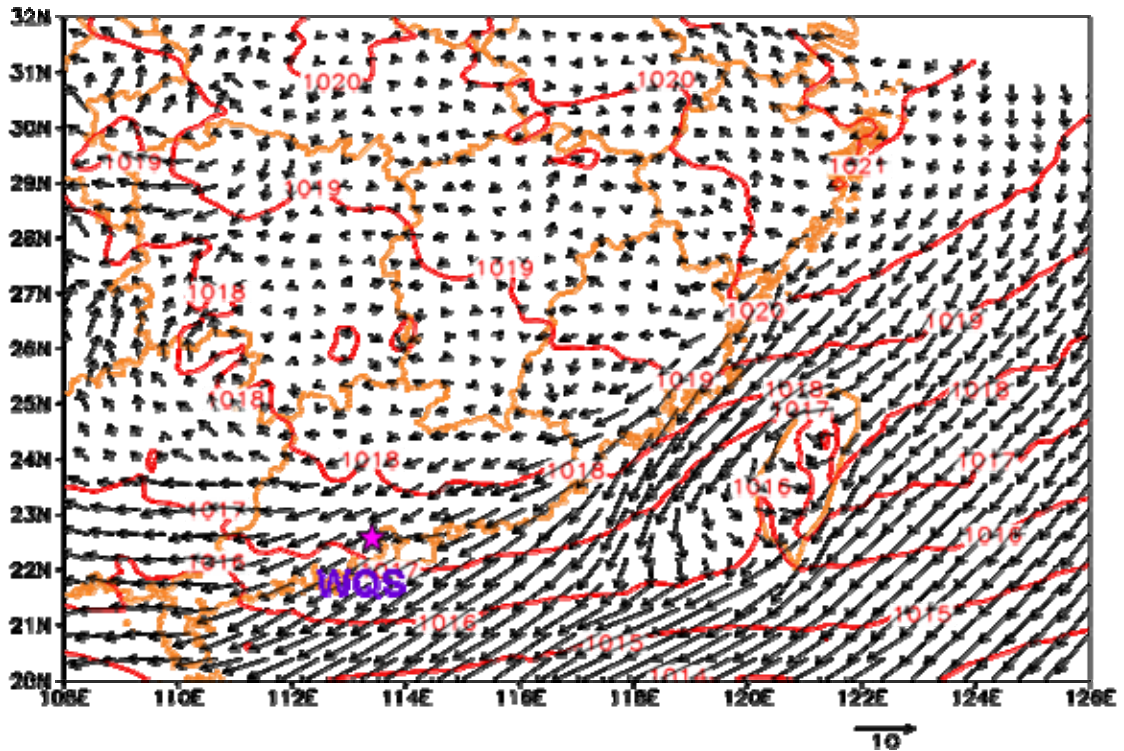


Fig.6.9. Climatological chart of wind field and surface pressure at 15:00 on 13 November, 2007

trajectory was defined as the base case experiment to calculate the POCP value of each VOC. Over a 72-hour period this particular air mass trajectory initialized from Lishui, Zhejiang province, passed over Fujian province including Fuzhou and Xiamen, then most parts of Guangdong province including Huizhou, Shenzhen and Dongguan, before ultimately arriving at WQS (Fig. 6.9). Wherever the air mass passed over, it picked up the local emissions of air pollutants. Based on the INTEX-B inventory, the 2006-based PRD emission inventory, and the MEGAN emission inventory, the time-integrated NO_x and VOC emissions for this air mass trajectory during the 72-hr period were 242 and 317 kg km^{-2} , respectively.

The Photochemical ozone creation potential (POCP) concept is to provide a

VOC ranking under conditions which lead to elevated ozone. Hence POCP's calculated using the base case photochemical trajectory model, would be appropriate for the region under similar conditions and can be used to describe the relative contribution of each VOC to O₃ formation at the regional scale (Section 1). The POCP for a given VOC 'i' is defined by Eq. (6.1),

$$\text{POCP}_i = \frac{\text{ozone increment with the } i\text{th VOC}}{\text{ozone increment with the ethene}} \times 100 \quad (6.1)$$

The POCP for each VOC was calculated from the result of a separate model experiment, each having the same mass increment in VOC emission (6.8% of the total integrated VOC emission across the entire model domain) above the base case experiment. The 72-hr PTM was rerun 139 times, once for each VOC species described in MCM. It is noteworthy that the choice of 6.8 % increase in the VOC emission was arbitrary and had no policy significance. It amounted to 21.6 kg km⁻² in a total VOC emission of 317 kg km⁻². The extra VOC emission stimulated additional O₃ formation over the base case, and this incremental quantity of O₃ can be defined for a particular point along the trajectory or integrated over the entire trajectory (Derwent et al., 1996, 1998; Saunders et al., 2003).

In this study, POCP values were calculated for all 139 non-methane VOCs using the extended MCM v3.1 (Table 6.1). Similar to previous studies (Jenkin et al., 2003; Saunders et al., 2003), alkanes and oxygenated organic compounds have relatively low POCP values while alkenes and aromatics have high POCP values. The POCP values for alkanes ranged from 9 to 48, with ethane showing

the lowest value (9). There was an increasing trend for POCP values with carbon number up to C₆, and then the POCP values remained relatively constant for carbon numbers from C₇ to C₁₂. The alkenes exhibited high POCP values, ranging from 75 (3-methyl-1-butene) to 229 (trans-2-butene). In addition, the POCP values of aromatics ranged from -85 to 197 with the highest value for 1,3,5-trimethylbenzene and the lowest POCPs (negative) for benzaldehyde and styrene. The low POCP value for benzaldehyde was likely due to its rapid photo-oxidation to nitrophenol. As a comparatively unreactive reservoir for both free radicals and NO_x, nitrophenol inhibits the O₃ formation. The negative POCP value for styrene may then also be attributed to its degradation to benzaldehyde, which is rapidly oxidized into nitrophenol (Derwent et al., 1996; Jenkin et al., 2003).

For the oxygenated organic compounds, aldehydes showed the highest mean POCP values, ranging from 30 to 116. The ethers and glycol ethers exhibited slightly lower mean POCPs (16 to 77), followed by the alcohols and glycols (9 – 65) and ketones (8 – 65). In particular, acetone, often used as a solvent, showed a remarkably low POCP value (8), indicating that it could be a potential substitute for the relatively higher reactivity aromatic VOCs in a solvent. It can be seen that esters have the second lowest mean POCP values among the oxygenated species (4-29) whereas organic acids presented the lowest values (2-13), suggesting their low contributions to O₃ formation. The halocarbons showed negligible mean POCP values (1-7), with the exception of the

chloroethenes (23 -68), which therefore should be considered in the assessment of target VOC reduction. The negligible POCP values of halocarbons may be attributed to their low reactivity with OH radicals and the reduced number of C-H bonds which decreased the number of HO₂ radicals formed (Derwent et al., 1996).

6.4.2 Comparison of POCPs with previous studies

[Fig. 6.10](#) compares the POCP values of VOCs in the PRD region obtained by the extended MCM v3.1, with those calculated in Europe by MCM v3 (Jenkin et al., 2003; Saunders et al., 2003). There was similar general trend in VOC POCP values between the two regions, especially for alkanes and some oxygenated organic compounds like ketones and alcohols, whereby their POCP values in the two regions were almost the same. However, there were distinct differences between the PRD region and Europe for the aromatics and alkenes, with consistently higher POCP values for alkenes and reactive aromatics in the PRD than in Europe, and lower values for the least reactive aromatics in the PRD than in Europe. For example, the trans-2-butene POCP was 229 in the PRD but 111 in Europe, while those of styrene and benzaldehyde were -33 and -85 in the PRD compared to 14.5 and -10.4 in Europe. The large difference between the POCP values may be attributed to different emissions of NO_x and VOCs, variable VOC distributions and meteorological conditions such as solar radiation and temperature between the PRD and Europe. Another factor for the

Table 6.1. POCP values for 139 volatile organic compounds relative to ethene (= 100).

VOC	POCP	VOC	POCP
Alkanes		Alcohols and Glycols	
Ethane	9	Methanol	11
Propane	13	Ethanol	34
n-Butane	30	n-Propanol	41
i-Butane	28	i-Propanol	21
n-Pentane	32	n-Butanol	43
i-Pentane	35	2-Butanol	45
tert-Pentane	14	2-Methyl-1-propanol	38
n-Hexane	36	2-Methyl-2-propanol	9
2-Methylpentane	38	3-Pentanol	49
3-Methylpentane	45	2-Methyl-1-butanol	46
2,2-Dimethylbutane	19	3-Methyl-1-butanol	50
2,3-Dimethylbutane	46	2-Methyl-2-butanol	22
n-Heptane	40	3-Methyl-2-butanol	45
2-Methylhexane	39	Cyclohexanol	65
3-Methylhexane	48	Diacetone alcohol	28
n-Octane	34	Propylene glycol	43
n-Nonane	36	Ethylene glycol	20
n-Decane	43	Methylbutenol	46
n-Undecane	42	2-Butoxy Ethanol	56
n-Dodecane	43		
Cyclohexane	38	Esters	
Alkenes		Methyl formate	26
Ethene	100	Methyl acetate	5
Propene	160	Ethyl acetate	17
1-Butene	102	n-Propyl acetate	22
cis-2-butene	216	i- Propyl acetate	22
trans-2-butene	229	n-Butyl acetate	22
Isobutene	91	s-Butyl acetate	29
1-Pentene	84	t-Butyl acetate	4
cis-2-Pentene	161	Ethers and Glycol Ethers	
trans-2-Pentene	161	Methyl ether	26
2-methyl-1-Butene	93	Diethyl ether	72
3-methyl-1-Butene	75	Methyl t-butyl ether	16
2-methyl-2-Butene	202	Diisopropyl ether	54
1-Hexene	91	tert-Butyl ethyl ether	29
cis-2-Hexene	141	Methyl proxitol	58
trans-2-Hexene	141	Methyl glycol	38
2-Butene	169	Ethyl glycol	54
Alkynes		Butyl oxitol	58
Ethyne	6	n-Butoxypropanol	77

Table 6.1 (continued)

VOC	POCP	VOC	POCP
Aromatics		Chloro and hydrochlorocarbons	
Benzene		Methylchloride	
Toluene	36	Methylene chloride	3
o-Xylene	91	Chloroform	1
m-Xylene	111	Methylchloroform	1
p-Xylene	88	Tetrachloroethene	2
Ethylbenzene	34	Trichloroethene	23
Propylbenzene	23	cis-1,2-Dichloroethene	37
i-Propylbenzene	24	trans-1,2-Dichloroethene	34
1,2,3-Trimethylbenzene	165	Vinyl chloride	68
1,2,4-Trimethylbenzene	179	1,2-Dichloroethane	4
1,3,5-Trimethylbenzene	197	1,1-Dichloroethene	58
o-Ethyl toluene	68	1,2-Dichloropropane	5
m-Ethyl toluene	85	1,1-Dichloroethane	4
p-Ethyl toluene	59	Chloroethane	7
5-Ethyl-m-xylene	170	1,1,2,2-Tetrachloroethane	7
3,5-Diethyl toluene	145	1,1,2-Trichloroethane	3
Styrene	-33	Organic Acids	
Benzaldehyde	-85	Methanoic acid	2
		Ethanoic acid	9
		Propanoic acid	13
Aldehydes			
Formaldehyde	67		
Acetaldehyde	116	Dialkenes	
Propionaldehyde	74	Isoprene	171
Butyraldehyde	63	1-3 Butadiene	113
1-Butyraldehyde	58		
Valeraldehyde	79	Monoterpenes	
Acrylaldehyde	30	α -pinene	152
Methacrylaldehyde	35	β -pinene	110
Crotonaldehyde	50		
		Hydrobromocarbons	
Ketones		Bromomethane	0
Acetone	8	1,2-Dibromoethane	1
Butanone	28		
Pentanone	45	Other species	
3-Pentanone	26	Dimethoxymethane	17
Eethyl 1-propyl ketone	33	Dimethyl carbonate	1
Methyl n-butyl ketone	47	Ethylene oxide	1
Ethyl n-propyl ketone	45		
Methyl 1-butyl ketone	65		
Methyl t-butyl ketone	18		
Cyclohexanone	39		

aromatic species may be that the mechanism used in this study (extended MCM v3.1) has been updated from that used in Europe study (MCM v3), in particular it represents aromatic degradation more completely and gives a more reasonable description of known organic product formation, even though previous studies have shown that the POCPs calculated with MCM v3.1 by Derwent et al. (2007b) are reasonably similar to those using MCM v3 by Jenkin et al. (2003) in Europe.

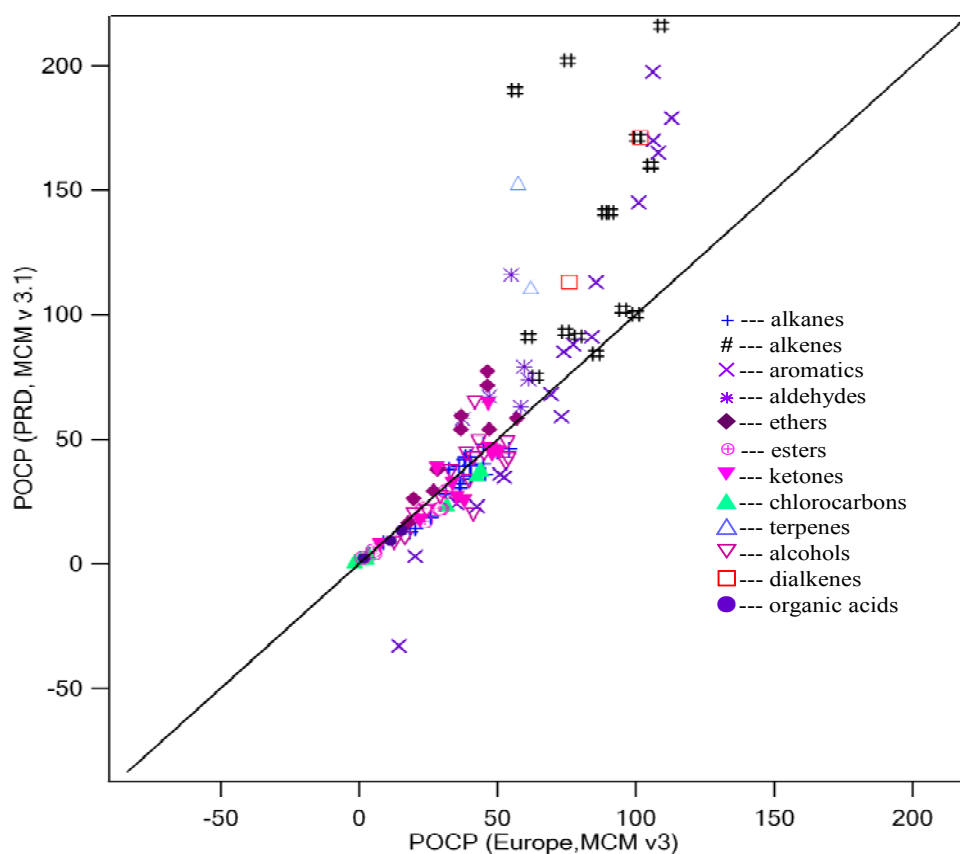


Fig.6.10 Comparison of POCP values of target VOCs in the PRD region (using MCM v3.1) with those reported in Europe (using MCM v3).

To further evaluate the PTM model results, we compared the POCP values obtained in this study with those predicted by the maximum incremental reactivity (MIR) method proposed by Carter (Carter, 1994) from smog chamber mechanism studies (Fig. 6.11). In general, the POCP values showed a good agreement with the MIR values ($R^2 = 0.80$, $p < 0.05$). Both values indicated that alkenes and aromatics were the most reactive and alkanes were least reactive even though the two methods were developed for different scenarios. However, there were some remarkable differences between the two schemes. The POCP method showed that trans-2-butene was the most reactive VOC species, compared to 1,3,5-trimethylbenzene for the MIR scale. The POCP scale also showed that alkenes were stronger contributors to O₃ formation compared to the MIR method. The difference between POCP and MIR schemes is likely because the POCPs obtained in this study focused on specific regional emissions, VOC distribution and long-range transport, while the MIR method was associated with the urban scale and was developed for Los Angeles condition (Carter, 1994).

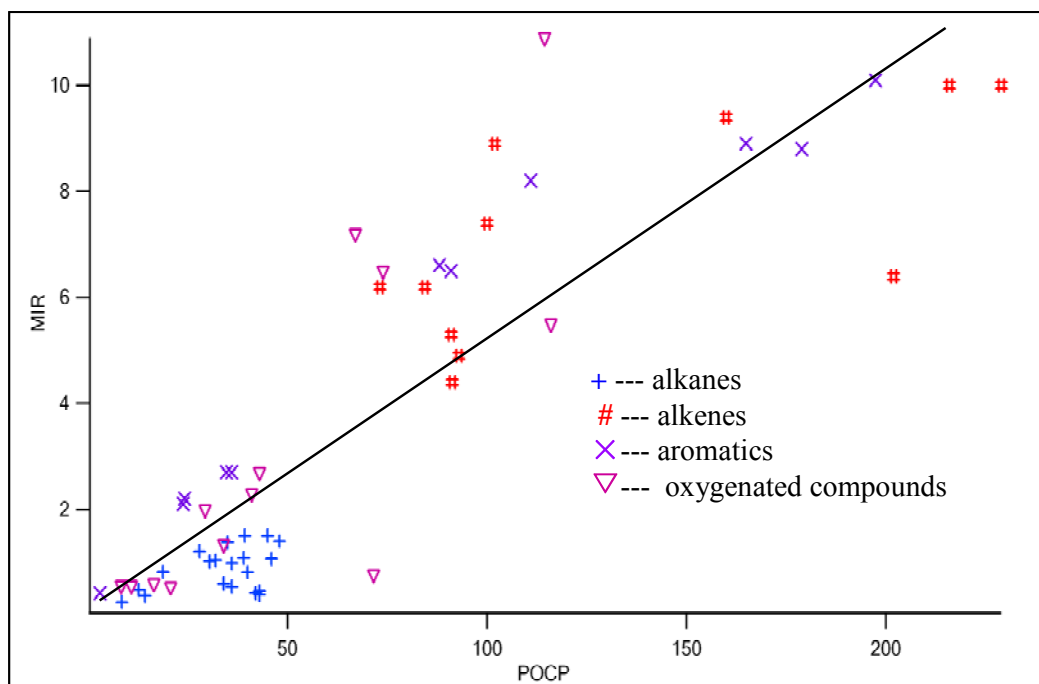


Fig6.11. Comparison of POCP and MIR values for 56 volatile organic compounds, which are available in both MCM (this study) and MIR (Carter, 1994)

6.4.3 The Contribution of VOC species to O₃ formation

To thoroughly understand the relative contribution of each VOC to O₃ formation in the PRD region, a method combining the POCP index with the emission inventories is adopted, in which the importance of each VOC towards O₃ formation potential is ranked using its POCP-weighted emission (Table 2). In other words, the POCP-weighted value of each VOC was obtained in terms of an ethene-equivalent method (i.e. the emission of the VOC in the PRD region (kt yr⁻¹) multiplies by its POCP value/100). Based on the PRD emission inventory, the sum of the anthropogenic and biogenic VOC emissions in this region (21°27'47"-23°56'13" N and 111°59'52"-115°24'48'E) is 1180.1 kt/yr (Zheng et

al., 2009). We used the total emission from the whole region to calculate the emissions of individual VOCs - rather than the emission in the grids where the trajectory passed over - as this would not affect the relative ranking of the VOCs in terms of their POCP-weighted value. [Table 6.3](#) lists the top 15 VOCs with the highest reactivity (POCPs) and emission rates (kt/yr) in the PRD region. Trans-2-butene, cis-2-butene, 2-methyl-2-butene, 1,3,5-trimethylbenzene, 2,3-Dimethylbut-2-ene, 1,2,4-trimethylbenzene, isoprene, and propene had high POCP values, while isoprene, toluene, benzene, ethene, and formaldehyde had elevated emission rates, accounting for 7.3%, 6.6%, 6.2%, 6.0%, and 4.1% of the total emission rates, respectively. Other species, such as m-xylene, ethyne, and ethane also exhibited high emission rates. The 15 most abundant VOC species accounted for 54.9% of the total VOC emission rates in the PRD region.

After taking into account both photochemical reactivity (POCP) and the emission amount of each VOC, isoprene, ethene, α -pinene, m-xylene, propene, formaldehyde, toluene, and 1,2,4-trimethylbenzene became the key emitted precursors to photochemical O₃ formation in the PRD region. We compared the ozone formation potentials (OFP) of each VOC species with those calculated from Zheng's study (Zheng et al., 2009). It was comparable for most species in both studies. For example, both studies have shown that some reactive VOCs like isoprene, *m,p*-xylene, ethyne, propene have the highest contributions to O₃ formation. However there were some discrepancies between the two studies, for example, Zheng's study showed that benzene and methanol are important O₃

precursors, while in this study, their effects on O₃ formation are very small. The different OFP values of some VOC species were caused by the different speciation methods of TVOC emission inventories and the method to determine the relative reactivity of each VOC species. In this study, POCP values calculated by PTM was use to get the relative reactivity of each VOC species, while MIR was used in Zheng's study (Carter 1994).

The top 15 species in terms of POCP-weighted emissions contributed 74% to the O₃ formation in the region but only accounted for 43% of the total VOC emissions, suggesting that species with either high reactivity or large emissions do not necessarily have high contributions to O₃ formation. For example, trans-2-butene was the most reactive compound among the VOCs studied, but its contribution to O₃ formation only ranked twelfth due to its low emission. In contrast, ethyne and benzene accounted for a relatively high percentage of the total VOC emission (3% and 5%, respectively), yet they had negligible contribution to O₃ formation because of their low reactivity. The results imply that the emission quantity together with reactivity of individual VOCs should be considered when strategies for photochemical O₃ pollution control are formulated and implemented. Furthermore, the sum of the most abundant 60 VOC species accounted for 92% of the total POCP-weighted emission of the 139 non-methane VOCs (Table 6.2). The rest (79 VOCs) were either emitted in small amount or were relatively unreactive, resulting in contributions of only 8% to the total POCP-weighted emissions. The results suggest that a relatively small number of

VOC species are responsible for regional scale O₃ formation in the PRD region.

The relative contribution of individual VOC species to O₃ formation in the PRD region was also investigated using an observation-based model (OBM) (Cheng et al., 2009). Both the OBM and PTM models used the same data set for model simulations. The results from both models showed that m,p-xylene, toluene, o-xylene, and formaldehyde were important precursor species to O₃ formation in the region, and that photochemical O₃ formation can be mainly attributed to a small number of VOC species. However, there were some important differences between the two modeling results. For example, POCP-weighted values using PTM showed that isoprene was the most important contributor to O₃ formation, whereas the OBM results found that isoprene had a negligible effect on the O₃ formation. The difference between the two models might be partly due to the fact that POCP-weighted values in the PTM incorporated the contributions of VOCs to O₃ formation at a regional scale, while the OBM results were relatively site-specific.

Table 6.2. 60 key volatile organic compounds included in the photochemical trajectory model together with their mass emission rates, POCPs and POCP-weighted emissions.

VOC species	Emission (kt/yr)	POCP	POCP- weighted*	VOC species	Emission (kt/yr)	POCP	POCP -weighted*
Isoprene	74.10	171	126.71	n-Hexane	7.94	36.17	2.87
Ethene	60.15	100	60.15	trans-2-Hexene	1.91	141.00	2.69
α -pinene	28.80	152	41.65	n-Butane	7.97	30.46	2.43
m-Xylene	37.45	111	43.78	cis-2-Hexene	1.64	140.88	2.30
Propene	25.59	160	41.06	i-Butane	7.81	27.58	2.15
Formaldehyde	40.92	67	27.51	2-Methylhexane	5.43	39.35	2.14
Toluene	66.93	36	24.32	Ethyne	35.92	5.90	2.12
1,2,4-Trimethylbenzene	13.55	179	24.18	3-methyl-1-Butene	2.49	74.74	1.86
β -pinene	20.80	110	19.76	trans-2-Pentene	1.09	170.72	1.86
Acetaldehyde	17.02	116	15.20	n-Octane	5.22	33.98	1.77
o-Xylene	16.73	91	22.88	3,5-Diethyl toluene	1.09	144.85	1.58
cis-2-butene	6.77	216	14.63	Propane	11.95	12.52	1.50
trans-2-butene	6.22	229	14.25	2,3-Dimethylbutane	3.16	45.76	1.44
1-Butene	13.37	102	13.69	n-Decane	3.38	42.68	1.44
1,3,5-Trimethylbenzene	5.58	197	10.97	n-Undecane	3.07	41.83	1.28
m-Ethyl toluene	11.95	85	10.17	2-methyl-1-Butene	1.09	92.51	1.01
i-Propylbenzene	42.23	24	9.99	1-Hexene	1.09	91.03	0.99
2-methyl-2-Butene	4.80	202	9.68	Isobutene	1.09	90.67	0.99
1-3 Butadiene	7.00	113	7.95	n-Nonane	2.63	36.38	0.96
1,2,3-Trimethylbenzene	4.78	165	7.92	p-Ethyl toluene	1.59	59.37	0.94
Methyl 1-butyl ketone	10.60	65	6.89	Propylbenzene	3.99	23.09	0.92
i-Pentane	16.87	35	5.90	n-Butoxypropanol	1.09	77.00	0.84
Ethylbenzene	15.93	34	5.34	Propionaldehyde	1.09	73.67	0.80
1-Pentene	6.22	84	5.25	Acetone	8.76	8.43	0.74
2-Methylpentane	13.78	38	5.23	Cyclohexanol	1.09	64.70	0.70
n-Pentane	14.13	32	4.57	1-Butyraldehyde	1.09	58.34	0.63
o-Ethyl toluene	5.58	68	3.82	2-Butoxy Ethanol	1.09	56.00	0.61
3-Methylhexane	7.17	48	3.47	Cyclohexane	1.44	38.26	0.55
Ethane	34.86	9	3.03	n-Butyl acetate	2.27	22.31	0.51
n-Heptane	7.61	40	3.02	2-Butanol	1.09	45.07	0.49

*= Emission amount x POCP value/100

Table 6.3. The top 15 VOCs with the highest reactivities (POCPs), and emission rates in the PRD region.

VOC	POCP	VOC	Emission rates (kt/yr)
trans-2-butene	229	Isoprene	74.1
cis-2-butene	216	Toluene	66.93
2-methyl-2-Butene	202	Benzene	62.90
1,3,5-Trimethylbenzene	197	Ethene	60.15
2,3-Dimethylbut-2-ene	190	Formaldehyde	40.92
1,2,4-Trimethylbenzene	179	m-Xylene	37.45
Isoprene	171	Ethyne	35.92
trans-2-Pentene	171	Ethane	34.86
cis-2-Pentene	171	α -pinene	28.8
5-Ethyl-m-xylene	170	Propene	25.59
1,2,3-Trimethylbenzene	165	β -pinene	20.8
Propene	160	Acetaldehyde	17.02
α -pinene	152	i-Pentane	16.87
3,5-Diethyl toluene	145	o-Xylene	16.73
trans-2-Hexene	141	n-Pentane	14.13

6.5 The contributions of VOC emission sources to O₃ formation

To determine the relative contributions of the main VOC emission source categories to O₃ formation, for a given source category each VOC's fraction by mass was multiplied by the total emission from that source category, then the emission of each VOC was multiplied by its POCP. The total POCP-weighted emissions for each source category were then summed for each VOC species, and the relative contribution of each source category to the O₃ formation was thus obtained.

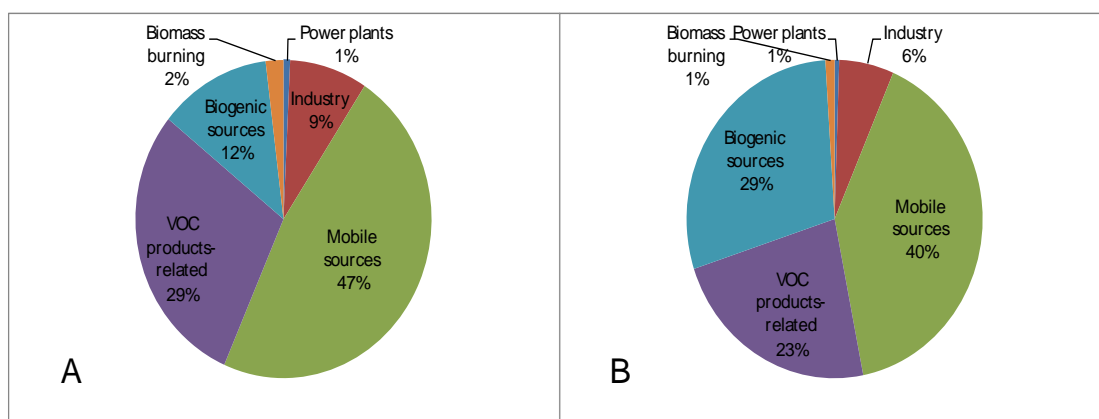


Fig.6.12. Source contributions to anthropogenic VOC emissions (A) and source contributions to regional ozone formation (B)

Based solely on the PRD emission inventory, there are six major sources of VOCs. Mobile sources were the most important contributors to VOC emissions in the PRD region (47%), followed by VOC product-related sources (29%), biogenic sources (12%), industry (8%), biomass burning (2%), and power plants (1%) (Fig.6.12). By comparison, when POCP-weighted emissions were taken into account, mobile sources remained the largest contributor to regional O₃ formation (40%), followed by biogenic sources (29%), VOC product-related sources (23%), industry (6%), biomass burning (1%), and power plants (1%). The highest contribution of mobile sources to regional O₃ formation is attributed to relatively more reactive compounds such as alkenes or aromatics present in vehicle exhaust emissions. The results also indicated that biogenic sources had a large contribution to regional O₃ formation in the PRD region.

6.6 Summary

A photochemical trajectory model (PTM), combining an updated version of the

MCM, boundary layer trajectories, precursor emissions and chemical processing, was modified and employed to simulate the formation of photochemical oxidants at WQS, Guangzhou during a photochemical pollution event from 12 to 17 November, 2007. This is the first time that the photochemical trajectory model containing detailed chemical mechanism was used in the PRD region to assess the relative influence of individual VOCs to regional O₃ formation. Good agreement between the simulated and observed diurnal variations of O₃ ($R^2 = 0.80$, $p < 0.05$) suggested that the PTM simulation could provide a reasonable description of O₃ formation in the PRD region. However, the model performance of NO_x simulation was inferior and most of the observed NO_x mixing ratios were higher than the simulated values. The apparent discrepancy may be due to chimney emissions of upwind power plants in Humen town of Dongguan, and/or the high vertical gradient of NO_x, and /or the high uncertainties in the 2006-based PRD emission inventory.

Model simulations showed that alkanes and oxygenated organic compounds had relatively low POCP values while alkenes and aromatics had high POCP values. After taking into account both POCP values and emission amounts, the top 15 VOC species contributed about 74% to the total POCP-weighted emission in the PRD region, and the top 60 VOC species accounted for 92%, indicating that regional-scale O₃ formation in the PRD region can be mainly attributed to a relatively small number of VOC species. Further analysis suggested that mobile source was responsible for 40% of the regional O₃ formation, followed by

biogenic sources (29%), VOC products-related (23%), industry (6%), biomass burning (1%), and power plants (1%). The results of this study should assist future policy development in targeting specific VOCs and emission source categories responsible for the air pollution episodes in the PRD region.

Chapter 7

Conclusions

In this study, an intensive field measurement study was conducted simultaneously for the first time at a site (WQS) within the inland Pearl River Delta (PRD) region and a site in Hong Kong (TC) from 22 October to 01 December 2007. Ambient air pollutants measured included ozone (O_3), nitrogen oxides (NO_x), carbon monoxide (CO), sulfur dioxide (SO_2), non-methane hydrocarbons (NMHCs), and carbonyls. The purpose is to improve our understanding of the interplay of O_3 pollution between Hong Kong and the inland PRD region, to explore the relationships between O_3 and its precursors, and to identify the key volatile organic compound (VOC) species and emission source categories contributing to the O_3 formation.

Thirteen O_3 episode days (>120 ppbv) were observed at WQS and only on 2 days at TC during the sampling period. The results indicate that O_3 pollution at WQS was more serious than that at TC. O_3 episodes usually occurred when weather systems were relatively stable. Analysis of the synoptic weather conditions and variations of air pollutants indicated that high O_3 levels were mainly attributed to local photochemical production. Various air pollutant ratios (SO_2/NO_x , CO/NO_x , *m*, *p*-xylene/ethylbenzene, *i*-butane/propane) suggested that air masses arriving at TC were mainly affected by local emissions superimposed by regional transport, whereas the air at WQS was highly influenced by regional emissions and was therefore more aged.

An OBM was developed to assess the ozone–precursors relationships as well as determine the relative contributions of different VOC species, particularly carbonyls, to photochemical O₃ production. The net O₃ production derived from the OBM agreed better with the observed O₃ increment after hourly carbonyl concentrations were included. When adding carbonyls to the OBM, the derived P_{O₃-NO} peak increased by 64% and 47%, and the HO₂ peak increased by 43% and 39% at WQS and TC, respectively. These results highlight the importance of carbonyls in the photochemistry in this region.

The OBM-derived RIRs support O₃ production being VOC-limited at WQS and TC, respectively. The AHC group showed the highest RIR, while BHC and CO showed positive but small RIRs. NO was negatively correlated with O₃ production, indicating that reducing NO would lead to an increase in O₃ production. Among the VOC species, primary formaldehyde had the highest RIR. Aromatics such as *m,p*-xylene, toluene, and *o*-xylene also showed high RIR at WQS. Primary formaldehyde, acetaldehyde, isoprene, *m,p*-xylene, ethene, 1-butene, and toluene were the dominant precursors with high RIR at TC. The summed RIR of the top 12 compounds accounted for 89% of the total RIR (VOC) at WQS and 85% at TC, respectively, suggesting that local photochemical O₃ formation was mainly attributed to a small number of VOC species.

To evaluate the OBM results, and deeply understand which specific VOCs contribute most to O₃ formation in the PRD region, a photochemical trajectory model (PTM), combining an updated version of the MCM, boundary layer

trajectories, precursor emissions and chemical processing, was developed and employed to simulate the formation of photochemical oxidants at WQS, Guangzhou, during a photochemical pollution event from the 12 to 17 November, 2007. This is the first time that the photochemical trajectory model containing detailed chemical mechanism was used in the PRD region to assess the relative influence of individual VOCs to regional O₃ formation. Good agreement between the simulated and observed diurnal variations of O₃ ($R^2 = 0.80$, $p < 0.05$) suggested that the PTM simulation could provide a reasonable description of O₃ formation in the PRD region. However, the model performance of NO_x simulation was inferior and most of the observed NO_x mixing ratios were higher than the simulated values. The apparent discrepancy may be due to chimney emissions of upwind power plants in Humen town of Dongguan, and/or the high vertical gradient of NO_x, and /or the high uncertainties in the 2006-based PRD emission inventory.

Model simulations showed that alkanes and oxygenated organic compounds had relatively low POCP values while alkenes and aromatics had high POCP values. After taking into account both POCP values and emission amounts, the top 15 VOC species including isoprene, ethene, α -pinene, *m*-xylene, propene, formaldehyde, toluene, 1,2,4-trimethylbenzene, β -pinene, acetaldehyde, *o*-xylene, *cis*-2-butene, *trans*-2-butene, 1-butene, and 1,3,5-trimethylbenzene contributed about 74% to the total POCP-weighted emission in the PRD region, and the top 60 VOC species accounted for 92%, indicating that regional-scale O₃ formation

in the PRD region can be mainly attributed to a relatively small number of VOC species.

The relative contribution of individual VOC species to O₃ formation in the PRD region has been investigated by using the OBM and the PTM in this study. The results from both models showed that *m,p*-xylene, toluene, *o*-xylene, and formaldehyde were important emitted precursor species to the O₃ formation in the region, and that photochemical O₃ formation can be mainly attributed to a small number of VOC species. However, there were some important differences between the two modeling results. For example, POCP-weighted values using PTM showed that isoprene was the most important contributor to O₃ formation, whereas the OBM results found that isoprene had a negligible effect on the O₃ formation. The difference between the two models might be partly due to the fact that POCP-weighted values in the PTM incorporated the contributions of VOCs to O₃ formation at a regional scale, while the OBM results were relatively site-specific.

Further analysis by the PTM suggested that mobile source was responsible for 40% of the regional O₃ formation, followed by biogenic sources (29%), VOC products-related (23%), industry (6%), biomass burning (1%), and power plants (1%). The results of this study should assist future policy development in targeting specific VOCs and emission source categories responsible for the air pollution episodes in the PRD region.

References

- Ancellet, G., Beekmann, M., 1997. Evidence for changes in the ozone concentrations in the free troposphere over Southern France from 1976 to 1995. *Atmospheric Environment* 31, 2835-2851.
- Atkinson, R., 1990. Gas-Phase Tropospheric Chemistry of Organic-Compounds - a Review. *Atmospheric Environment Part a-General Topics* 24, 1-41.
- Atkinson, R., 1997. Gas-phase tropospheric chemistry of volatile organic compounds .1. Alkanes and alkenes. *Journal of Physical and Chemical Reference Data* 26, 215-290.
- Atkinson, R., 2000. Atmospheric chemistry of VOCs and NOx. *Atmospheric Environment* 34, 2063-2101.
- Atkinson, R., Arey, J., 2003. Gas-phase tropospheric chemistry of biogenic volatile organic compounds: a review. *Atmospheric Environment* 37, S197-S219.
- Barletta, B., Meinardi, S., Rowland, F.S., Chan, C.Y., Wang, X.M., Zou, S.C., Chan, L.Y., Blake, D.R., 2005. Volatile organic compounds in 43 Chinese cities. *Atmospheric Environment* 39, 5979-5990.
- Barletta, B., Meinardi, S., Simpson, I.J., Khwaja, H.A., Blake, D.R., Rowland, F.S., 2002. Mixing ratios of volatile organic compounds (VOCs) in the atmosphere of Karachi, Pakistan. *Atmospheric Environment* 36, 3429-3443.
- Barletta, B., Meinardi, S., Simpson, I.J., Zou, S.C., Rowland, F.S., Blake, D.R., 2008b. Ambient mixing ratios of nonmethane hydrocarbons (NMHCs) in two major urban centers of the Pearl River Delta (PRD) region: Guangzhou and Dongguan. *Atmospheric Environment* 42, 4393-4408.
- Blake, D.R., Rowland, F.S., 1995. Urban Leakage of Liquefied Petroleum Gas and Its Impact on Mexico-City Air-Quality. *Science* 269, 953-956.
- Borbon, A., Locoge, N., Veillerot, M., Galloo, J.C., Guillermo, R., 2002. Characterisation of NMHCs in a French urban atmosphere: overview of the main sources. *Science of the Total Environment* 292, 177-191.
- Cardelino, C.A., Chameides, W.L., 1995. An Observation-Based Model for Analyzing Ozone Precursor Relationships in the Urban Atmosphere. *Journal of the Air & Waste Management*

Association 45, 161-180.

Cardelino, C.A., Chameides, W.L., 2000. The application of data from photochemical assessment monitoring stations to the observation-based model. *Atmospheric Environment* 34, 2325-2332.

Carnero, J.A.A., Bolivar, J.P., de la Morena, B.A., 2010. Surface ozone measurements in the southwest of the Iberian Peninsula (Huelva, Spain). *Environmental Science and Pollution Research* 17, 355-368.

Carter, W.P.L., 1990. A Detailed Mechanism for the Gas-Phase Atmospheric Reactions of Organic-Compounds. *Atmospheric Environment Part a-General Topics* 24, 481-518.

Carter, W.P.L., 1994. Development of Ozone Reactivity Scales for Volatile Organic-Compounds. *Journal of the Air & Waste Management Association* 44, 881-899.

Chameides, W.L., Fehsenfeld, F., Rodgers, M.O., Cardelino, C., Martinez, J., Parrish, D., Lonneman, W., Lawson, D.R., Rasmussen, R.A., Zimmerman, P., Greenberg, J., Middleton, P., Wang, T., 1992. Ozone Precursor Relationships in the Ambient Atmosphere. *Journal of Geophysical Research-Atmospheres* 97, 6037-6055.

Chan, L.Y., Chan, C.Y., Qin, Y., 1998a. Surface ozone pattern in Hong Kong. *Journal of Applied Meteorology* 37, 1153-1165.

Chan, L.Y., Chu, K.W., Zou, S.C., Chan, C.Y., Wang, X.M., Barletta, B., Blake, D.R., Guo, H., Tsai, W.Y., 2006a. Characteristics of nonmethane hydrocarbons (NMHCs) in industrial, industrial-urban, and industrial-suburban atmospheres of the Pearl River Delta (PRD) region of south China. *Journal of Geophysical Research-Atmospheres* 111, 9.

Chan, L.Y., Chu, K.W., Zou, S.C., Chan, C.Y., Wang, X.M., Barletta, B., Blake, D.R., Guo, H., Tsai, W.Y., 2006b. Characteristics of nonmethane hydrocarbons (NMHCs) in industrial, industrial-urban, and industrial-suburban atmospheres of the Pearl River Delta (PRD) region of south China. *Journal of Geophysical Research-Atmosphere* 111.

Chan, L.Y., Lau, W.L., Wang, X.M., Tang, J.H., 2003. Preliminary measurements of aromatic VOCs in public transportation modes in Guangzhou, China. *Environment International* 29, 429-435.

Chan, L.Y., Liu, H.Y., Lam, K.S., Wang, T., Oltmans, S.J., Harris, J.M., 1998b. Analysis of the seasonal behavior of tropospheric ozone at Hong Kong. *Atmospheric Environment* 32,

159-168.

Chang, C.C., Chen, T.Y., Lin, C.Y., Yuan, C.S., Liu, S.C., 2005. Effects of reactive hydrocarbons on ozone formation in southern Taiwan. *Atmospheric Environment* 39, 2867-2878.

Chen, T.Y., Simpson, I.J., Blake, D.R., Rowland, F.S., 2001. Impact of the leakage of liquefied petroleum gas (LPG) on Santiago air quality. *Geophysical Research Letters* 28, 2193-2196.

Cheng, H.R., Guo, H., Wang, X.M., Saunders, S.M., Lam, S.H.M., Jiang, F., Wang, T.J., Ding, A.J., Lee, S.C., K.F. H., 2010. On the relationship between ozone and its precursors in the Pearl River Delta: application of an observation-based model (OBM). *Environmental Science and Pollution Research* 17, 547-560.

Chou, C.C.K., Liu, S.C., Lin, C.-Y., Shiu, C.-J., Chang, K.-H., 2006. The trend of surface ozone in Taipei, Taiwan, and its causes: Implications for ozone control strategies. *Atmospheric Environment* 40, 3898-3908.

Colbeck, Mackenzie, 1994. *Air Pollution by Photochemical Oxidants*. Elsevier Amsterdam, 232.

Cooper, O.R., Moody, J.L., Parrish, D.D., Trainer, M., Ryerson, T.B., Holloway, J.S., Hubler, G., Fehsenfeld, F.C., Oltmans, S.J., Evans, M.J., 2001. Trace gas signatures of the airstreams within North Atlantic cyclones: Case studies from the North Atlantic Regional Experiment (NARE '97) aircraft intensive. *Journal of Geophysical Research-Atmospheres* 106, 5437-5456.

Curtis, A.R., Sweetenham, W.P., 1987. *FACSIMILE release H user's manual*. AERE Report R11771 (HMSO), London.

Derwent, R.G., Davies, T.J., Delaney, M., Dollard, G.J., Field, R.A., Dumitrean, P., Nason, P.D., Jones, B.M.R., Pepler, S.A., 2000. Analysis and interpretation of the continuous hourly monitoring data for 26 C-2-C-8 hydrocarbons at 12 United Kingdom sites during 1996. *Atmospheric Environment* 34, 297-312.

Derwent, R.G., Jenkin, M.E., 1991. Hydrocarbons and the long-range transport of ozone and pan across Europe. *Atmospheric Environment. Part A. General Topics* 25, 1661-1678.

Derwent, R.G., Jenkin, M.E., Passant, N.R., Pilling, M.J., 2007a. Photochemical ozone

creation potentials (POCPs) for different emission sources of organic compounds under European conditions estimated with a Master Chemical Mechanism. *Atmospheric Environment* 41, 2570-2579.

Derwent, R.G., Jenkin, M.E., Saunders, S.M., 1996. Photochemical ozone creation potentials for a large number of reactive hydrocarbons under European conditions. *Atmospheric Environment* 30, 181-199.

Derwent, R.G., Jenkin, M.E., Saunders, S.M., Pilling, M.J., 1998. Photochemical ozone creation potentials for organic compounds in northwest Europe calculated with a master chemical mechanism. *Atmospheric Environment* 32, 2429-2441.

Derwent, R.G., Jenkin, M.E., Saunders, S.M., Pilling, M.J., Simmonds, P.G., Passant, N.R., Dollard, G.J., Dumitrean, P., Kent, A., 2003. Photochemical ozone formation in north west Europe and its control. *Atmospheric Environment* 37, 1983-1991.

Derwent, R.G., Simmonds, P.G., Manning, A.J., Spain, T.G., 2007b. Trends over a 20-year period from 1987 to 2007 in surface ozone at the atmospheric research station, Mace Head, Ireland. *Atmospheric Environment* 41, 9091-9098.

Ding, A., Wang, T., Zhao, M., Wang, T., Li, Z., 2004. Simulation of sea-land breezes and a discussion of their implications on the transport of air pollution during a multi-day ozone episode in the Pearl River Delta of China. *Atmospheric Environment* 38, 6737-6750.

Ding, A.J., Wang, T., Thouret, V., Cammas, J.P., Nedelec, P., 2008. Tropospheric ozone climatology over Beijing: analysis of aircraft data from the MOZAIC program. *Atmospheric Chemistry and Physics* 8, 1-13.

Dodge, M.C., 2000. Chemical oxidant mechanisms for air quality modeling: critical review. *Atmospheric Environment* 34, 2103-2130.

Draxler, R.R., Rolph, G.D., 2003. HYSPLIT (HYbrid Single-Particle Lagrangian Integrated Trajectory) Model access via NOAA ARL READY Website (<http://www.arl.noaa.gov/ready/hysplit4.html>). NOAA Air Resources Laboratory, Silver Spring, Maryland, USA.

Evtuygina, M.G., Pio, C., Nunes, T., Pinho, P.G., Costa, C.S., 2007. Photochemical ozone formation at Portugal West Coast under sea breeze conditions as assessed by master chemical mechanism model. *Atmospheric Environment* 41, 2171-2182.

Fan, S., Wang, B., Tesche, M., Engelmann, R., Althausen, A., Liu, J., Zhu, W., Fan, Q., Li, M., Ta, N., Song, L., Leong, K., 2008. Meteorological conditions and structures of atmospheric boundary layer in October 2004 over Pearl River Delta area. *Atmospheric Environment* 42, 6174-6186.

Forastiere, F., Peters, A., Kelly, F.J., T.HolgTE, S., 2005. Air Quality Guidelines. WHO regional Office for Europe, 331-377.

Geng, F.H., Zhao, C.S., Tang, X., Lu, G.L., Tie, X.X., 2007. Analysis of ozone and VOCs measured in Shanghai: A case study. *Atmospheric Environment* 41, 989-1001.

Gery, M.W., Whitten, G.Z., Killus, J.P., Dodge, M.C., 1989. A Photochemical Kinetics Mechanism for Urban and Regional Scale Computer Modeling. *Journal of Geophysical Research-Atmospheres* 94, 12925-12956.

Godish, T., 2003. Air Quality 4th Edition. Lewis Publishers.

Godish, T., 2004. Air Quality. 4th edition Lewis Publishers, Boca Raton, USA.

Government, G.P., 2008. Guangdong Statistical Yearbook. Guangdong Provincial Government.

Grosjean, E., Grosjean, D., Rasmussen, R.A., 1998a. Ambient concentrations, sources, emission rates, and photochemical reactivity of C-2-C-10 hydrocarbons in Porto Alegre, Brazil. *Environmental Science & Technology* 32, 2061-2069.

Grosjean, E., Rasmussen, R.A., Grosjean, D., 1998b. Ambient levels of gas phase pollutants in Porto Alegre, Brazil. *Atmospheric Environment*. 32, 3371-3379.

Guenther, A., Karl, T., Harley, P., Wiedinmyer, C., Palmer, P.I., Geron, C., 2006. Estimates of global terrestrial isoprene emissions using MEGAN (Model of Emissions of Gases and Aerosols from Nature). *Atmospheric Chemistry and Physics* 6, 3181-3210.

Guo, H., Jiang, F., Cheng, H.R., Simpson, I.J., Wang, X.M., Ding, A.J., Wang, T.J., Saunders, S.M., Wang, T., Lam, S.H.M., Blake, D.R., Zhang, Y.L., Xie, M., 2009. Concurrent observations of air pollutants at two sites in the Pearl River Delta and the implication of regional transport. *Atmospheric Chemistry and Physics* 9, 7343-7360.

Guo, H., Lee, S.C., Louie, P.K.K., Ho, K.F., 2004a. Characterization of hydrocarbons, halocarbons and carbonyls in the atmosphere of Hong Kong. *Chemosphere* 57, 1363-1372.

Guo, H., So, K.L., Simpson, I.J., Barletta, B., Meinardi, S., Blake, D.R., 2007. C-1-C-8

volatile organic compounds in the atmosphere of Hong Kong: Overview of atmospheric processing and source apportionment. *Atmospheric Environment* 41, 1456-1472.

Guo, H., Wang, T., Blake, D.R., Simpson, I.J., Kwok, Y.H., Li, Y.S., 2006. Regional and local contributions to ambient non-methane volatile organic compounds at a polluted rural/coastal site in Pearl River Delta, China. *Atmospheric Environment* 40, 2345-2359.

Guo, H., Wang, T., Louie, P.K.K., 2004b. Source apportionment of ambient non-methane hydrocarbons in Hong Kong: Application of a principal component analysis/absolute principal component scores (PCA/APCS) receptor model. *Environmental Pollution* 129, 489-498.

Guo, H., Wang, T., Simpson, I.J., Blake, D.R., Yu, X.M., Kwok, Y.H., Li, Y.S., 2004c. Source contributions to ambient VOCs and CO at a rural site in Eastern China. *Atmospheric Environment*. 38, 4551-4560.

Harrison, R.M., 2007. Principles of Environmental chemistry.

Hidy, G.M., 2000. Ozone process insights from field experiments - part I: overview. *Atmospheric Environment* 34, 2001-2022.

HKEPD, 2009. http://www.epd.gov.hk/epd/english/environmentinhk/air/air_maincontent.html

Ho, K.F., Lee, S.C., Guo, H., Tsai, W.Y., 2004. Seasonal and diurnal variations of volatile organic compounds (VOCs) in the atmosphere of Hong Kong. *Science of The Total Environment* 322, 155-166.

Huang, J.P., Fung, J.C.H., Lau, A.K.H., 2006. Integrated processes analysis and systematic meteorological classification of ozone episodes in Hong Kong. *Journal of Geophysical Research-Atmospheres* 111, 14.

Huang, J.P., Fung, J.C.H., Lau, A.K.H., Qin, Y., 2005. Numerical simulation and process analysis of typhoon-related ozone episodes in Hong Kong. *J. Geophys. Res.-Atmos.* 110.

Jacob, D.J., Logan, J.A., Murti, P.P., 1999. Effect of rising Asian emissions on surface ozone in the United States. *Geophysical Research Letters* 26, 2175-2178.

Jaffe, D., Price, H., Parrish, D., Goldstein, A., Harris, J., 2003. Increasing background ozone during spring on the west coast of North America. *Geophysical Research Letters* 30, 4.

Jaffe, D., Ray, J., 2007. Increase in surface ozone at rural sites in the western US. *Atmospheric Environment* 41, 5452-5463.

Jenkin, M.E., 2008. Trends in ozone concentration distributions in the UK since 1990: Local, regional and global influences. *Atmospheric Environment* 42, 5434-5445.

Jenkin, M.E., Saunders, S.M., Pilling, M.J., 1997. The tropospheric degradation of volatile organic compounds: A protocol for mechanism development. *Atmospheric Environment* 31, 81-104.

Jenkin, M.E., Saunders, S.M., Wagner, V., Pilling, M.J., 2003. Protocol for the development of the Master Chemical Mechanism, MCM v3 (Part B): tropospheric degradation of aromatic volatile organic compounds. *Atmospheric Chemistry and Physics* 3, 181-193.

Jiang, F., Wang, T., Wang, T., Xie, M., Zhao, H., 2008. Numerical modeling of a continuous photochemical pollution episode in Hong Kong using WRF-chem. *Atmospheric Environment* 42, 8717-8727.

Kleinman, L., Lee, Y.N., Springston, S.R., Nunnermacker, L., Zhou, X.L., Brown, R., Hallock, K., Klotz, P., Leahy, D., Lee, J.H., Newman, L., 1994. Ozone Formation at a Rural Site in the Southeastern United-States. *Journal of Geophysical Research-Atmospheres* 99, 3469-3482.

Kleinman, L.I., 2000. Ozone process insights from field experiments - part II: Observation-based analysis for ozone production. *Atmospheric Environment* 34, 2023-2033.

Kok, G.L., Lind, J.A., Fang, M., 1997. An airborne study of air quality around the Hong Kong Territory. *Journal of Geophysical Research-Atmospheres* 102, 19043-19057.

Krzyscin, J., Krizan, P., Jaroslowski, J., 2007. Long-term changes in the tropospheric column ozone from the ozone soundings over Europe. *Atmospheric Environment* 41, 606-616.

Kurokawa, J., Ohara, T., Uno, I., Hayasaki, M., Tanimoto, H., 2009. Influence of meteorological variability on interannual variations of springtime boundary layer ozone over Japan during 1981-2005. *Atmospheric Chemistry and Physics* 9, 6287-6304.

Lam, K.S., Wang, T.J., Chan, L.Y., Wang, T., Harris, J., 2001. Flow patterns influencing the seasonal behavior of surface ozone and carbon monoxide at a coastal site near Hong Kong. *Atmospheric Environment* 35, 3121-3135.

Lam, K.S., Wang, T.J., Wu, C.L., Li, Y.S., 2005. Study on an ozone episode in hot season in Hong Kong and transboundary air pollution over Pearl River Delta region of China. *Atmospheric Environment* 39, 1967-1977.

- Lary, D.J., Shallcross, D.E., 2000. Central role of carbonyl compounds in atmospheric chemistry. *Journal of Geophysical Research-Atmospheres* 105, 19771-19778.
- Lee, S., Akimoto, H., Nakane, H., Kurnosenko, S., Kinjo, Y., 1998. Lower tropospheric ozone trend observed in 1989-1997 at Okinawa, Japan. *Geophysical Research Letters* 25, 1637-1640.
- Lee, S.C., Chiu, M.Y., Ho, K.F., Zou, S.C., Wang, X.M., 2002. Volatile organic compounds (VOCs) in urban atmosphere of Hong Kong. *Chemosphere* 48, 375-382.
- Lee, Y.C., Calori, G., Hills, P., Carmichael, G.R., 2002. Ozone episodes in urban Hong Kong 1994-1999. *Atmospheric Environment* 36, 1957-1968.
- Lee, Y.C., Savtchenko, A., 2006. Relationship between air pollution in Hong Kong and in the Pearl River Delta region of south China in 2003 and 2004: An analysis. *J. Appl. Meteorol. Climatol.* 45, 269-282.
- Lelieveld, J., Dentener, F.J., 2000. What controls tropospheric ozone? *Journal of Geophysical Research-Atmospheres* 105, 3531-3551.
- Lin, C.Y.C., Jacob, D.J., Munger, J.W., Fiore, A.M., 2000. Increasing background ozone in surface air over the United States. *Geophysical Research Letters* 27, 3465-3468.
- Liu, H.P., Chan, J.C.L., 2002. Boundary layer dynamics associated with a severe air-pollution episode in Hong Kong. *Atmospheric Environment* 36, 2013-2025.
- Liu, Y., Shao, M., Fu, L.L., Lu, S.H., Zeng, L.M., Tang, D.G., 2008a. Source profiles of volatile organic compounds (VOCs) measured in China: Part I. *Atmospheric Environment* 42, 6247-6260.
- Liu, Y., Shao, M., Lu, S.H., Liao, C.C., Wang, J.L., Chen, G., 2008b. Volatile organic compound (VOC) measurements in the pearl river delta (PRD) region, China. *Atmospheric Chemistry and Physics* 8, 1531-1545.
- Manahan, S.E., 2001. *Fundamentals of environmental chemistry* Boca Raton, Fla.: Lewis Publishers.
- Monks, P.S., 2000. A review of the observations and origins of the spring ozone maximum. *Atmospheric Environment* 34, 3545-3561.
- Morikawa, T., Wakamatsu, S., Tanaka, M., Uno, I., Kamiura, T., Maeda, T., 1998. C-2-C-5 hydrocarbon concentrations in central Osaka. *Atmospheric Environment* 32, 2007-2016.

NRC, N.R.C., 1991. Rethinking the Ozone Problem in Urban and Regional Air Pollution. National Academic Press, Washington, DC.

Oltmans, S.J., Lefohn, A.S., Harris, J.M., Galbally, I., Scheel, H.E., Bodeker, G., Brunke, E., Claude, H., Tarasick, D., Johnson, B.J., Simmonds, P., Shadwick, D., Anlauf, K., Hayden, K., Schmidlin, F., Fujimoto, T., Akagi, K., Meyer, C., Nichol, S., Davies, J., Redondas, A., Cuevas, E., 2006. Long-term changes in tropospheric ozone. *Atmospheric Environment* 40, 3156-3173.

Oltmans, S.J., Lefohn, A.S., Harris, J.M., Shadwick, D.S., 2008. Background ozone levels of air entering the west coast of the US and assessment of longer-term changes. *Atmospheric Environment* 42, 6020-6038.

Pang, X., Mu, Y., 2006. Seasonal and diurnal variations of carbonyl compounds in Beijing ambient air. *Atmospheric Environment* 40, 6313-6320.

Parrish, D.D., Dunlea, E.J., Atlas, E.L., Schauffler, S., Donnelly, S., Stroud, V., Goldstein, A.H., Millet, D.B., McKay, M., Jaffe, D.A., Price, H.U., Hess, P.G., Flocke, F., Roberts, J.M., 2004. Changes in the photochemical environment of the temperate North Pacific troposphere in response to increased Asian emissions. *Journal of Geophysical Research-Atmospheres* 109, 16.

Penkett, S.A., 1988. Chemistry of the Natural Atmosphere - Warneck, P. *Nature* 336, 322-322.

Pinho, P.G., Lemos, L.T., Pio, C.A., Evtuygina, M.G., Nunes, T.V., Jenkin, M.E., 2009. Detailed chemical analysis of regional-scale air pollution in western Portugal using an adapted version of MCM v3.1. *Science of the Total Environment* 407, 2024-2038.

Possanzini, M., Palo, V.D., Cecinato, A., 2002. Sources and photodecomposition of formaldehyde and acetaldehyde in Rome ambient air. *Atmospheric Environment* 36, 3195-3201.

Sahu, L.K., Lal, S., 2006. Distributions of C-2-C5NMHCs and related trace gases at a tropical urban site in India. *Atmospheric Environment* 40, 880-891.

Saunders, S.M., Jenkin, M.E., Derwent, R.G., Pilling, M.J., 2003. Protocol for the development of the Master Chemical Mechanism, MCM v3 (Part A): tropospheric degradation of non-aromatic volatile organic compounds. *Atmospheric Chemistry and*

Physics 3, 161-180.

Shao, M., Tang, X.Y., Zhang, Y.H., Li, W.J., 2006. City clusters in China: air and surface water pollution. *Frontiers in Ecology and the Environment* 4, 353-361.

Shao, M., Zhang, Y., Zeng, L., Tang, X., Zhang, J., Zhong, L., Wang, B., 2009. Ground-level ozone in the Pearl River Delta and the roles of VOC and NO_x in its production. *Journal of Environmental Management* 90, 512-518.

Shiu, C.J., Liu, S.C., Chang, C.C., Chen, J.P., Chou, C.C.K., Lin, C.Y., Young, C.Y., 2007. Photochemical production of ozone and control strategy for Southern Taiwan. *Atmospheric Environment* 41, 9324-9340.

Sillman, S., 1999. The relation between ozone, NO_x and hydrocarbons in urban and polluted rural environments. *Atmospheric Environment* 33, 1821-1845.

Sillman S., 2003. Tropospheric ozone and photochemical smog. *Environmental Geochemistry*, Vol. 9 *Treatise on Geochemistry* 407-432.

Sin, D.W.M., Wong, Y.C., Louie, P.K.K., 2000. Monitoring of ambient volatile organic compounds at two urban sites in Hong Kong from 1997 to 1998. *Indoor Built Environ.* 9, 216-227.

So, K.L., Wang, T., 2003. On the local and regional influence on ground-level ozone concentrations in Hong Kong. *Environmental Pollution* 123, 307-317.

So, K.L., Wang, T., 2004. C-3-C-12 non-methane hydrocarbons in subtropical Hong Kong: spatial-temporal variations, source-receptor relationships and photochemical reactivity. *Science of the Total Environment* 328, 161-174.

Staehelin, J., Harris, N.R.P., Appenzeller, C., Eberhard, J., 2001. Ozone trends: A review. *Rev. Geophys.* 39, 231-290.

Stockwell, W.R., Middleton, P., Chang, J.S., Tang, X.Y., 1990. The 2nd Generation Regional Acid Deposition Model Chemical Mechanism for Regional Air-Quality Modeling. *Journal of Geophysical Research-Atmospheres* 95, 16343-16367.

Stohl, A., 1998. Computation, accuracy and applications of trajectories - A review and bibliography. *Atmospheric Environment* 32, 947-966.

Streets, D.G., Yu, C., Bergin, M.H., Wang, X.M., Carmichael, G.R., 2006. Modeling study of air pollution due to the manufacture of export goods in China's Pearl River Delta.

Environmental Science & Technology 40, 2099-2107.

Tang, J.H., Chan, L.Y., Chan, C.Y., Li, Y.S., Chang, C.C., Liu, S.C., Wu, D., Li, Y.D., 2007. Characteristics and diurnal variations of NMHCs at urban, suburban, and rural sites in the Pearl River Delta and a remote site in South China. *Atmospheric Environment* 41, 8620-8632.

Tang, J.H., Chan, L.Y., Chan, C.Y., Li, Y.S., Chang, C.C., Wang, X.M., Zou, S.C., Barletta, B., Blake, D.R., Wu, D., 2008. Implications of changing urban and rural emissions on non-methane hydrocarbons in the Pearl River Delta region of China. *Atmospheric Environment* 42, 3780-3794.

Tanimoto, H., 2009. Increase in springtime tropospheric ozone at a mountainous site in Japan for the period 1998-2006. *Atmospheric Environment* 43, 1358-1363.

Tanimoto, H., Furutani, H., Kato, S., Matsumoto, J., Makide, Y., Akimoto, H., 2002. Seasonal cycles of ozone and oxidized nitrogen species in northeast Asia - 1. Impact of regional climatology and photochemistry observed during RISOTTO 1999-2000. *Journal of Geophysical Research-Atmospheres* 107.

Tie, X., Brasseur, G.P., Zhao, C., Granier, C., Massie, S., Qin, Y., Wang, P., Wang, G., Yang, P., Richter, A., 2006. Chemical characterization of air pollution in Eastern China and the Eastern United States. *Atmospheric Environment* 40, 2607-2625.

Tiwari, S., Rai, R., Agrawal, M., 2008. Annual and seasonal variations in tropospheric ozone concentrations around Varanasi. *International Journal of Remote Sensing* 29, 4499-4514.

Tsui, J.K.Y., Guenther, A., Yip, W.K., Chen, F., 2009. A biogenic volatile organic compound emission inventory for Hong Kong. *Atmospheric Environment* 43, 6442-6448.

Tu, J., Xia, Z.G., Wang, H.S., Li, W.Q., 2007. Temporal variations in surface ozone and its precursors and meteorological effects at an urban site in China. *Atmospheric Research* 85, 310-337.

Utembe, S.R., Jenkin, M.E., Derwent, R.G., Lewis, A.C., Hopkins, J.R., Hamilton, F.H., 2005. Modelling the ambient distribution of organic compounds during the August 2003 ozone episode in the southern UK. *Faraday Discuss.* 130, 311-326.

Vingarzan, R., 2004. A review of surface ozone background levels and trends. *Atmospheric Environment* 38, 3431-3442.

- Vingarzan, R., Taylor, B., 2003. Trend analysis of ground level ozone in the greater Vancouver/Fraser Valley area of British Columbia. *Atmospheric Environment* 37, 2159-2171.
- Vukovich, F.M., Fishman, J., Browell, E.V., 1985. The Reservoir of Ozone in the Boundary-Layer of the Eastern-United-States and Its Potential Impact on the Global Tropospheric Ozone Budget. *Journal of Geophysical Research-Atmospheres* 90, 5687-5698.
- Walker, H.L., Derwent, R.G., Donovan, R., Baker, J., 2009. Photochemical trajectory modelling of ozone during the summer PUMA campaign in the UK West Midlands. *Science of the Total Environment* 407, 2012-2023.
- Wang, H.Q., Jacob, D.J., Le Sager, P., Streets, D.G., Park, R.J., Gilliland, A.B., van Donkelaar, A., 2009a. Surface ozone background in the United States: Canadian and Mexican pollution influences. *Atmospheric Environment* 43, 1310-1319.
- Wang, J.-L., Wang, C.-H., Lai, C.-H., Chang, C.-C., Liu, Y., Zhang, Y., Liu, S., Shao, M., 2008. Characterization of ozone precursors in the Pearl River Delta by time series observation of non-methane hydrocarbons. *Atmospheric Environment* 42, 6233-6246.
- Wang, J.T., Lam, K.S., Xie, M., Wang, X.M., Carmichael, G., Li, Y.S., 2006. Integrated studies of a photochemical smog episode in Hong Kong and regional transport in the Pearl River Delta of China. *Tellus Ser. B-Chem. Phys. Meteorol.* 58, 31-40.
- Wang, T., Cheung, T.F., Li, Y.S., Yu, X.M., Blake, D.R., 2002a. Emission characteristics of CO, NO_x, SO₂ and indications of biomass burning observed at a rural site in eastern China. *Journal of Geophysical Research-Atmospheres* 107.
- Wang, T., Cheung, V.T.F., Lam, K.S., Kok, G.L., Harris, J.M., 2001a. The characteristics of ozone and related compounds in the boundary layer of the South China coast: temporal and vertical variations during autumn season. *Atmospheric Environment* 35, 2735-2746.
- Wang, T., Guo, H., Blake, D.R., Kwok, Y.H., Simpson, I.J., Li, Y.S., 2005a. Measurements of trace gases in the inflow of South China Sea background air and outflow of regional pollution at Tai O, Southern China. *Journal of Atmospheric Chemistry* 52, 295-317.
- Wang, T., Kwok, J.Y.H., 2003. Measurement and analysis of a multiday photochemical smog episode in the Pearl River delta of China. *Journal of Applied Meteorology* 42, 404-416.
- Wang, T., Lam, K.S., Lee, A.S.Y., Pang, S.W., Tsui, W.S., 1998. Meteorological and

chemical characteristics of the photochemical ozone episodes observed at Cape D'Aguilar in Hong Kong. *Journal of Applied Meteorology* 37, 1167-1178.

Wang, T., Poon, C.N., Kwok, Y.H., Li, Y.S., 2003. Characterizing the temporal variability and emission patterns of pollution plumes in the Pearl River Delta of China. *Atmospheric Environment* 37, 3539-3550.

Wang, T., Wu, Y.Y., Cheung, T.F., Lam, K.S., 2001b. A study of surface ozone and the relation to complex wind flow in Hong Kong. *Atmospheric Environment* 35, 3203-3215.

Wang, X.M., Carmichael, G., Chen, D.L., Tang, Y.H., Wang, T.J., 2005a. Impacts of different emission sources on air quality during March 2001 in the Pearl River Delta (PRD) region. *Atmospheric Environment* 39, 5227-5241.

Wang, X.M., Chen, F., Wu, Z.Y., Zhang, M.G., Tewari, M., Guenther, A., Wiedinmyer, C., 2009. Impacts of Weather Conditions Modified by Urban Expansion on Surface Ozone: Comparison between the Pearl River Delta and Yangtze River Delta Regions. *Advances in Atmospheric Sciences* 26, 962-972.

Wang, X.M., Sheng, G.Y., Fu, J.M., Chan, C.Y., Lee, S.G., Chan, L.Y., Wang, Z.S., 2002. Urban roadside aromatic hydrocarbons in three cities of the Pearl River Delta, People's Republic of China. *Atmospheric Environment* 36, 5141-5148.

Wang, X.M., Tang, Y.H., Carmichael, G., 2005b. A modeling study on regional air pollutions transport patterns over the pearl river delta in the fall season. *Modern Physics Letters B* 19, 1735-1738.

Wu, B.Z., Chang, C.C., Sree, U., Chiu, K., Lo, J.G., 2006. Measurement of non-methane hydrocarbons in Taipei city and their impact on ozone formation in relation to air quality. *Analytica Chimica Acta* 576, 91-99.

Xie, S.D., Zhang, Y.H., Li, Q., Tang, X.Y., 2003. Spatial distribution of traffic-related pollutant concentrations in street canyons. *Atmospheric Environment* 37, 3213-3224.

Xu, J., Zhang, Y.H., Wang, W., 2006. Numerical study on the impacts of heterogeneous reactions on ozone formation in the Beijing urban area. *Advances in Atmospheric Sciences* 23, 605-614.

Xu, J.L., Zhu, Y.X., Li, J.L., 1999. Case studies on the processes of surface ozone pollution in Shanghai. *J. Air Waste Management Association* 49, 716-724.

- Xu, X., Lin, W., Wang, T., Yan, P., Tang, J., Meng, Z., Wang, Y., 2008. Long-term trend of surface ozone at a regional background station in eastern China 1991-2006: enhanced variability. *Atmospheric Chemistry and Physics* 8, 2595-2607.
- Zhang, B.N., Kim Oanh, N.T., 2002. Photochemical smog pollution in the Bangkok Metropolitan Region of Thailand in relation to O₃ precursor concentrations and meteorological conditions. *Atmospheric environment* 36, 4211-4222.
- Zhang, J., Wang, T., Chameides, W.L., Cardelino, C., Kwok, J., Blake, D.R., Ding, A., So, K.L., 2007. Ozone production and hydrocarbon reactivity in Hong Kong, Southern China. *Atmospheric Chemistry and Physics* 7, 557-573.
- Zhang, Q., Streets, D.G., Carmichael, G.R., He, K.B., Huo, H., Kannari, A., Klimont, Z., Park, I.S., Reddy, S., Fu, J.S., Chen, D., Duan, L., Lei, Y., Wang, L.T., Yao, Z.L., 2009. Asian emissions in 2006 for the NASA INTEX-B mission. *Atmospheric Chemistry and Physics* 9, 5131-5153.
- Zhang, y.H., S. Xie, L. Zeng and H. Wang 1999. The traffic emission and its impact on air quality in Guangzhou area *J. Environmental Sciences* 11, 355-360.
- Zhang, Y.H., Shao, K. S., Tang, X. Y., and Li, J. L., 1998a. The study of urban photochemical smog pollution in China. *Acta Scientiarum Naturalium Universitatis Pekinensis* 33, 393-399.
- Zhang, Y.H., Shao, K., Tang, X., Li, J., 1998b. The Study of Urban Photochemical Smog Pollution in China *Acta Scientiarum Naturalium Universitatis Pekinensis* 34, 392-400.
- Zhang, Y.H., Su, H., Zhong, L.J., Cheng, Y.F., Zeng, L.M., Wang, X.S., Xiang, Y.R., Wang, J.L., Gao, D.F., Shao, M., Fan, S.J., Liu, S.C., 2008. Regional ozone pollution and observation-based approach for analyzing ozone-precursor relationship during the PRIDE-PRD2004 campaign. *Atmospheric Environment* 42, 6203-6218.
- Zheng, J.Y., Zhang, L.J., Che, W.W., Zheng, Z.Y., Yin, S.S., 2009. A highly resolved temporal and spatial air pollutant emission inventory for the Pearl River Delta region, China and its uncertainty assessment. *Atmospheric Environment* 43, 5112-5122.
- Zheng, J.Y., Zhong, L.J., Wang, T., Louie, P.K.K., Li, Z.C., 2010. Ground-level ozone in the Pearl River Delta region: Analysis of data from a recently established regional air quality monitoring network. *Atmospheric Environment* 44, 814-823.